

©2018

David P. Caronia

ALL RIGHTS RESERVED

NEW TECHNIQUES FOR THE REHABILITATION OF CONCRETE AND STEEL
STRUCTURES

By

DAVID P. CARONIA

A Dissertation submitted to the

School of Graduate Studies

Rutgers, The State University of New Jersey

In partial fulfillment of the requirements

For the degree of

Doctor of Philosophy

Graduate Program in Civil and Environmental Engineering

Written under the direction of

Dr. Perumalsamy N. Balaguru

And Approved by

New Brunswick, New Jersey

May, 2018

ABSTRACT OF THE DISSERTATION

NEW TECHNIQUES FOR THE REHABILITATION OF CONCRETE AND STEEL STRUCTURES

by DAVID PAUL CARONIA

Dissertation Director:

Dr. P.N. Balaguru

The results presented in this dissertation focus on the development of a durable repair system for concrete structures and an enhanced protocol for durability and corrosion resistance testing of concrete repair materials and coatings for steel structures. The primary characteristics of the repair material are: rapid strength gain, low shrinkage, flowable and develop good bond with aged concrete. The objective was to obtain a matrix composition with shrinkage strains less than the tensile cracking strain capacity. Tensile strain capacity of the matrix was increased using discrete fibers. In the area of accelerated testing, a new test protocol was developed for accelerated testing of coatings and thin repair layers. The objective was to develop response variables that provides clear quantitative measures. This was achieved by incorporating direct tensile pull-off strength of the virgin and deteriorated coatings as the main response variable for determining the durability of coating.

Review of the current state of the art indicated that there is a need for durable repair systems and a protocol for accelerated testing. A rapid-set composite formulation that has minimum shrinkage was chosen based on extensive review of all the products that are currently available. The chosen commercial product performance was further improved in the areas of shrinkage strain reduction and improvement of mechanical properties, with specific focus on increasing the tensile strain capacity. Use of admixtures and fibers were found to provide substantial improvements for both areas. The new formulation was used for both horizontal and non-horizontal patch repairs. For accelerated testing, a new response variable, namely, direct tensile (adhesion) strength of coating at various levels of exposures was found to be an excellent quantitative measure. For the exposure itself, deep freezing was added in addition to the current practice of exposure to ultra violet and salt water spray. Tests were conducted on five commercially available coatings to establish the viability of the proposed protocol.

Based on the experimental results and analysis presented in this dissertation, it is possible to formulate long lasting rapid repairs for both horizontal and non-horizontal patches. The system identified gains more than 6500 psi in compressive strength in 3 hours, an ultimate shrinkage strain of 0.000230 in/in has a modulus of rupture of 1198 psi at 28 days with a tensile strain capacity of 0.000457 in/in. The combination of the tensile strain capacity and ultimate shrinkage strain makes it possible to produce durable crack free repairs. The proposed test protocol for accelerated durability test provides a distinct quantitatively measurable response variable. In the current practice corrosion growth measured after long exposure durations are typically less than a few millimeters. The measurement is also difficult because of fuzzy corrosion growth. In the proposed

method, growth up to 6 millimeters of corrosion was established using pull-off tests. Pull test values decreased from 1018 psi to 158 psi. The method can also be used for thin repair systems.

ACKNOWLEDGEMENTS

“Nothing in this world can take the place of persistence”

-Calvin Coolidge

First and foremost, I would like to express my sincere gratitude to my advisor, Dr. Perumalsamy Balaguru for the continuous support of my Ph.D. study, for his patience, motivation and immense knowledge. His guidance helped me in all the time of research and writing of this thesis. I could not have imagined a better advisor and mentor for my Ph.D. study.

I would like to extend a special thanks to my committee members: Dr. H. Najm, Dr. H. Wang, and Dr. G. Venkateela. Further thanks goes to Dr. H. Najm for his assistance through my instruction of the undergraduate civil engineering laboratory courses and providing career advice. Appreciation is also given to Dr. N. Gucunski for giving me the opportunity to fund my graduate school education by teaching, for which I will always be grateful.

Special appreciation is given to the staff of the Civil Engineering department. Linda Szary and Gina Cullari for their support above and beyond the call of duty. A special thanks to Ed Wass Sr. for assisting me with tasks that I could not do myself, as well as making my time working in the lab much more entertaining.

A special appreciation to Ed Wass Jr., John Hencken, and Austin Taterka. Without your help in the hot summer sun, the logistics of my research would not have been possible. A special thanks to my undergraduate research assistants throughout the past four years, Jimmy Givas, Scott Buxbaum, Adam Davenport and Rick Vogt; your assistance was

invaluable. To Marko Lyszyk and Adi Abu-Obeidah, your friendship helped me maintain a level of sanity throughout this graduate school process.

Finally, a deep feeling of gratitude and appreciation to my family who have supported me through the good times and the bad. A very special appreciation goes to Henna Nain, for her steadfast dedication, confidence, support and ability to handle my nonsense through the long four years. I love you all.

TABLE OF CONTENTS

ABSTRACT OF THE DISSERTATION ii

ACKNOWLEDGEMENTS v

LIST OF TABLES xv

LIST OF FIGURES xviii

CHAPTER 1 – INTRODUCTION 1

CHAPTER 2 – RESEARCH OBJECTIVES AND STATE OF THE ART 5

 2.1 Introduction 5

 2.2 Introduction on Concrete Rehabilitation 6

 2.2.1 Background on Rapid Set Cement Systems 10

 2.2.2 Phosphate Cement 11

 2.2.3 Calcium Sulfoaluminate Cement..... 14

 2.2.4 Portland Cement with Additives..... 17

 2.2.5 Polymer Concrete 20

 2.3 Background on Rapid Set Durability Tests..... 23

 2.3.1 Current Methods for Concrete Repair Bond Durability 24

 2.3.2 Rapid Set Formulation: Research Objective 26

 2.4 Selection of Promising Rapid Set Cement System 26

 2.5 Introduction on Thin Coating Systems..... 27

2.5.1 Thin Coating: Surface Preparation	31
2.5.2 Thin Coating: Application Techniques.....	32
2.6 State of the Art: Evaluations of Thin Coatings	33
2.6.1 Thin Coating Performance Evaluation: Field Conditions	33
2.6.2 Thin Coating Performance Evaluation: Laboratory Conditions.....	38
2.6.3 Thin Coatings: Research Objective	43
2.7 Summary	43
 CHAPTER 3 – FORMULATIONS OF AN ENHANCED RAPID-SET CEMENT	
SYSTEM (RSHPR) AND MECHANICAL PROPERTIES.....	46
3.1 Introduction	46
3.2 Part 1: Processing Variables to Develop the Promising Rapid Set System	46
3.2.1 Test Variables	48
3.2.2 Response Variables.....	48
3.2.3 Cements Types	49
3.2.4 Fiber Types	49
3.2.5 Water to Cement Ratios.....	51
3.2.6 Admixtures	52
3.2.7 Small Diameter Aggregate (Pea Gravel)	54
3.2.8 Mixing and Curing Techniques	55
3.2.9 Determining the Optimal Composition	56

3.2.10 Flowability and Workability Trials	56
3.2.11 Flowability and Workability Trial Results for CSA Cement Formulations...	61
3.2.12 Flowability and Workability Trial Results for Modified Portland Cement Formulations	63
3.2.13 Drying Free Shrinkage Trials	66
3.2.14 Drying Free Shrinkage Trial Observations and Analysis	71
3.2.15 Compressive Strength Trials	71
3.2.14 Compressive Strength Trial Observations and Analysis	72
3.2.16 Flexural Strength Trial.....	73
3.2.17 Flexural Strength Trial Observations and Analysis.....	73
3.2.18 Selection of the Promising Rapid Set System (RSHPR).....	74
3.3 Part 2: Mechanical Properties of the Promising Rapid Set System (RSHPR)	75
3.3.1 Compressive Strength.....	75
3.3.2 Compressive Strength Observations and Analysis.....	76
3.3.3 Free Drying Shrinkage.....	78
3.3.4 Free Drying Shrinkage Observations and Analysis.....	79
3.3.5 Splitting Tensile.....	80
3.3.6 Splitting Tensile Observations and Analysis.....	81
3.3.8 Modulus of Elasticity.....	82
3.3.9 Modulus of Elasticity Observations and Analysis.....	84

3.3.10 Restrained Drying Shrinkage.....	84
3.3.11 Restrained Drying Shrinkage Observations and Analysis.....	85
3.3.12 Flexural Strength	85
3.3.13 Flexural Strength Analysis and Observations	92
3.4 Tensile Strain Capacity of Fiber Reinforced Rapid Set Concrete.....	93
3.4.1 Test Set-Up.....	94
3.4.2 Test Results.....	95
3.4.3 Flexural Modulus of Elasticity Analysis and Observations	102
3.5 Physical Property Relationships.....	104
3.5.1 Compressive Strength versus Modulus of Elasticity	104
3.5.1 Compressive Strength versus Splitting Tensile Strength	106
3.5.3 Flexural Strength versus Splitting Tensile Strength.....	111
3.6 Summary	114
 CHAPTER 4 – FIELD EVALUATION AND REPAIR OF NON-HORIZONTAL SURFACES	
4.1 Introduction.....	116
4.2 Horizontal Structural Patch Repair	116
4.2.1 Laboratory Horizontal Structural Patch Repair Test Overview	116
4.2.2 Horizontal Structural Patch Repair Field Test Overview	117
4.2.3 Horizontal Structural Patch Repair Laboratory Test Preparation.....	118

4.2.4 Horizontal Structural Patch Repair Field Test Preparation	120
4.2.5 Test Procedure	122
4.2.6 Laboratory Horizontal Structural Repair Test Results	123
4.2.7 Field Horizontal Structural Repair Test Results.....	125
4.2.8 Horizontal Structural Patch Repair Observations and Analysis.....	126
4.3 Patching Repairs of Non-Horizontal Surfaces	127
4.3.1 Test Overview.....	127
4.3.2 Non-Horizontal Patch Preparation.....	129
4.3.3 Non-Horizontal Patch Test Set Up	129
4.3.4 Non-Horizontal Patch Repair Test Result	131
4.3.5 Non-Horizontal Patch Observations and Analysis	133
4.4 Summary	133
 CHAPTER 5 – MECHANICAL ANCHORS TO PREVENT DE-BONDING OF REPAIR MATERIALS	 135
5.1 Introduction	135
5.2 Specimen Preparation.....	137
5.3 Horizontal Patch Repair Test Set Up	141
5.4 Horizontal Patch Repair Test Results.....	144
5.5 Mechanical Anchors Observations and Analysis.....	150
5.6 Summary	153

CHAPTER 6 – TEST CRITERIA FOR ACCELERATED CORROSION TESTING..	154
6.1 Selection of Criteria	154
6.2 Description of Criteria.....	155
6.3 Description of Test Set Up.....	157
6.4 Development of the Chamber for Accelerated Testing.....	159
6.5 Testing Scheme for the Chamber for Accelerated Testing	161
6.6 Summary	163
CHAPTER 7 – EXPERIMENTAL SETUP: ACCELERATED TESTING.....	165
7.1 Introduction	165
7.2 Salt Water Spray System.....	165
7.3 Salt Water Solution Preparation.....	169
7.4 Specimen Holding Rack.....	170
7.5 Heat and UV Exposure System.....	172
7.6 Deep Freezer	173
7.7 Chamber for Accelerated Testing Maintenance.....	174
7.8 Summary	175
CHAPTER 8 – DURABILITY TESTS: THIN COATINGS	176
8.1 Introduction	176
8.2 Thin Coating Specimen Preparation	176
8.3 Test Procedure.....	181

8.3.1 Response Variable: Pull Off Testing	182
8.3.2 Interpretation of Pull off Test Result	184
8.3.3 Response Variable: Color Change.....	185
8.3.4 Response Variable: Thickness Change.....	186
8.3.5 Response Variable: Visual Inspection	187
8.4 Test Results	187
8.5 Pull of Test Results Discussion.....	207
8.6 Color Change Results Discussion	208
8.7 Thickness Change Results Discussion	209
8.8 Visual Inspection Change Results Discussion	209
8.5 Discussion of Test Results	210
8.6 Proposed Acceptance Criteria	210
8.5 Summary	211
CHAPTER 9 – DURABILITY TESTS: RAPID REPAIR SYSTEMS.....	213
9.1 Introduction	213
9.2 Rapid Repair Durability: Test Set Up	213
9.3 Rapid Repair Durability: Specimen Preparation.....	215
9.4 Rapid Repair: Test Schedule	218
9.5 Rapid Repair Durability: Test Procedure	219
9.6 Test Results	221

9.7 Discussion of Test Results	229
9.8 Summary	229
CHAPTER 10 – CONCLUSIONS	231
REFERENCES	235

LIST OF TABLES

Table 2.1– Risk Based Acceptance Criteria for Coating Thickness and Adhesion (ASTM D3359, 2017)	34
Table 2.2 – Distribution of Condition Ratings For Coating Within Each Category (Ault & Farsschon, 2011)	37
Table 2.3 – Representative Mean Creepage from Scribe Reference Table (ASTM D 1654, 2016)	42
Table 3.1 - Fiber Types and Dimensions	51
Table 3.2 – Flowability and Workability Trial Results	61
Table 3.3 – Passing Rapid Set Formulations	66
Table 3.4 – Compressive Strength at 3 Hours	72
Table 3.5 – Three Hour Flexural Modulus of Rupture	73
Table 3.6 – RSHPR Specimen Flexural Strength	88
Table 3.7 – Highly Flowable RSHPR Specimen Flexural Strength	90
Table 3.8 - Sample 1 Load, Deflection & Strain Results.....	96
Table 3.9 – Sample 2 Load, Deflection & Strain Results.....	96
Table 3.10 – Sample 3 Load, Deflection & Strain Results.....	97
Table 3.11 – Sample 4 Load, Deflection & Strain Results.....	97
Table 3.12 – Flexural Modulus of Elasticity Results.....	98
Table 3.13 – Estimated Flexural Tensile Strain Capacity of RSHPR.....	103
Table 4.1 - RSHPR Simulated Slab Pull Off Test Results	124
Table 4.2 - Simulated Unprepared Surface Pull Off Test Results	124

Table 4.3 - Route 18, County Road 516 Bridge Pull Off Test Results.....	125
Table 4.4 - Pull Off Test Failure Location.....	126
Table 5.1 – Failure Location Percentage from Tensile Test.....	146
Table 5.2 – Substrate Tensile Capacity & Failure Mode.....	147
Table 5.3 – RSHPR & Tensile Capacity Results.....	148
Table 5.4 – Type 1 Mechanical Anchor Tensile Capacity & Failure Mode Results	148
Table 5.5 – Type 2 Mechanical Anchor Tensile Capacity & Failure Mode Results	149
Table 5.6 – Pull Off Test Results Distribution	150
Table 8.1 – Thin Coating Systems.....	187
Table 8.2 – Thin Coating Systems Allowable Minimum & Maximum Thickness	188
Table 8.3 – Thickness Readings: Thin Coating System 1	194
Table 8.4 – Thickness Readings: Thin Coating System 2	195
Table 8.5 – Thickness Readings: Thin Coating System 3	196
Table 8.6 – Thickness Readings: Thin Coating System 4	197
Table 8.7 – Thickness Readings: Thin Coating System 5	198
Table 8.8 – Average Thickness Change	198
Table 8.9 - Color Recordings: Thin Coating System 1.....	199
Table 8.10 - Color Recordings: Thin Coating System 2.....	199
Table 8.11 - Color Recordings: Thin Coating System 3.....	200
Table 8.12 - Color Recordings: Thin Coating System 4.....	200
Table 8.13 - Color Recordings: Thin Coating System 5.....	201
Table 8.14 - Color Recordings: Percent Change from Cycle 0 to Cycle 100.....	201

Table 8.15 - Visual Inspection: Thin Coating System 1	202
Table 8.16 - Visual Inspection: Thin Coating System 2	202
Table 8.17 - Visual Inspection: Thin Coating System 3	203
Table 8.18 - Visual Inspection: Thin Coating System 4	203
Table 8.19 - Visual Inspection: Thin Coating System 5	204
Table 9.1 – Pull Off Testing: Rapid Repair Durability Specimen 1	221
Table 9.2 – Pull Off Testing: Rapid Repair Durability Specimen 2	222
Table 9.3 – Pull Off Testing: Rapid Repair Durability Specimen 3	222
Table 9.4 – Pull Off Testing: Rapid Repair Durability Specimen 4	223
Table 9.5 – Pull Off Testing: One-Month Testing After Durability Specimen Chamber Removal	223
Table 9.6 – Average Percentage Loss of Tensile Stress Over 56 Cycles	224

LIST OF FIGURES

Figure 2.1 – The Effects of Shrinkage Between a Repair Material and Substrate Concrete (Vaysburg et al., 2014).....	9
Figure 2.2- Coating System for Highway Bridges (SPCC, 2014)	30
Figure 2.3 - Percent of Surface Rusted Reference Table (ASTM D 610, 2012)	35
Figure 2.4 - Typical Salt Fog (Corrosion) Test Set Up with Scribed Samples.....	39
Figure 2.5 - Scribe cuts on painted steel specimens ready for evaluation	40
Figure 2. 6 – Typical Old Decommissioned Bridge Components	42
Figure 3.1 – Typical W/C Ratio related to Drying Shrinkage (Krishna, V & Kumar, R, 2016)	52
Figure 3.2 – Rapid Set Identification: 1SF	67
Figure 3.3 - Rapid Set Identification: 2SF	68
Figure 3.4 - Rapid Set Identification: 0.5SF2	68
Figure 3.5 - Rapid Set Identification: 1SF2	69
Figure 3.6 - Rapid Set Identification: 2SF2	69
Figure 3.7 - Rapid Set Identification: 2SF_25G	70
Figure 3.8 - Rapid Set Identification: 2SF2_50G	70
Figure 3.9 – Three Hour Load versus Deflection	74
Figure 3.10 – Compressive Strength of the Promising Rapids Set Formulations	76
Figure 3.11 – Percent of Compressive Strength Increase Over 100 Days	77
Figure 3.12 – RSHPR Compressive Specimen in the Forney 250-Kip Compression Machine.....	78
Figure 3.13 – RSHPR Dry Free Shrinkage.....	79

Figure 3.14 – Highly Flowable RSHPR Dry Free Shrinkage	80
Figure 3.15 – Average Splitting Tensile Capacity	82
Figure 3.16 – Modulus of Elasticity	84
Figure 3.17 – Restrained Shrinkage Ring Sample	85
Figure 3.18 – RSHPR Load versus Deflection	91
Figure 3.19 – Highly Flowable RSHPR Load versus Deflection	91
Figure 3.20 – Flexural Strength Fractured Specimen	92
Figure 3.21 - C2A-06-125LW-120 Strain Gauge Attached to RSHPR Flexural Sample	94
Figure 3.22 – Sample 1 Flexural Stress versus Strain	98
Figure 3.23 – Sample 2 Flexural Stress versus Strain	99
Figure 3.24 – Sample 3 Flexural Stress versus Strain	99
Figure 3.25 – Sample 4 Flexural Stress versus Strain	100
Figure 3.26 – Sample 1 Load versus Deflection Curve	100
Figure 3.27 – Sample 2 Load versus Deflection Curve	101
Figure 3.28 – Sample 3 Load versus Deflection Curve	101
Figure 3.29 – Sample 4 Load versus Deflection Curve	102
Figure 3.30 – Flexural Modulus of Elasticity versus Compressive Modulus of Elasticity	102
Figure 3.31 – Correlation between RSHPR Modulus of Elasticity and Square Root of Compressive Strength	105
Figure 3.32 – Correlation between Highly Flowable RSHPR Modulus of Elasticity and Square Root of Compressive Strength	106
Figure 3.33 – Correlation Between RSHPR Splitting Tensile Strength and Square Root of	

Compressive Strength	107
Figure 3.34 – Correlation Between Highly Flowable RSHPR Splitting Tensile Strength and Square Root of Compressive Strength	107
Figure 3.35 – Correlation Between RSHPR Flexural Strength and the Square Root of Compressive Strength	109
Figure 3.36 – Correlation Between Highly Flowable RSHPR and the Square Root of Compressive Strength	109
Figure 3.37 – Correlation Between RSHPR Flexural Strength and Splitting Tensile Strength	111
Figure 3.38 – Correlation Between Highly Flowable RSHPR Flexural Strength and Splitting Tensile Strength	111
Figure 3.39 – Correlation Between CSA Cement Manufacturer Flexural Strength and Splitting Tensile Strength	113
Figure 4.1 - Route 18, County Road 516 overpass bridge repaired with RSHPR	118
Figure 4.2 - Laboratory RSHPR Slab with attached Pull Off Dollies	119
Figure 4.3 - 20-Millimeter Pull Off Dolly Attached to RSHPR Casted on Un-prepared Surface	120
Figure 4.4 – 20-millimeter Pull Off Test Dolly	121
Figure 4.5 - Attached Pull Off Dollies on RSHPR Patch Repair.....	121
Figure 4.6 - PosiTest® AT-M Manual Adhesion Tester	122
Figure 4.7 – Schematic of Failure Modes (ASTM C1583, 2016)	123
Figure 4.8 – Non-Horizontal Surface Patch Repair Applicator Plate	128
Figure 4.9 – Non-Horizontal Surface Patch Repair Application System	128

Figure 4.10 – Non-Horizontal Surface: Before Repair	129
Figure 4.11 – Non-Horizontal Surface Repair: Patch Repair Test Set Up	130
Figure 4.12 – Non-Horizontal Surface Repair: After Completion of Repair	132
Figure 4.13 - Non-Horizontal Surface Repair: Two Years After Completion of Repair.....	131
Figure 5.1 – Typical Simulated Patch.....	138
Figure 5.2 – Type 1 Mechanical Anchor	139
Figure 5.3 – Type 2 Mechanical Anchor	139
Figure 5.4 – Type 1 Mechanical Anchor Installation	140
Figure 5.5 – Type 2 Mechanical Anchor Installation	140
Figure 5.6 – Core Drill and Wet Core Bit Used to Make Circular Cuts.....	142
Figure 5.7 - Pull Off Test Dollies Attached to Repaired Patch	142
Figure 5.8 - Pull Off Test Conducted on Repaired Patch with a PosiTest® AT-M Manual Adhesion Tester	143
Figure 5.9 - Schematic of Failure Modes (ASTM C1583, 2016).....	144
Figure 5.10 – Average Tensile Capacity.....	145
Figure 5.11 – Typical RSHPR & Substrate Pull Off Result	146
Figure 5.12 – Typical Anchor Pull Out	147
Figure 5.13 – Magnified x25 Interface of RSHPR and Substrate Concrete	149
Figure 5.14 – Diagram of Mechanical Anchor in Patch Repair	152
Figure 7.1 - 150 Gallon Polyethylene Plastic Tub and Salt Water Solution Reservoir ..	166
Figure 7.2 - Salt Water Solution Reservoir Connection to the Pump.....	166
Figure 7.3 - Salt Sprayer Layout.....	167

Figure 7.4 - PVDF Flat Spray Nozzles	168
Figure 7.5 - Salt Water Sprayer Assembly	168
Figure 7.6 – Specimen Holding Rack.....	171
Figure 7.7 - Shoulder Screws Installed on the Specimen Holding Rack	171
Figure 7.8 - Infrared and UV Light Frame	172
Figure 7.9 - Removable Shelf for the Freezer.....	174
Figure 8.1 – Typical ½ inch diameter holes in steel specimens	177
Figure 8.2 - Typical 1-inch-long welds on steel specimens.....	177
Figure 8.3 – O-rings attached to steel specimen.....	177
Figure 8.4 - Aurand hand held steel toothed cleaning machine.....	178
Figure 8.5 – Low Pressure Spray Apparatus	179
Figure 8.6 – Spray Painting Specimens	180
Figure 8.7 – Thickness gage used for measuring the thickness of paint layers	180
Figure 8.8 – Painted steel specimen with O-rings removed	181
Figure 8.9 – 20 Millimeter Pull Off Dolly: Epoxied to Thin Coated Steel Specimen....	183
Figure 8.10 – Typical Pull Test.....	184
Figure 8.11 - Konica Minolta CR-10 Plus Color Reader.....	186
Figure 8.12 - Direct Tensile Stress versus Master Cycles: Thin Coating System 1	188
Figure 8.13 - Direct Tensile Stress versus Master Cycles: Thin Coating System 2	189
Figure 8.14 - Direct Tensile Stress versus Master Cycles: Thin Coating System 3	189
Figure 8.15 - Direct Tensile Stress versus Master Cycles: Thin Coating System 4	190
Figure 8.16 - Direct Tensile Stress versus Master Cycles: Thin Coating System 5	190
Figure 8.17 - Effective Radius versus Cycles: Thin Coating System 1	191

Figure 8.18 - Effective Radius versus Cycles: Thin Coating System 2.....	191
Figure 8.19 - Effective Radius versus Cycles: Thin Coating System 3.....	192
Figure 8.20 - Effective Radius versus Cycles: Thin Coating System 4.....	192
Figure 8.21 - Effective Radius versus Cycles: Thin Coating System 5.....	193
Figure 8.22 – Typical Corrosion Pitting at Simulated Bolt Hole & Weld.....	204
Figure 8.23 – Poor & Best Performing Thin Coating System Pull Test Dollies: Cycle 0 to Cycle 42	205
Figure 8.24 – Poor & Best Performing Thin Coating System Pull Test Dollies: Cycle 56 to Cycle 100	206
Figure 8.25 – Removed Paint After Pull Off Test	207
Figure 9.1 – Simulated Damage Patch Design Plan	216
Figure 9.2 – Mesh Wire Placed in Formwork Mold for Simulated Damage Patch.....	217
Figure 9.3 – Ferrocement Specimen with Simulated Damage Patch.....	217
Figure 9.4 – RSHPR Durability Specimen After Simulated Patch Repair	218
Figure 9.5 – Pull Off Dollies Epoxied on a Rapid Set Repair Durability Specimen	220
Figure 9.6 – Tensile Stress versus Cycles: Rapid Set Durability Specimen 1.....	224
Figure 9.7 – Tensile Stress versus Cycles: Rapid Set Durability Specimen 2.....	225
Figure 9.8 – Tensile Stress versus Cycles: Rapid Set Durability Specimen 3.....	225
Figure 9.9 – Tensile Stress versus Cycles: Rapid Set Durability Specimen 4.....	226
Figure 9.10 – Average Percentage Loss of Tensile Stress versus Cycles.....	226
Figure 9.11 – Typical Pull Off Specimens.....	227
Figure 9.12 – Typical Pull Outs on Durability Specimens	227
Figure 9.13 – RSHPR Patch Repair: 10 Months After Placement	228

Figure 9.14 – RSHPR Patch Repair: 10 Months After Placement 228

CHAPTER 1 – INTRODUCTION

The results presented in this dissertation focus on the development of a durable repair system for concrete structures and an enhanced protocol for durability and corrosion resistance testing of concrete repair materials and coatings for steel structures. The primary characteristics of the repair material are: rapid strength gain, low shrinkage, flowable and develop good bond with aged concrete. The objective was to obtain a matrix composition with shrinkage strains less than the tensile cracking strain capacity. Tensile strain capacity of the matrix was increased using discrete fibers. In the area of accelerated testing, a new test protocol was developed for accelerated testing of coatings and thin repair layers. The objective was to develop response variables that provides clear quantitative measures. This was achieved by incorporating direct tensile pull-off strength of the virgin and deteriorated coatings as the main response variable for determining the durability of coating.

Chapter 2 is divided into two parts. The first part provides an overview of the history and state-of-the-art of rapid concrete repair systems. Rapid set repair systems and application recommendations are summarized. The advantages and disadvantages of each rapid set system are given. The authors opinion is that durable repair systems are not currently available. The shrinkage strain of the available systems exceeds the tensile strain capacity of the repair material. Therefore, micro cracks will occur leading to further deterioration. The second part provides an overview of the history and state-of-the art of steel thin coating evaluation methods. Current evaluation methods for thin coating systems are discussed and shortcomings with the accepted methods are highlighted. The

authors opinion is that the current evaluation methods utilize difficult subjective measurements, and do not provide an indicator of actual field performance.

Chapter 3 discusses the formulation of an enhanced rapid-set cement system (RSHPR). Specifically, the optimized items are flowability, reduction of shrinkage strains, compressive strength gain in three hours, flexural strength and toughness. In the first part, the process of formulating and processing the variables for the mix designs are discussed. The second part of the chapter focuses on the selected promising formulations mechanical properties. The selected promising formulations combination of the tensile strain capacity and ultimate shrinkage strain makes it possible to produce durable crack free repairs. The discussion includes specimen preparation, test set-up and test results.

Chapter 4 presents field applications of the selected rapid set formulation (RSHPR). RSHPR is used to repair horizontal structural patches on an active Route 18, County Road 516 overpass bridge deck located in Old Bridge, New Jersey and to repair a non-horizontal patch conducted outside of the CAIT laboratory on Rutgers Livingston campus in Piscataway, New Jersey.

Chapter 5 is an experimental investigation of implementing mechanical anchors to prevent the de-bonding of repair materials and substrate concrete. Outside of the CAIT laboratory on Rutgers Livingston campus, a horizontal patch repair was conducted using RSHPR and mechanical anchors on a Route 18, County Road 516 overpass bridge deck donated by the New Jersey Department of Transportation. The use of an adhesion pull tester and pull off dollies were used to determine the tensile strength capacity increase of the mechanical anchors.

The selection of test criteria for accelerated corrosion testing is discussed in chapter 6. The fundamental weakness of the current testing is that the tests do not provide the estimate of service life in actual field conditions. The tests are intended only for comparative evaluations. A new economical chamber for accelerated corrosion testing was developed, that effectively provides a more realistic simulation of the interaction of these factors than is found in current accepted tests.

Chapter 7 discusses the fabrication of the chamber for accelerated testing. The chamber developed is fully automatic except for the manual replacement of salt water and placement of the specimens from the deep freezer to the chamber. To prevent any negative effects such as material creep or corrosion, the chamber had to be created out of strong durable materials. A recirculating salt water system is utilized for the chamber to effectively recycle and distribute the salt water. A system for the freezing, thawing and UV exposure was also developed and installed to ensure the required temperature and UV exposure metrics are achieved.

Chapter 8 deals with the specimen preparation, durability testing protocol and test results for thin coating systems. The thin coated steel specimens are placed into the chamber for accelerated testing, and monitored for 100 master-cycles. A new response variable, namely, direct tensile (adhesion) strength of coating at various levels of exposures was found to be an excellent quantitative measure.

Chapter 9 deals with the durability testing protocol for rapid-set cement systems. The specimen preparation, durability testing protocol and test results for rapid-set cement systems are presented. Based on the results, a new durability evaluation by incorporating

direct tensile pull-off strength of the virgin and deteriorated rapid-set cement durability specimens as the main response variable is recommended.

Chapter 10 discusses the major conclusions from the experimental results and provides recommendations for further research.

CHAPTER 2 – RESEARCH OBJECTIVES AND STATE OF THE ART

2.1 Introduction

In general, the United States highway system dates from the 1940's and 1950's. Many of the original pavements and structures still exist today, but are in poor condition. The American infrastructure is in great need of improvement and rehabilitation as the American Society of Civil Engineers "2017 Report Card for America's Infrastructure" issued a C+ grade for bridges where 9.1% of bridges are structurally deficient, and issued the roadways a D grade where 1 out of every 5 miles of highway pavement is in poor condition. Developing methodologies to efficiently repair and rehabilitate these structures is critical.

Rapid repair of concrete structures such as bridges is becoming more necessary so that there is minimal disruption to the public that utilizes the road ways. Rapid is used in the context to describe materials that gain strength at an accelerated rate where a structure can be reopened to traffic within 1 to 3 hours after placement of the repair material.

Many factors affect the effectiveness of rapid repair materials, such as the repair materials mechanical properties and the environment it is placed in. Repair materials will be constantly subjected to harsh environments such as freezing and thawing, chloride exposure, drying and wetting, and its properties need to be able to withstand these conditions for indefinite amounts of time. Hence it is necessary for the rapid material to not only gain rapid strength, but have long term durability properties as well.

Steel bridges represent more than 30% of the total number of highway bridges in the United States (Soliman & Frangopol, 2014). Steel bridges that are under severe chloride exposure due to deicing salts or marine environments require frequent maintenance and

repair activities to extend their service life and maintain an adequate performance level. Without proper maintenance of steel bridges, corrosion will weaken the metal, putting additional pressure on the concrete and ultimately compromise the structural integrity of the bridge. According to a FHWA study conducted in 2002, it was determined that the direct cost of corrosion in the United States is \$276 billion dollars on an annual basis. It was estimated in this study that 25% to 30% of annual corrosion cost in the U.S. could be saved if optimum corrosion management practices were employed. One such method is the application of thin coating paints, which help inhibit the expansion of corrosion on bridges.

The first part of this chapter will look at the state of the art information about rapid set repair materials and the characteristics they have to effectively rehabilitate concrete structures. The second part of this chapter will look at the state of the art information about thin coating paints, the application and the evaluating process of thin coating paints.

2.2 Introduction on Concrete Rehabilitation

Concrete shrinkage is an age old problem, identified as early as 1897 by J.B. Johnson in his *Treatise for Engineers on the Strength of Engineering Materials*. Other early publications on this subject include the papers published in American Concrete Institute Journals by Abrams, Davis and White. Shrinkage continues to be a problem that needs to be addressed by creating new materials, methods and type of fabrication to reduce the shrinkage strains. For example, low-shrinkage mixtures are needed to:

- Minimize cracking in bridge decks, with the ultimate goal of boosting service life
- Minimize curling and thereby help meet the increasing demand for very flat and level industrial floors
- Prevent delamination of repairs, and
- Cracking of slabs

In addition, shrinkage of concrete contributes to loss of prestress, redistribution of stresses between steel and concrete in reinforced concrete, increase in deflections and relaxation of fixity over continuous supports. Shrinkage strains for typical concrete mixtures range from 800 to 1200 micro strains.

Drying shrinkage is the reduction in volume caused principally by the loss of water during the drying process. Drying shrinkage in high strength concrete is smaller than normal strength concrete due to the smaller quantities of free water after hydration (Gilbert, R.I, 2001). If the concrete is free to move, drying shrinkage is not a problem. If the concrete is restrained in any way, drying shrinkage will introduce tensile stresses which, if they exceed the tensile strength of the concrete, will cause the concrete to crack. Shrinkage cracks, as opposed to flexural cracks are parallel sided and in the case of slabs usually extend right through the slab thickness. Such cracks can cause water penetration/leakage and ultimately impair the durability of the concrete element (CCAA, 2002). Therefore, controlling the cracking due to drying free shrinkage of concrete will reduce the tensile stresses, and eliminate cracking.

If the cement based materials are free to shrink, it'll just become shorter without any defects or distress. However, this is not the case with a concrete composite repair system.

Shrinkage of hardened cement-based materials, when restrained by bond to the substrate, produces tensile stresses. Since the tensile strength capacity of the material is very low, it usually cracks. As shrinkage stresses accumulate, the repair material resists cracking until the stress exceeds the tensile capacity of the repair material. Repair distress is triggered by the stress concentrations at the interface, a region where the probability of failure is as high as in the material itself. The load-carrying capacity of the repair material does not come into play when the repair material fails to fill the cavity as designed, because of the effects of shrinkage (Vaysburd et. al, 2014). Figure 2.1 shows the stress distribution around a new repair material that does not carry its part of the load.

The best solution is to obtain concrete that has zero shrinkage but this is practically impossible. The next best solution is to restrict the shrinkage strains to the tensile strain capacity of concrete which range from 200 to 300 micro strains. If this can be achieved, the restrained shrinkage cracking problem can be solved resulting in durable structures that can last for centuries.

The repair materials adhesion to the substrate concrete needs to be considered when selecting a repair material. A composite concrete slab consisting of a base and a bonded overlay is significantly stronger and stiffer than a composite slab with an unbonded overlay (Silfwerbrand, 2017). A sufficiently good bond between base layer concrete and concrete overlay is mandatory for bonded overlays; not only to obtain monolithic action between the two concrete layers, but also to promote crack control in the overlay and prevent the transport of water and detrimental substances in the interfacial zone between the two layers. The bond between the base layer concrete (substrate) and a concrete overlay (repair material) is very comprehensive with many factors affecting the bond

strength. Silfwerbrand and Beuhausen defined three classes of importance: major, intermediate, and minor influencers for overlay bond to the substrate concrete.

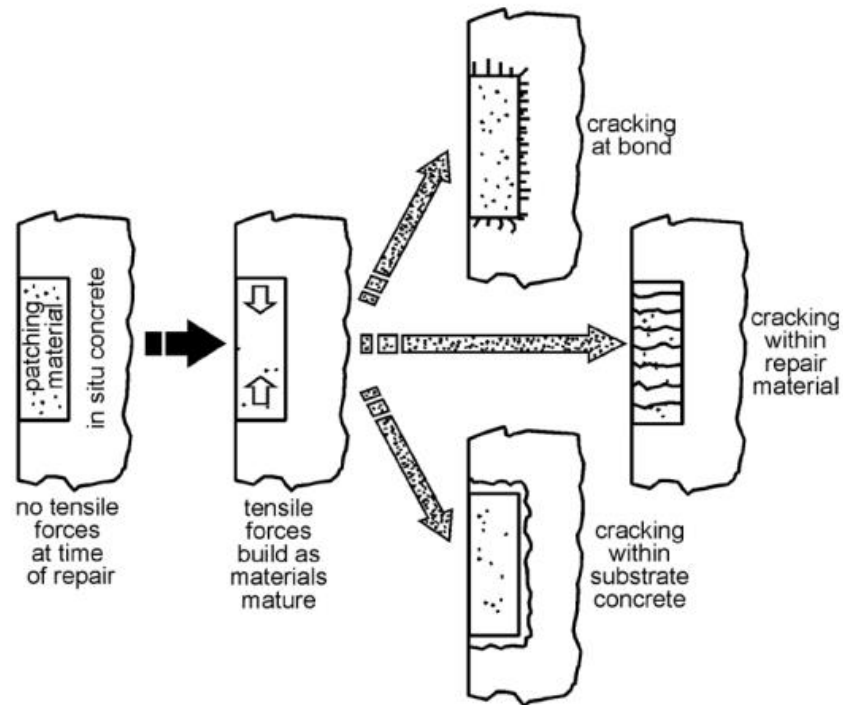


Figure 2.1 – The Effects of Shrinkage Between a Repair Material and Substrate Concrete (Vaysburg et al., 2014)

Major influencers are as identified as

- A substrate free of microcracking;
- A substrate free of laitance;
- A clean substrate surface during overlay placement;
- Sufficient compaction of the overlay;
- Good curing during a sufficiently long period after placement.

Intermediate influencers are identified as:

- Prewetting of the substrate;

- Overlay properties;
- Time after overlay placement.

Minor influencers are identified as:

- Substrate properties and roughness;
- Bonding agents;
- Overlay placement method;
- Early traffic and fatigue;
- Environment.

Based on Silberbrand and Beuhausen's observations, a successful bond between substrate and repair material must meet the demands of the listed influencers.

State of the art on concrete materials that provide low shrinkage strains are presented in this chapter. The focus is to develop low shrinkage formulations that are field usable for rapid repair and rehabilitation of concrete structures.

2.2.1 Background on Rapid Set Cement Systems

Rapid set cements are a class of materials that can obtain a compressive strength of 3,000 psi in 1 to 3 hours. This aspect is particularly important for repair of transportation structures because the structures cannot be taken out of service for extended durations.

Typical rapid set cements have low shrinkage characteristics. In the case of repairs, low-shrinkage is another important factor for lasting repairs. Shrinkage of repairs will lead to delamination, cracking at the junctions, cracking of repair patch and damage to parent concrete surface. In overhead applications delamination could lead to safety issues

because the delaminated patch could fall on vehicles traveling underneath the structures. Fortunately, shrinkage strains of rapid set formulations are typically lower than traditional Portland cement mixes. Rapid set formulations are an important class of materials due of their extensive and effective use in repairs.

There are multiple types of rapid set formulations commonly used. For this chapter, phosphate cement, calcium sulfoaluminate cement, portland cement with additives and polymer concrete will be discussed due to the know mechanical property of being able to reach a compressive strength of 3000 psi within 1 to 3 hours.

2.2.2 Phosphate Cement

Magnesium phosphate concrete, a type of rapid- hardening concrete, is composed of magnesium phosphate cement (MPC), instead of common Portland cement, as well as other cementitious materials such as fly ash, aggregate (generally a coarse aggregate such as gravel limestone or granite, plus a fine aggregate such as sand), water, and chemical admixtures. The density of magnesium phosphate concrete is generally less than the density of normal concrete, $2,400 \text{ kg/m}^3$ (150 lb/ft^3). Magnesium phosphate concrete has two specific characteristics that are suitable for rapid repairs encountered in transportation infrastructures. First, the concrete sets rapidly and can achieve the required strengths in less than 2 hours. In addition, Magnesium Phosphate concretes are known to provide very little shrinkage.

A number of investigators have evaluated the shrinkage characteristics of Magnesium phosphate concrete and the conclusion is that these concretes undergo limited shrinkage strains. For example, Yang, Zhu and Xu reported that Magnesium Phosphate mortar had

a shrinkage strain of 34 micro strains whereas Portland cement mortar had shrinkage strain of 3000 to 5000 micro strain (Yang, Zhu & Xu, 2000). Yue and Bing reported a similar shrinkage strain of 35 micro strain (Yue & Bing, 2002). Key characteristics of these cements are rapid strength gain, excellent bonding to Portland cement substrates and low shrinkage. The mechanical properties of concrete made with these classes of cements are comparable to that of concrete made with Portland cements.

Magnesium phosphate cement is a blend of magnesium oxide and some form of phosphate. Ammonium phosphate is used in commercial products but this formulation releases gases. Therefore, for this chapter, mono-potassium, di-phosphate (KH_2PO_4) also called MKP was further investigated. These ingredients react with water, rapidly producing strength and heat. The reaction product is magnesium potassium phosphate ($\text{MgKPO}_4 \cdot 6\text{H}_2\text{O}$). Compared with Portland cement, this type of cement can obtain several thousand psi compressive strength and over thousand psi modulus of rupture in a very short time. Fly ash, sand, gravel, fiber and other admixtures and fillers can be incorporated to improve the economy and mechanical properties. Some of these cements are available as packaged patching material, such as Euro-Speed MP which requires only the addition of water. Thin formulations are also being used as a coating material.

The fundamental work for these classes of phosphate cements, dates back to 1950, when Kingery published the results of his investigation. His work dealt with the fundamental aspects of phosphate bonding in refractory cement systems. Interestingly, none of the US patents reference this work. This reference could have been ignored (missed) since the classical cement compositions are based on calcium silicates. However, refractory cement systems encompass a number of composition systems that include magnesium phosphate.

Note that the refractory cements must be able to tolerate exposure to corrosive environments at elevated temperatures.

The formulation and preparation of magnesium (or Ca or Al) phosphate based cements are based on the reaction of an acidic phosphate salt with an alkaline source product of magnesium oxide (or calcium oxide or aluminum oxide, respectively). The combination of these 2 components, in the right ratio, when exposed to water will result in an acid-base reaction that forms a very stable cementitious product. Early published and patented work was based on the use of phosphoric acid directly and/or in combination with acid phosphate salts including monosodium phosphate (MSP) and mono-ammonium phosphate (MAP).

- In 1950 Kingery publishes work on the fundamentals of phosphate bonding systems in refractory cement compositions; this sets the foundation for the use of magnesium phosphate and related phosphate systems for use as refractory cement compositions that are still used today.
- Mid '60's / early '70's, US patents were granted on the preparation and use of MgO in combination with phosphoric acid and/or acidic phosphate salts such as MAP, MSP, mono-magnesium phosphate for producing rapid-set concretes. These products were used for a variety of applications including road repair and building construction.
- In the 1980's researchers started to improve the properties magnesium phosphate cement in the area of quality assurance. Consistent results were obtained by controlling the reaction mechanism. In most of the published work, the principal acid phosphate source used was mono-ammonium

phosphate (MAP). MAP was usually preferred because it was readily available and economical. Note that MAP was also used as a fertilizer product.

- In the late 1990's / early 2000, Argonne National Labs completed work and patented the application of the magnesium phosphate based cement systems for encapsulation of nuclear and hazardous waste. They promoted a formulation based on the use of MgO with MKP.

In early 2000's, Argonne National Laboratories extended their work and obtained patents covering the use of magnesium phosphate for various construction applications.

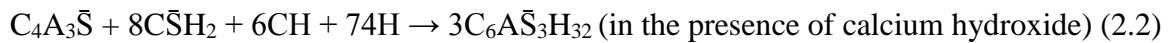
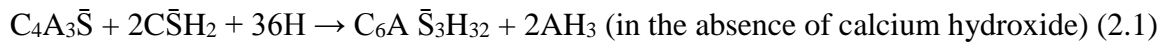
The mechanical properties of Magnesium-Phosphate Concrete (MPC) are very similar to Portland cement concrete. These include: compressive strength, modulus of elasticity, modulus of rupture and strain capacities in tension and compression. The primary differences are setting time and shrinkage strains. MPC bonds well to concretes made with Portland cement.

2.2.3 Calcium Sulfoaluminate Cement

In the 1950's Alexander Klein invented Calcium Sulfoaluminate Cement (CSA) at the University of California, Berkeley. CSA is considered an eco-friendly binder thanks to its lower environmental impact than ordinary portland cement, linked to the reduced CO₂ emission achieved by a lower production process temperature and a different chemical composition (Tortelli & Marchi, 2015).

The hydration process for CSA cement involves the very rapid development of ettringite needles within the structure of the cement paste causing rapid strength gain. As Pera and

Ambrose explain, CSA contains the phases belite (C_2S), tetracalcium trialuminate sulfate (C_4A_3S), and gypsum (CSH_2) as their main constituents, as well as other phases such as C_4AF , $C_{12}A_7$, C_3A , and C_6AF_2 . When CSA hydrates, ettringite ($C_6AS_3H_{32}$) is formed according to the following reactions:



The microstructure of ettringite is strongly dependent on the presence of lime. Ettringite produced by the reaction equation 2.1 is expansive and this property is exploited in special applications such as shrinkage-restraint and self-stressing cements. Ettringite formed in the absence of lime in equation 2.2 is non expansive and generates high early strength in cementitious systems. The property in equation 2.2 is exploited in the manufacturing process to develop concretes with high early strength (40 MPa (5800 psi) after 6 hours of age) and workability.

In many rapid set cements the temperature development is often explosive which can lead to further moisture loss. The temperature development in CSA is significantly lower and shorter, which provides a curing stage of only several hours. This guarantees durable and stable strengths.

A study started in 2010 by Shadravan at the University of Oklahoma supported by the Oklahoma Transportation Center, was conducted to develop an innovative, economical and practical concrete pavement system that would have superior serviceability and durability. In this investigation, 15 slabs with the dimensions of 3-inch x 36-inch x 240-inch were casted on top of a 4-inch sand sub-base placed on a soil base (to duplicate a

true slab exposed to a realistic environment). The types of mixes tested were Type K shrinkage compensated concrete, calcium sulfoaluminate (CSA) based rapid set concrete, Portland cement based normal concrete, high performance concrete and normal concrete with two types of shrinkage reducing admixtures. The slabs were regularly visually inspected for surface cracking, and surface strain and joint opening measurements were taken using Demec targets and vibrating wire strain gauges up to 600 days. Shadravan determined that CSA has negligible shrinkage while the other mixes, specifically the high performance concrete exhibited the largest shrinkage in both early age, short and long term. The conclusion made by the researchers is that CSA increases the dimensional stability of the slab in comparison to the other types of Portland cement based concretes, even at an extreme testing age.

A study conducted by the CTL Group on behalf of the Hawaii Department of Transportation (HDOT) to develop a more fatigue and shrinkage resistant concrete mixture for use in bridge decks. HDOT reported that spalling of cover concrete has been observed in bridge decks, which was attributed to fatigue damage. It was also reported that spalling was not associated with corrosion, but generally occurred due to a combination of shrinkage stresses and trapped bleed water surrounding the reinforcing steel. Hence an investigation was conducted to address concerns of long-term durability by investigating the mechanical properties of concrete that affect fatigue life, and by reducing shrinkage, which is a source of tensile stress that contributes to cracking in bridge decks. The study concluded that CSA cement has higher flexural strengths and does not exhibit bleeding as compared to the other four Portland cement based repair materials. The compressive strength and reinforcement bond strength of the CSA cement

was found to be satisfactory in relation to the other repair material compositions. The CSA cement did not crack during the 31-day testing period for the restrained cracking test, therefore it is not likely to exhibit early age cracking due to shrinkage. The CSA bond strength tests resulted in sufficient strength to prevent delamination upon opening to traffic (above 250 psi), however in this study the failure occurred at the unprepared substrate concrete surface interface; so the bond strength would be improved by using surface preparation methods.

2.2.4 Portland Cement with Additives

A characteristic of ordinary Portland cement is that after mixing with water it sets to a final product having very considerable strength. However, one of the properties of such compositions is that early strength development is slow. This causes delays in construction sequencing such as forming, casting and form stripping cycle on a job-placed concrete can require at least one and usually several days. Providing a fast setting cement with Portland cements strength characteristics would increase the turnover rates, allowing for decreases in construction costs. Increased setting time would also allow for rapid repair of structures such as bridge decks, and airfields, reducing the amount of time the structure is out of service for repair. Developing a portland cement that hardens rapidly and has high early strength is beneficial.

The primary compounds found in Portland cement are tricalcium silicate (C_3S), dicalcium silicate (C_2S), tricalcium aluminate (C_3A), and tetracalcium aluminoferrite (C_4AF).

Tricalcium silicate hardens rapidly and is largely responsible for initial set and early strength. Dicalcium Silicate hardens slowly and contributes largely to strength increases

at ages beyond 7 days. Tricalcium aluminate liberates a large amount of heat during the first few days of hardening, and together with tricalcium silicate increase early strength of the cement. Tetracalcium aluminoferrite contributes little to the strength gain, it mostly affects the color of the cement. This produces ordinary portland cement that approximately reaches its serviceable compressive strength at 28 days, and shrinkage strains from 800 to 1200 micro strains. Hence this provides motivation for exploring alternatives to improve Portland cement from its shortcomings in certain applications and environments.

A number of modified cements have been produced that have the traditional components of Portland cement, and the addition of expansive agents to mitigate the shrinkage and fasten the set time of portland cement. The addition of Calcium Sulfoaluminate Cement (CSA) and Calcium Aluminate Cement (CAC) are typical expansive agents blended into fast set modified Portland cements. The reaction of CAC with CSA is strongly affected by the chemical activity and proportions between the Al_2O_3 (aluminum oxide) and $CaSO_4$ (Calcium Sulfate) bearing compounds added to the portland cement. The amount of each added into the portland cement will determine the rate and amount of ettringite formed at the appropriate time to give the expansion but also the source of sulfate and calcium ions which provide an environment to stabilize ettringite crystals. This is an important process because ettringite will begin to form immediately after water is added to the cement; in order to have proper expansion effect, a large percentage of the ettringite must form after some degree of strength has been achieved (Noncun-Wczelik et. al, 2011). Together this system produces special properties such as fast setting, rapid strength development, and shrinkage compensation (Bizzozero & Scrivener, 2015).

Morgan (1996) defines compatibility as the balance of physical, chemical and electrochemical properties and dimensions between a repair material and the existing substrate that will ensure that the repair can withstand all the stresses induced by volume changes and chemical and electrochemical effects without distress and deterioration over a designated period of time. Maintaining a composition of portland cement in the rapid repair material will provide mechanical properties closest to the substrate concrete, allowing for more compatibility between the repair and surrounding concrete.

Application of a fast set modified portland cement also has the advantage of being well covered by national codes and standards that are based around portland cement based materials (Morgan, 1996). This may make it more likely for a portland cement with additives repair material to be accepted by the design engineer.

Several authors studied the effect of blending ordinary portland cement and CSA/CAC to obtain a mortar with enhanced properties. Tortelli and Marchi report that the replacement of Portland Cement with CSA by 30% by mass will reduce shrinkage significantly. The study found that the replacement of portland cement with CSA by 30% mass produced shrinkage strains no greater than 380 microstrains at one year, as compared to the plain ordinary portland cement having shrinkage strains of 700 microstrains at one year. The replacement of ordinary portland cement with CSA/CAC by 15% by mass enhances early strength. The other mechanical properties of portland cement with additives concrete are very similar to Portland cement concrete. These include: compressive strength, modulus of elasticity, modulus of rupture and strain capacities in tension and compression. The primary differences are setting time and shrinkage strains.

2.2.5 Polymer Concrete

Polymer concrete was introduced in the late 1950's and became well known in the 1970's for its use in repair, thin overlays, floors and precast components (Bedi et al., 2013).

Polymer concretes are still widely used as a repair material in transportation structures.

Polymer concrete is a part of group of concretes that use polymers to supplement or replace cement as a binder. For a given type of polymer concrete, the properties are dependent upon binder content, aggregate size distribution, nature and content of micro-filler and curing conditions. The most commonly used resins for polymer concrete are unsaturated polyester resin, methyl methacrylate, epoxy resins, furan resins, polyurethane resins, and urea formaldehyde resin (Omaha, 1997). The types of polymer concrete are:

- Polymer impregnated concrete (PIC), where the portland cement concrete is treated by soaking and polymerization
- Polymer Modified Concrete (PMC), where the polymer is mixed with portland cement
- Polymer concrete (PC), where the binder is a polymer that replaces Portland cement

Polymer concrete has advantages compared to ordinary concrete repair materials as follows (Bedi et al., 2013):

- Rapid curing at ambient temperatures,
- High tensile, flexural and compressive strengths,
- Strong adhesion to most surfaces,
- Good long term durability with respect to freeze and thaw cycles,

- Low permeability to water and aggressive solutions,
- Good resistance against corrosion.

Disadvantages of polymer concrete as a repair material include according to Bedi et al. (2013) are:

- Difficulty to manipulate due to its strength and density
- It tends to be brittle in nature, i.e. if no reinforcement is provided there is a tendency to form cracks
- Polymer concretes are viscoelastic and will fail under a sustained compressive loading at stress levels greater than 50 percent of the ultimate strength.
- Polymer materials are costly, approximately up to five times the cost of ordinary concrete (Adams et al. 1975)
- Strength, stiffness, and bond to concrete varies with different types of polymers (Adams et al., 1975)

Lack of understanding of polymer concrete and cement concrete interaction is frequently the source of failure in practice as a repair material (Vaysburd et. al, 2014). This is due to many factors; polymer-based materials cover an extremely broad range of chemical/physical properties. The physical properties of polymer are uniquely different to those of concrete (i.e., mismatch). Polymer material properties are sensitive to the effects of relatively small temperature changes, and the harden properties can be markedly affected by the environment in which the material is applied.

Sprinkel (1985) reported that the temperature changes to which bridge decks are typically subjected can be sufficient to cause deterioration and eventual failure of polymer concrete overlays. According to Sprinkel, overlay failures can be grouped into three basic types:

1. The formation of vertical cracks through the thickness of the overlay. The formation of vertical cracks increases the permeability of the overlay and reduces its effectiveness in preventing the infiltration of chlorides. It will be the predominant mode of failure on bridges where the shear strength of the base concrete and the bond strength are high or the modulus of elasticity of the overlay is high, or the tensile strength is low. Failure will likely remain bonded to the base concrete until freezing and thawing action causes delamination.
2. The shearing of portland cement concrete below the bond line. Shearing of the concrete below the bond line causes the overlay to delaminate with concrete remaining bonded to its underside. Failure is most likely to occur when the shear strength of the base concrete is low, the bond is good, and the tensile strength of the overlay is high. Failure will likely occur after a few cycles of temperature change and will result in the delamination of the polymer concrete overlay.
3. The delamination of the bond between the polymer concrete overlay and the base concrete causes the overlay to delaminate with no concrete remaining on the underside. Failure is likely to occur when either the surface preparation prior to the installation is poor or when the shear strength of the base concrete and the tensile strength of the overlay are high. Where the initial bond is good, a significant number of cycles may be required to complete the failure.

2.3 Background on Rapid Set Durability Tests

Concrete's durability is a key characteristic that led to its wide spread use. Concrete must be able to resist weathering action, chemical attack, abrasion and other process of deterioration. Durable concrete will maintain its original form and, quality and serviceability when exposed to its environment (ACI 201.2R-08, 2008). This also is an important factor for concrete patch repairs, as a repair material that is not durable will ultimately reduce the effectiveness of the repair.

Many concrete repairs are conducted on outdoor structures, such as bridges, which are exposed to freeze and thaw cycles, ultra violet (UV) radiation, wetting and drying and salt exposure. This is due to the fact that bridges are outdoor structures, exposed to air on all four sides. These exposure environments can accelerate deterioration of concrete repairs and ultimately the longevity of the structures life span by providing an environment for deterioration to occur. For example, in repeated cycles of freezing and thawing in a wet environment, water enters the cracks during the thawing portion of the cycle and, during the subsequent freezing, the expansive stress results in progressive deterioration. This can reduce the effectiveness and lifespan of the repair material, as well as the damaged structure.

There are many factors that play a role in the effectiveness of a concrete repair, one of the most important being the repair materials ability to remain bonded to the substrate concrete. According to ASTM Subcommittee C09.25 on Organic Materials for bonding the response variables are:

- The near-surface tensile strength of the substrate as an indicator of the adequacy of surface preparation before applying repair or overlay material;
- The bond strength of a repair or an overlay material after the material has been applied to the substrate;
- The tensile strength of a repair material after the material has been applied to a surface; and
- The adhesive strength of bonding agents.

The mentioned response variables are typically evaluated on recently placed repair materials. Evaluating these variables will inform the investigator if there is a sufficient bond between the repair and substrate, but it does not indicate the long term durability of the bond that will be exposed to environmental conditions. A test procedure is developed to determine rapid set formulations durability by evaluating the direct tensile capacity while specimens undergo cyclic wetting, drying and freezing.

2.3.1 Current Methods for Concrete Repair Bond Durability

Concrete and concrete repair materials must be able to resist environmental factors, chemical attacks and any other process that can deteriorate it. The repair materials that retains its original form, bond strength and serviceability while undergoing environmental conditions is a durable material. According to Furr and Ingram, the important bond and durability evaluations for concrete repairs are the following:

- Shear Bond Tests
- Freeze-Thaw Durability
- Cyclical Flexure Tests

- Cold Temperature Cyclical Flexure Tests

Shear bond tests are to be conducted to determine the shear bond strength of bonding agents used to bond overlays to the base concrete. Freeze-thaw tests are to determine the durability of bonding agents and overlay materials. Cyclical flexure tests are to determine the effect of overlays and repeated loadings on the stiffness of a reinforced beam, and to determine the effect of repeated loads on the bonding agents. Cold temperature cyclical flexure tests are applied to determine the fatigue characteristics of overlaid beams in freezing environments. The importance is that bond strength, freeze-thaw resistance, and fatigue resistance are critical variables for a repair material. Note that not all of these variables are tested simultaneously.

A study by Li et al. was conducted at the University of Connecticut to determine the most effective method of determining a concrete repair materials bond strength. An analysis was carried out on five common bond strength tests to determine the evaluation method with the least amount of variation. The bond strength tests analyzed are as follows:

- Direct Tension Test
- Indirect Tension Test
- Direct shear
- Shear-Compression (Shear Bond Test)
- Pull Off Test

The investigation determined that pull off tests, prism splitting, and slant shear tests had lower coefficient of variation than direct tension and direct shear tests. For this investigation it is decided to apply pull off testing.

Road salts are commonly used throughout the United States where snow and ice are an issue. The road salts lower the freezing point of water that forms ice which leads to melting of the ice and snow; unfortunately, the road salts also deteriorate concrete.

Deterioration from road salts is a result of physical and chemical effects that occur whether or not the deicers cause significant scaling damage (Darwin et al., 2007).

According to Darwin et al., the damage caused by the deicing road salts is due to the effects of crystal growth within concrete pores. It is known that the application of deicing salts over the life of a structure or pavement will negatively impact the long term durability of the concrete, but there are currently no ASTM standards for test methods to assess the effects of deicer salt and freeze-thaw cycling on the durability of concrete repair materials and the concrete substrate.

2.3.2 Rapid Set Formulation: Research Objective

To better simulate field conditions and deterioration caused by outdoor exposure rapid set durability specimens will be placed into a developed chamber for accelerated testing.

The specimens will undergo cyclical wetting, drying, salt solution exposure, ultra violet exposure and freezing. A new evaluation method is developed to give a quantifiable performance evaluation of the rapid set patch repair to determine the repairs effectiveness when exposed to environmental conditions.

2.4 Selection of Promising Rapid Set Cement System

Based on information found on literature, and the requirements to solve the problem in this investigation, it was decided to pursue Calcium Sulfoaluminate Cement (CSA) and Portland Cement with additives. CSA and portland cement with additives are easily

obtainable, with numerous proven proprietary blends readily available. The mechanical properties of these two rapid set cement systems provide evidence that it is possible to achieve crack free concrete that could be used as a rapid repair material. Chapter 3 will discuss in detail the process of developing the selected rapid set system, as well as the selected rapid set systems mechanical properties.

2.5 Introduction on Thin Coating Systems

A common practice for maintaining and repairing existing structural steel is to apply an epoxy mastic urethane over coating. The Society for Protective Coatings (SSPC) defines this practice as follows:

Over coating is defined as the application of coating materials over an existing coating in order to extend its service life, including use of the appropriate cleaning methods. The procedure includes preparation of rusted or degraded areas, feathering edges of existing paint, low-pressure water washing of the entire structure to remove contaminants, application of a full intermediate coat over repaired areas, and optional application of a full topcoat over the entire structure (The Society for Protective Coatings, 1997)

Over coating offers significant advantages over repainting a structural steel bridge. The principal advantage is cost. According to a FHWA article “Over Coating”, full removal of paint can cost vaysburdas much as \$35 per square foot, because the old paint typically includes lead, which is a hazardous material to humans and the environment. In contrast, overcoat applications can cost an agency in the order of \$6 to \$10 per square foot (FHWA Bridge Coatings Technical Note, 2000).

However, over coating may be susceptible to poor performance based on several factors. According to a FHWA Bridge Over Coating Technical Note, original construction of structural steel bridges incorporated single component oil-alkyds containing lead or lead/chromate pigmentation. Over the years, environmental exposure resulted in alkyds becoming brittle and inflexible, with heavily chalked areas occurring where exposed to direct sunlight. This aging and deterioration, results in poor adhesion of the original paint system on structural steel.

In addition to the original coat system, bridges constructed over 40 years ago were fabricated from steel covered in mill scale. Mill scale is the flaky surface of hot rolled steel, consisting of iron oxides FeO , Fe_2O_3 , and Fe_3O_4 . In the short-term, mill scale provided bridges with corrosion protection. However, as moisture and chlorides penetrated the mill scale layer, the mill scale itself would help accelerate electrochemical processes corroding the bare steel. The mill scale also served as a poor surface for coating adhesion. The presence of mill scale can greatly increase the risk of corrosion failure in the rehabilitated structural steel when using over coating.

Prior to 1965 over coatings were generally oil- or alkyd-based and contained pigments using lead and/or chromium compounds as the corrosion inhibitors. The old axiom was “the more paint the better,” as additional coating thickness meant that more inhibitive pigment was applied to resist corrosion. These paints were expected to last about eight to ten years before requiring some level of maintenance intervention. As a result, there were so many coating layers on some bridges, that the weight of the coatings would overcome the adhesion to one another and/or the mill scale and fall off, sometimes in sheets (Kline, 2009).

Around 1965 many departments of transportations in the United States began specifying the use of blast cleaning to a near white condition in order to completely remove mill scale, and coatings that contained metallic zinc powder as the pigment providing corrosion resistance, as well as other paints became the standard. Today there are multiple types of paints used, for different applications. Figure 2.2 is a table from the Society for Protective Coatings describing what type of coating paint system should be used for highway bridges based on the painting application (new bridge versus over coating maintenance).

Coating System	Highway Bridges (New)	Highway Bridges (Maintenance 1)	Highway Bridges (Maintenance 2)
Inorganic Zinc-Rich Primer/Polyamide Epoxy/Acrylic Polyurethane	√		
Organic Zinc-Rich Primer/Polyamide Epoxy/Acrylic Polyurethane	√	√	
Organic Zinc-Rich Primer/ Polyamide Epoxy/Polysiloxane	√		
Organic Zinc-Rich Primer/ Polyamide Epoxy/Fluoropolymer	√	√	
Organic Zinc-Rich Primer/Polyurea	√	√	
Moisture Cure Urethane Zinc-Rich Primer/Moisture Cure Urethane/ Moisture Cure Urethane	√	√	
Moisture Cure Urethane Zinc-Rich Primer/Moisture Cure Urethane/Acrylic Polyurethane	√	√	
Inorganic Zinc-Rich Primer/Water- borne Acrylic	√		
Polyurea/Polyurethane Hybrid	√	√	
Organic Zinc-Rich Primer/ Water- borne Acrylic		√	
Thermal Spray Coating/Sealer	√	√	
Epoxy Sealer/Epoxy Mastic/Acrylic Polyurethane			√
Epoxy Mastic/ Acrylic Polyurethane			√
Epoxy Mastic/ Waterborne Acrylic			√
Moisture Cure Urethane Sealer/Moisture Cure Urethane/ Moisture Cure Urethane			√
Moisture Cure Urethane/Moisture Cure Urethane/Acrylic Polyurethane			√
Alkyd/Silicone Alkyd			√
Calcium Sulfonate Alkyd (2 coats)			√

Figure 2.2- Coating System for Highway Bridges (SPCC, 2014)

While there are several proven strategies for over coating corrosion protection of steel, there is no universal solution. A proper protection system must be chosen to accommodate cost, fabrication and productivity, long-term performance and maintenance. The various superimposed coats within a painting systems have, of course, to be compatible with one another.

Lastly, surface conditions can greatly affect the performance of coating systems. In-service bridges are exposed to a variety of environmental and industrial pollutants, as

well as dirt and debris over their life. The presence of these pollutants and debris build-up result in contamination that must be removed prior to over coating. Paint performance will be affected by the surface conditions during application. Over coating performance will be dependent on the underlying layer, and poor conditions will likely result in failure of the coating. Hence it is critical to properly prepare the steel surface before thin coating application as the lack of alternative over coating paint systems presents a challenge in maintaining a state of good repair for bridges constructed using painted structural steel elements.

2.5.1 Thin Coating: Surface Preparation

Surface preparation must be conducted to allow the over coating paint to adhere to the application surface. Typical methods for surface preparation involves either abrasive blasting, power tool, hand tool or high pressure water cleaning.

Abrasive blasting is the predominant method for surface preparation of bridges prior to painting. Abrasive blasting is typically uses recyclable steel grit or expendable abrasives. The advantage of the steel grit is the reduction of the volume of waste because the steel grit can be recycled. Typical steel cleaned rates for bridge abrasive blasting ranges from 50 to 250 square feet of steel cleaned per man hour of blasting.

Power tool cleaning is labor intensive, with slow production rates. It is only suitable for preparation of surfaces without extensive deterioration and for cleaning and repairing small areas in an already existing over coating. Power tool cleaning with vacuum system generally requires much less stringent containment and produces less waste than abrasive blasting.

Cleaning methods using high-pressure water have started to become prevalent in the industry. This approach has a low dust production, and a reduction in surface chemical containments (i.e. chlorides) as compared to the other dry surface preparation techniques. A downside of high pressure water blasting is it is unable to remove mill scale beneath original paint systems. Since water alone, regardless of pressure, will not give a surface profile, this limits the application of this technology for bridges intended for painting over a fully cleaned and profiled surface.

The level of cleaning specified is dependent upon a number of factors, including the severity of the environment, the extent of paint failure and corrosion, the location/area of failed paint, the desired service life of the applied maintenance system, the type of paint system to be used, and the availability of budget for the operation. Dependent on the level of cleaning, this step will remove loose particles, to various degrees, tight mill scale and paint. Proper surface preparation is required for strong adhesion between the thin coating and steel.

2.5.2 Thin Coating: Application Techniques

Typical paint coatings are applied by spraying, brushing, or rolling based on the requirements of the particular assignment. According to the Society for Protective Coatings most coating applications are applied using airless spray. However, in many cases where nearby traffic or facilities may be impacted by overspray, transportation authorities may restrict the use of spray equipment; brushing or rolling may be required in lieu of spraying in containment. With the use of containment on blasting jobs,

specifications commonly require the containment to remain in place for spraying of the primer and subsequent topcoats.

2.6 State of the Art: Evaluations of Thin Coatings

2.6.1 Thin Coating Performance Evaluation: Field Conditions

There are multiple standards for the performance rating of over coating paints in field conditions. The most commonly used standards will be discussed.

The current accepted rapid method of measuring paint adhesion and performance in the field is ASTM D 3359, Methods for Measuring Adhesion by Tap Test. In this specification a sharp blade is used to scribe through the coating to the substrate. There are two methods for forming the scribe, based on the paints thickness. The thickness of the aged paint system should be determined in accordance with SSPC PA-2, Measurement of Dry Paint Thickness with Magnetic Gages. Dry film thickness should be measured for each representative component of the structure. Film thickness may be categorized as thin ($0 < 10$ mils), medium (10 – 20 mils), or thick (> 20 mils). Method A employs an X-shaped scribe and is used for paint films thicker than 5.0 mils. Method B calls for a series of cuts in a Crosshatch pattern, and is used for relatively thin film coatings.

The specified tape is applied to and removed from the scribed area and the adhesion is rated based on the amount of paint removed from the substrate. Table 2.1 shows the ASTM D3359 risk-based acceptance criteria for coating thickness and adhesion. In practice Method A is almost always used when assessing coating adhesion in the field. The adhesion should be measured at a minimum of five random locations on each type of

representative component identified during the visual assessment. For large components or structures, a minimum of 5 measurements per 10,000 square feet should be performed.

Coating Thickness	Thin (<10 mils)	Medium (10-20 mils)	Thick (>20 mils)
5A or 5B	NONE	NONE	NONE
4A or 4B	NONE	NONE	NONE
3A or 3B	NONE	NONE	LOW
2A or 2B	LOW	LOW	MODERATE
1 A or 1 B	MODERATE	HIGH	HIGH
OA or OB	CERTAIN	CERTAIN	CERTAIN

Table 2.1– Risk Based Acceptance Criteria for Coating Thickness and Adhesion (ASTM D3359, 2017)

Patch testing should be applied to judge the risk associated with over coating a particular structure. Surfaces and components representative of the structure should be tested. The condition of areas to be evaluated should be assessed using visual and physical inspection techniques. Cleaning, surface preparation, and over coat materials should be identical to those proposed for use on the structure. The over coat materials should be applied to the prepared test areas, re-inspected after cure, and re-evaluated using the visual and physical inspection techniques.

The test patches are re-inspected after short-term (14 days) or long term (6 months minimum) curing. Ideally the test exposure period should span at least one winter season. The degree of rusting is recorded following the guidelines of ASTM D610, Standard Practice for Evaluating Degree of Rusting on Painted Steel Surfaces and ASTM D3359, Methods for Measuring Adhesion by Tap Test.

ASTM D610 estimates the percentage of surface area rust on a painted area by visual inspection, electronic scanning techniques or other agreed upon methods. After determining the rust surface area, the inspector refers to a chart supplied by ASTM to

determine the rust grade (Figure 2.3). The rust grade is a metric from 0 to 10, where 0 is greater than 50 percent surface area rust, and 10 is less than or equal to 0.01 percent surface area rust.

Rust Grade	Percent of Surface Rusted
10	Less than or equal to 0.01 percent
9	Greater than 0.01 percent and up to 0.03 percent
8	Greater than 0.03 percent and up to 0.1 percent
7	Greater than 0.1 percent and up to 0.3 percent
6	Greater than 0.3 percent and up to 1.0 percent
5	Greater than 1.0 percent and up to 3.0 percent
4	Greater than 3.0 percent and up to 10.0 percent
3	Greater than 10.0 percent and up to 16.0 percent
2	Greater than 16.0 percent and up to 33.0 percent
1	Greater than 33.0 percent and up to 50.0 percent
0	Greater than 50 percent

Figure 2.3 - Percent of Surface Rusted Reference Table (ASTM D 610, 2012)

It should be noted that these procedures only provide quantitative evidence based on subjective visual inspection, and the over coating paint sampling location.

There are not many studies conducted on the longevity and effectiveness of over coating paints, as when deterioration begins to show, the paint is replaced. Fortunately, a study with strong documentation of the longevity of bridge over coating paint systems was conducted by the New Jersey Department of Transportation. A 1986 study incorporated 47 different coating systems to various individual spans on Route 37 Mathis Bridge located in southern New Jersey (Ault & Farsschon, 2011). The coating system selections consisted of eighteen manufactured products. The experimental coating systems consisted of inorganic and organic zinc coatings, epoxies, aluminum epoxy urethanes, vinyl, urethanes, oil-alkyds, zinc metallizing, aluminum metallizing, rust converters and others.

Surface preparation varied from SSPC-SP2 through SSPC-SP10. Systems were then graded based on performance on annual inspections over a 20-year period. Thus, the study provides information on a 20-year field exposure performance.

The performance was rated using ASTM D610 rating system by assigning a score based on a 1 to 10 scale, 1 being worst and 10 being best. Two systems received a rating of 9 and 11 systems received a rating between 7 and 8. These systems were also evaluated after 1 year of exposure. Therefore, a good correlation can be obtained between short-term (1 year) and long-term (20 year) performance.

The results of an inspection conducted in 2007, nominally 20 years after the initial coating application inspection, showed varied service lives associated with the different coating systems. Some of the systems were in excellent condition after 20 years, while others had extensive deterioration. The study showed that the two-metallizing systems performed extremely well, even after 20 years. At the 20-year inspection, the first signs of rusting were noted on both the zinc and 85 Zn-15 Al metallized spans. The inorganic zinc systems performed quite well as a class. Of the eight inorganic zincs tested, only one system performed unacceptably as defined by the authors. The organic zinc systems performed quite well as a class. Of the seven systems tested, one system that did not perform well was applied with a urethane topcoat over an SP 6 prepared surface. As a class, the alkyd systems generally performed well over the first eight years. One system over SP 2 had an unacceptable level of failure on the flange just after one-year. Epoxy systems were among the worst performers at the 8 and 20-year inspections. Notice that all of these systems were applied to an SP 6 surface preparation, where most of the existing lead-based coating would have been removed and where visible amounts of

corrosion should be removed before painting. The report includes a table summarizing performance by coating systems. Table 2.2 is added here for reference:

	D610 Rating at 8 Years			D610 Rating at 20 Years		
	>7	7-4	<4	>7	7-4	<4
Metallizing Systems (2)	2	0	0	2	0	0
Inorganic Zinc Systems (8)	7	0	1	2	5	1
Organic Zinc Systems (7)	5	2	0	2	4	1
Miscellaneous Systems (5)	3	2	0	1	3	1
Alkyd Systems (6)	4	2	0	1	3	2
Urethane Systems (5)	2	3	0	1	2	2
Aluminum Systems (8)	1	4	3	0	4	4
Epoxy Systems (6)	0	4	2	0	0	6

Table 2.2 – Distribution of Condition Ratings For Coating Within Each Category (Ault & Farsschon, 2011)

As the table indicates, epoxy systems performed poorly in comparison with other systems. The report goes on to provide conclusions of their 20-year study. The following conclusions presented verbatim are of particular interest:

- “the epoxy mastic system provided a wide range of performance”
- “surface preparation did not play a major role in long-term performance”
- “aluminum mastic systems and epoxy systems performed the worst”

The findings provide a solid basis for the selection of systems for this investigation. The focus of the evaluation is the test methods to be used for the approving the products. The following criteria will be used for the selection:

- Number of coats needed, with preference given to two coat systems if they provide long term durability

- Sensitiveness of the system for the surface preparation. Since focus of this research is over coating, systems that are very sensitive to surface preparation may not be suitable
- Cost of the product including cost of materials and any special application methods.

2.6.2 Thin Coating Performance Evaluation: Laboratory Conditions

For the performance testing of over coating paints in a laboratory environment, the thin coated specimens are placed into accelerated and atmospheric corrosion test chambers.

The transportation authorities in the United States follow ASTM B117, and ASTM D5894 for the accelerated and atmospheric corrosion test chambers to evaluate the protective over coating paints. The fundamental weakness of the current chamber testing is that the tests do not provide the estimate of service life in actual field conditions. The tests are intended only for comparative evaluations.

To evaluate over coating paints exposed to an accelerated and atmospheric corrosion environment, the commonly accepted evaluation method is ASTM D1654, Standard Test Method for Evaluation of Painted or Coated Specimens subjected to Corrosive Environments. ASTM D1654 is applied to compare basic corrosion performance of the substrate, pretreatment, and/or coating system. In this evaluation, painted steel specimens are prepared for testing by scribing it in such a manner that the scribe is exposed lengthwise when it is placed into the testing cabinet, to allow solution droplets to run lengthwise along the scribe. The scribing, a deliberate simulation of coating failure, is used to simulate the failure observed when coated products are subjected to abrasion or

accidental damage and then exposed to corrosive influences. The scribe produced should be a sufficient length to cover the test area, but not contact the edge of the specimen. The depth of the scribe should be predetermined as to test the effective focus of the test. If one scribe cut per sample is not enough, the standard allows for more scribe cuts but they must all be produced in the same direction. It is allowed to use scribe lines other than single, straight lines, such as an X cut shape. Following the scribe cuts, the specimens then undergo the accelerated and atmospheric corrosion procedures (figure 2.4).



Figure 2.4 - Typical Salt Fog (Corrosion) Test Set Up with Scribed Samples

All the coating systems are supposed to be exposed for a minimum duration of 3,000 hours. The blistering, peeling, rust creepage, and other surface defects will be evaluated at each 500-hour increment of exposure. After test cabinet evaluation, the specimens unscribed areas and formed edges (bends, dimples, or other areas of interest) are evaluated following the procedure outlined in ASTM D714, Standard Test Method for Evaluating Degree of Blistering of Paints. The formation of blisters on paints is related

to system weakness, this procedure provides a methodology to describe the size and density of the blisters so comparative evaluations can be made to other specimens. The specimens are visually inspected and then compared to photographic reference standards to determine the size and frequency of the blisters. Based from the photographic references this observation is then correlated to a number, which can be used as a comparative metric between over coating paints. Figure 2.5 displays scribes after undergoing an accelerated and atmospheric corrosive environment. After the completion of the blister evaluation, the paint on the specimens need to be removed to evaluate the corrosion on the substrate.



Figure 2.5 - Scribe cuts on painted steel specimens ready for evaluation

The paint can be removed by scraping, picking off loose coatings with a knife, soaking the specimens in paint thinner, air blow-off or power washing. The removal procedure needs to be done carefully, as to not accidentally remove any corrosion off of the specimen. Accidental removal of corrosion can result in inaccurate interpretations. After removal of the paint, the specimens are to be rated following the equation given in ASTM D1654 (equation 2.3). First the maximum and minimum creepage from the scribe is recorded,

and noted whether or not the maximum is an isolated spot. The mean is determined by making at least 6 measurements of the width of the zone of corrosion uniformly distributed along the scribe, ignoring 3 mm (0.125 in.) of each end of the scribe. The arithmetic mean is calculated and equation 2.3 is used to calculate the rust creepage.

$$c = \frac{w_c - w}{2} \quad (2.3)$$

Where:

c = Rust creepage (millimeters or inches)

w_c = mean overall width of the corrosion zone (millimeters or inches)

w = width of the original scribe (millimeters or inches)

After calculating the rust creepage, table 2.3 is used to determine the rating of failure at scribe from 0 to 10. A rating of 0 is the best performing, a rating of 10 is the worst performing. This value is then used as a comparative metric between different over coating paints.

Representative Mean Creepage From Scribe		
Millimetres	Inches (Approximate)	Rating Number
Zero	0	10
Over 0 to 0.5	0 to $\frac{1}{64}$	9
Over 0.5 to 1.0	$\frac{1}{64}$ to $\frac{1}{32}$	8
Over 1.0 to 2.0	$\frac{1}{32}$ to $\frac{1}{16}$	7
Over 2.0 to 3.0	$\frac{1}{16}$ to $\frac{1}{8}$	6
Over 3.0 to 5.0	$\frac{1}{8}$ to $\frac{3}{16}$	5
Over 5.0 to 7.0	$\frac{3}{16}$ to $\frac{1}{4}$	4
Over 7.0 to 10.0	$\frac{1}{4}$ to $\frac{3}{8}$	3
Over 10.0 to 13.0	$\frac{3}{8}$ to $\frac{1}{2}$	2
Over 13.0 to 16.0	$\frac{1}{2}$ to $\frac{5}{8}$	1
Over 16.0 to more	$\frac{5}{8}$ to more	0

Table 2.3 – Representative Mean Creepage from Scribe Reference Table (ASTM D 1654, 2016)

This testing procedure requires the removal of paint by an abrasive method, producing the possibility of removing corroded sections, as well as only providing comparative results. The metrics determined from these analyses do not provide a system for rating the performance of the over coating paints for actual field conditions.



Figure 2. 6 – Typical Old Decommissioned Bridge Components

2.6.3 Thin Coatings: Research Objective

Based on the results and evaluation of the information collected during this chapter, a new protocol and testing procedure is developed in this thesis to better evaluate thin coating systems. The procedure developed will use the current guidelines and ASTM specifications and any additional tests that will provide information on the long-term durability of these coatings in adverse environmental conditions. To better simulate field conditions and deterioration caused by outdoor exposure, the steel specimens with thin coating paint will be placed into the developed chamber for accelerated testing. The specimens will undergo cyclical wetting, drying, salt solution exposure, ultra violet exposure and freezing. The preparation of the samples will apply a scribe to allow salt solution entry, but at the end of the prescribed testing length, a new evaluation method is applied to give a quantifiable performance evaluation of the over coating paint to determine the paint's effectiveness in actual field conditions. Chapter 6 will further discuss the selection of test criteria for the evaluation of thin coatings.

2.7 Summary

The following points are noted in regard to rapid set systems:

- Rapid set cements are a class of materials that can obtain a compressive strength of 3,000 psi in 1 to 3 hours.
- Shrinkage of repairs will lead to delamination, cracking at the junctions, cracking of repair patch and damage to parent concrete surface; typical rapid set cements have low shrinkage characteristics.

- Shrinkage strains of rapid set formulations are typically lower than traditional Portland cement mixes.
- Phosphate cement, calcium sulfoaluminate cement, portland cement with additives and polymer concrete are rapid set formulations with known mechanical property of being able to reach a compressive strength of 3000 psi within 1 to 3 hours.

The following points are noted in regard to rapid set repair durability evaluations:

- Rapid set repair material must be able to resist weathering action, chemical attack, abrasion and other process of deterioration.
- Important response variables to evaluate to determine a rapid set repairs durability are bond strength, and freeze-thaw resistance.
- Direct pull off tests provide the least amount variation when determining rapid set repair material bond strength.
- Currently there are no ASTM standards for test methods to assess the effects of deicer salt and freeze-thaw cycling on the durability of concrete repair materials and concrete substrate.

The following points are noted in regard to thin coatings for steel structures:

- Over coating offers significant advantages over repainting a structural steel bridge. The principal advantage is cost.
- Over the years, environmental exposure resulted in alkyds becoming brittle and inflexible, with heavily chalked areas occurring where exposed to direct sunlight.

This aging and deterioration, results in poor adhesion of the original paint system on structural steel.

- While there are several proven strategies for over coating corrosion protection of steel, there is no universal solution. A proper protection system must be chosen to accommodate cost, fabrication and productivity, long-term performance and maintenance. The various superimposed coats within a painting systems have, of course, to be compatible with one another.

The following points are noted in regard to durability evaluations of thin coatings:

- Cleaning, surface preparation, and over coat materials applied to testing specimens should be identical to those proposed for use on the structure
- The fundamental weakness of the current chamber testing is that the tests do not provide the estimate of service life in actual field conditions. The tests are intended only for comparative evaluations.
- Removal of paint procedures for current thin coating evaluations risk disturbing the corrosion growth. Accidental removal of corrosion can result in inaccurate evaluations.
- Inorganic and Organic Zinc thin coating systems are better performing than aluminum mastic and epoxy mastic based on a 20-year field durability evaluation.

CHAPTER 3 – FORMULATIONS OF AN ENHANCED RAPID-SET CEMENT SYSTEM (RSHPR) AND MECHANICAL PROPERTIES

3.1 Introduction

One of the aims of this thesis is to formulate a variation of previously described fiber reinforced cement composites specifically for use in rapid repair systems for concrete bridge decks and their sub-structures. Since the basic mechanical properties of the cement materials are already known and documented, the mix can be optimized to increase those properties with respect to the application systems. Specifically, the optimized items are flowability, reduction of shrinkage strains, compressive strength gain in three hours, flexural strength and toughness. This chapter will divide into two parts. In the first part, the process of formulating and processing the variables for the mix designs will be discussed. The second part of this chapter will focus on the selected promising formulations mechanical properties.

3.2 Part 1: Processing Variables to Develop the Promising Rapid Set System

Concrete is an extraordinarily versatile building material used for many purposes in bridges, buildings, tunnels and many other structures. Composed of a mixture of sand, gravel, crushed stone, or other coarse material bound together with cement, concrete undergoes a chemical reaction and hardens when water is added. Inserting reinforcement adds tensile strength to structural concrete elements. The use of reinforcement contributes significantly to the range and size of building and structure types that can be constructed with concrete.

While modern concrete is often considered to be permanent, it is, like all materials subject to deterioration. Concrete deterioration occurs primarily because of corrosion of

the embedded steel, degradation of concrete itself, use of improper techniques or materials in construction, or structural problems.

Selection and design of proper repair materials is a critical component of the repair project. The decision process of selecting a repair material requires evaluation of the performance, characteristics, and limitations of the repair materials. Factors to select an appropriate repair system include economic factors; service record; appearance; environmental considerations; compatibility issues; durability and performance; and safety requirements (Gaudette et al., 2007).

Achieving compatibility between repair work and original concrete may be difficult, especially given the variability often present in concrete materials and finishes (Gaudette et al., 2007). According to the American Concrete Institute Committee (ACI) 564R-04 the current ways to place the repair material is as follows:

- Cast-in-place concrete (most frequently used)
- Shotcrete (pneumatically placed concrete)
- Preplaced-aggregate concrete
- Troweling (hand applied repairs)
- Injection grouting (used to fill cracks, open joints and interior voids)

The basic categories of repair materials are cementitious materials (the best choice to match the properties of concrete as closely as possible, which is often an important selection criterion) and polymer materials.

Common issues with concrete repair materials include disintegration; scaling; efflorescence; erosion due to abrasion; spalling and popouts. It is necessary to develop a

repair material that is compatible between the repair material and existing substrate as this reduces the probability of these common issues occurring (McDonald et. al., 2002).

The research objective is to determine a rapid set formulation that has low shrinkage, is durable, has high early strength gains, could be consolidated with no vibration and could produce a uniform fiber matrix. To develop the promising rapid set system different types of rapid set cements, varying fiber types and lengths, water to cement ratios, admixtures and mixing techniques were applied to produce the optimal formulation.

3.2.1 Test Variables

The following are test variables used for this investigation. Each test variable will be further discussed in this chapter.

- Cement Types
- Varying fiber types and lengths
- Varying water cement ratios
- Admixtures to lower the water to cement ratio
- Varying concentrations of small diameter aggregate

3.2.2 Response Variables

The following are response variables used for this investigation. Each response variable will be further discussed in this chapter.

- Compressive strength gain over time
- Free drying shrinkage
- Splitting tensile strength

- Compressive Modulus of Elasticity
- Restrained drying shrinkage
- Flexural Strength

3.2.3 Cements Types

The rapid-set cements chosen for this investigation were Quikrete – Commercial Grade FastSet™ Non-Shrink grout, a Modified Portland cement and CTS Rapid Set Cement All, a Calcium Sulfoaluminate Cement (CSA). The Quikrete-Commercial Grade FastSet™ Non-Shrink grout was supplied by Lowe’s Home Improvement located in East Rutherford, New Jersey. The CTS Rapid Set Cement All was supplied by The Home Depot located in South Plainfield, New Jersey. These rapid set formulations were chosen due to their easy availability, wide spread use, low shrinkage, and high early strength characteristics.

3.2.4 Fiber Types

According to ACI 544.1, fibers enhance the properties (of concrete) including the tensile strength compressive strength, elastic modulus, crack resistance, crack control, durability, fatigue life, resistance to impact and abrasion, shrinkage, expansion, thermal characteristics, and fire resistance. A multitude of fibers of various materials, lengths, and volume fractions were used to determine an optimal composition. Micro fibers and macro fibers were investigated, and combined together for this investigation. Micro-fibers provide superior resistance to the formation of plastic shrinkage cracks, but are unable to provide any resistance to further crack width openings cause by drying shrinkage, structural load or other forms of stress. Typical fiber lengths for micro fibers

range from 3 millimeters to 19 millimeters. Macro fibers will be implemented to enhance the rapid set materials durability, toughness and the ability to provide limited structural capacity. Macro fibers are intended to carry load, and therefore, used to replace traditional reinforcement in certain non-structural applications as well as minimize and/or eliminate both early and late age cracking. Typical lengths for macro fibers are greater than or equal to 1 inch.

The fiber types investigated are steel, carbon fiber, polypropylene and brass coated steel fibers. Steel fibers provide high flexural, and fatigue strength, improved abrasion, spalling and impact resistance, resulting in durable concrete. Steel fibers randomly distribute ensuring that crack free stress accommodation occurs throughout the concrete, and steel fibers are very economical (approximately \$1.00 per pound). Disadvantages of steel fibers is producing a higher specific gravity of concrete (more weight), and corrosion of the steel fibers. For this investigation any increase of weight due to the increased specific of gravity due to the steel fibers can be ignored because the amount used for repairs is small. Carbon fibers have strong tensile strength, high stiffness, lightweight and excellent durability because carbon fiber does not rust and is resistant to chlorides. Disadvantages of carbon fibers are their high costs (approximately ten times the cost of steel fibers), and brittleness. Polypropylene fibers are flexible, ductile and cannot corrode, but have low tensile strength and modulus of elasticity. Brass coated steel fibers have the same advantages and disadvantages as steel fibers, but have an improved corrosion resistance due to the brass coating. Table 3.1 shows the different fiber lengths, widths, and type of fibers used for this investigation.

Fiber Type	Fiber Material	Shape	Length (mm)	Equivalent Diameter (mm)
Macro	Steel	Double Hooked Ends	30	0.5
Micro	Steel	Straight	3.6	0.055
Micro	Steel	Straight	6	0.07
Macro	Polypropylene	Straight	50	0.6
Micro	Brass Coated Steel Fiber	Straight	6	0.05
Micro	Brass Coated Steel Fiber	Straight	13	0.075
Micro	Carbon Fiber	Straight	6	0.07

Table 3.1 - Fiber Types and Dimensions

3.2.5 Water to Cement Ratios

The hydration of cement is very necessary for the strength development, shrinkage prevention and durability of concrete. When the water to cement ratio is above 0.42, there will be greater capillary water and the greater the volume of capillary network. This reduces the strength and durability of the concrete. Therefore, having a lower water to cement ratio helps reduce shrinkage strains and increase strength. Figure 3.1 shows the effect of the water to cement (W/C) ratio has on drying shrinkage.

Rapid set materials typically have much lower water to cement ratios than traditional Portland cement, which contributes to their lower shrinkage and early strength gain properties. The lower water to cement ratio also produces a stiffer composition, reducing the workability. Part of this investigation is to vary the water to cement ratio with the addition of chemical admixtures to produce a lower water to cement ratio that is workable and self-consolidating, but maintains the same or better mechanical properties of traditional rapid set cements.

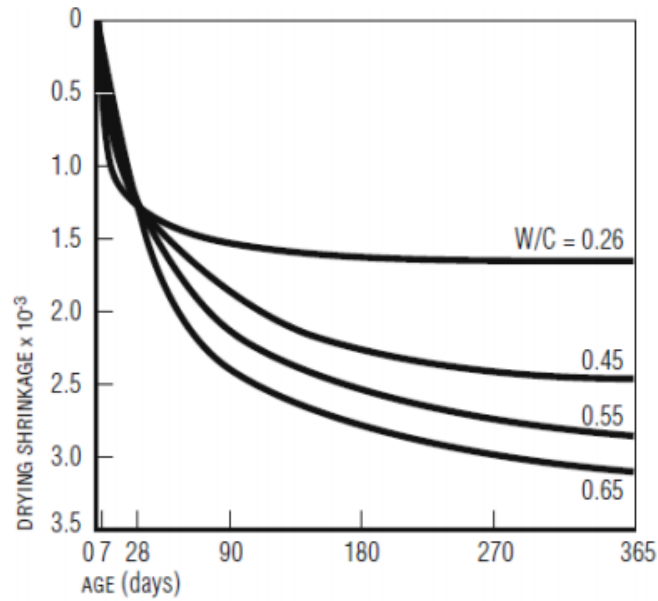


Figure 3.1 – Typical W/C Ratio related to Drying Shrinkage (Krishna, V & Kumar, R, 2016)

3.2.6 Admixtures

The application of admixtures for this investigation is to ensure a self-compacting rapid set formulation, while being able to reduce the water to cement ratio. The specific type of admixture that can most effectively achieve this goal is a High Range Water Reducer (HRWR), also known as super plasticizer. HRWR have an advantage over normal water reducers as they have a lower risk for excessive retardation, bleeding and air entrainment at higher doses. This is the justification for selecting HRWR formulations over normal water reducers for this investigation. High Range Water Reducers are used to reduce the amount of water needed for concrete by 12 percent to 30 percent, while maintaining a certain level of consistency and workability. The addition of HRWR are commonly utilized to produce flowing concrete used in heavy reinforced structures with inaccessible areas. HRWR also provide a delay in set time for concrete; the formulation of the HRWR dictates the increase in the set time (Fisher, 1994). There are four classes of

super plasticizers which are lignosulphonates, sulphonated melamine formaldehyde, sulphonated naphthalene formaldehyde and polycarboxylic ether. The most commonly used HRWR is sulphonated naphthalene formaldehyde based HRWR. Polycarboxylic ether based HRWR are currently gaining popularity due to their chemical structure that enables good particle distribution with low dosages. Sulphonated naphthalene formaldehyde based HRWR can add up to an additional 10 to 15 minutes of fluidity as compared to polycarboxylate ether HRWR has a lesser longevity of fluidity (Santhanam, 2013).

HRWR's are a powerful mechanism for improving the mechanical properties of concrete, but there are some disadvantages. A study conducted by Kronlöf et al. determined that a high percentage of plasticizer by weight can put a freshly casted mortar element at risk of excessive evaporation, due to excessive retardation, leading to significant shrinkage that causes cracking. Excessive addition of superplasticizers can cause undesirable side effects such as segregation, where particulate solids in concrete/mortars tend to segregate by differences in the size, density, shape and other properties of the particles of the composition (Neville, A.M., 2012).

The two types of HRWR investigated are a sulfonated naphthalene formaldehyde based High Range Water Reducing agent (Eucon 37) and a polycarboxylate ether based High Range Water Reducing agent (Plastol 5000). Both Eucon 37 and Plastol 5000 were supplied by Euclid Chemicals from the Euclid Chemical's East Brunswick, New Jersey location.

3.2.7 Small Diameter Aggregate (Pea Gravel)

Mineral aggregates are the predominant civil engineering material in terms of volume use. They are used with cementing matrices (in this case the rapid set material), to form composite materials (Young et al., 1998). Aggregates in concrete physically restrain the shrinkage of hydrating cement paste. Hard, rigid aggregates are difficult to compress and provide more restraint to shrinkage than softer, less rigid aggregates. Drying shrinkage can also be reduced by avoiding aggregates that have high drying shrinkage properties, and aggregates containing excessive amounts of clay. Quartz, granite, feldspar, limestone, and dolomite aggregates generally produce concretes with low drying shrinkages (Kosmatka, S.H. et al., 2011). Aggregates strongly influence concrete's freshly mixed and hardened properties, mixture proportions, and economy. Selection of aggregate is an important process. Although some variation in aggregate properties is expected, characteristics that are considered include:

- Grading
- Durability
- Particle shape and surface texture
- Abrasion and skid resistance
- Unit weights and voids
- Absorption and surface moisture

For this investigation an aggregate needed to be chosen that kept the rapid set formulation workable, flowable and self-compacting as well as provide resistance to shrinkage. It was decided to choose an aggregate with a diameter no larger than $\frac{1}{4}$ inch, commonly

known as pea gravel, to keep the formulation flowable and workable. The pea gravel chosen is a ¼ inch diameter quartz pea gravel supplied by The Home Depot in South Plainfield, New Jersey. First the pea gravel is thoroughly washed to remove any dust or dirt particles that could negatively affect the rapid set formulation. All moisture is then removed from the pea gravel by placing the aggregate in an oven until weight measurements confirmed that there is no moisture in the aggregate. This was done to ensure that there is no excess water being added into the rapid set formulation. For this investigation, varying concentrations of pea gravel in the formulation was tested to determine any beneficiary effects.

3.2.8 Mixing and Curing Techniques

To simulate rapid repair field conditions, specimens produced were air cured in the Rutgers Civil Engineering Laboratory on Busch Campus, Piscataway, NJ, since placing the samples in water or placing the specimens in a 100 hundred percent humidity chamber is not an option in field conditions.

For each rapid set formulation, the manufacturer specifications for mixing the composition was followed to ensure a correct reaction. If there were any admixtures added, first the minimum mixing time for the rapid set formulation is first reached, then the admixture is added, then continually mixed per the required amount of mixing time as per the admixtures manufactures specification.

For the addition of fibers and pea gravel, a trial and error testing methodology was used. During the mixing process it needed to be ensured that the rapid set formulation is uniformly mixed, the fibers do not clump, the formulation is flowable, and there is no

segregation between any of the components. Upon successful mixing and placement, results from the mechanical properties testing of the formulations were analyzed to determine the optimal mixing technique.

3.2.9 Determining the Optimal Composition

To determine the optimal composition, a total of ninety-eight formulations were developed and tested. The ninety-eight mixes were developed over an initial testing regiments flowability and workability. If the compositions were unable to pass these two initial tests, the conclusion was to disregard them as a formulation design, as it does not meet the research objective. After passing the flowability and workability investigations, the following step was to produce drying free shrinkage samples of the passing formulations. If the formulations were able to produce a dry free shrinkage of less than 300 microstrains, the following step was to test the high early strength gain. If the samples were able to satisfactorily surpass a compressive strength of 3000 psi within three hours, the selection would be further investigated. Following successful compressive strength testing, the samples then underwent Flexural Testing at three hours after casting. After the three-hour flexural testing of the specimens were analyzed, the two promising formulations were selected. One formulation to be easily applied in field conditions and the other to be highly flowable for pumping operations. The selected promising formulations mechanical properties were then further investigated.

3.2.10 Flowability and Workability Trials

Flowability for this research investigation will be defined as the formulations ability to take on the shape of its container, self-consolidate and maintain its composition matrix.

Workability will be defined as the rapid set formulations ease of use, ease to mix and effective placement without issue, and have a workability time of at least 10 minutes but no more than 30 minutes before initial setting.

To determine flowability, a modified flow test was developed. A three-inch diameter, three-inch height, non-absorbent plastic ring and 12 inch by 12 inch by $\frac{1}{4}$ inch thick non-absorbent acrylic plate were utilized. The rings center is first aligned and placed on the center of the acrylic plate, and placed on a flat, non-disturbed (free of vibrations) surface, then lightly dampened with potable water. Trial rapid set formulations would then be poured into the ring until full, forming a formulation volume of 21.2 in^3 . The ring would then be pulled straight up at a rate of 3 ± 1 second, with no twisting or jerking motions. The distance the rapid set formulation flowed, measured by the radius of the spread from the center point of the acrylic plate to the nearest eighth inch, as well as the time it took the rapid set formulation to reach its maximum spread were recorded. Formulations that flowed at least twice the radius of the ring from the center (3 inches), were then further investigated.

Workability was determined by the time it took a formulation to no longer be flowable, and the time until a formulation was no longer workable (any indents or errors could no longer be repaired by trowel). Once a rapid set is no longer workable, this is classified as initial setting of the material. According to the data sheets supplied by Quikrete and CTS, the typical average final set time of the selected rapid set cements typically occurs within 15 minutes after placement. For this research investigation, the minimum requirements were 5 minutes of flowability, and a minimum of 10 minutes of workability.

Rapid Set Identification	Rapid Set Type	W/C	Super Plasticizer (%)	Super Plasticizer Type	Mix Description	Flowability Measurement (inches)	Workability Measurement (Minutes)
M	CSA	0.1	0	N/A	Effective Water to Cement ratio to hydrate and mix cement	1.5	1
M2	CSA	0.11	0	N/A	Manufacturer Plastic Recommendation	2	3
M3	CSA	0.152	0	N/A	Manufacturer Flowable Recommendation	2.5	6
M4	CSA	0.19	0	N/A	Manufacturer Fluid Recommendation	3	10
MSP	CSA	0.1	0.5	Sulfonated Napthalene		1.625	3
MSP2	CSA	0.1	1	Sulfonated Napthalene		2	6
MSP3	CSA	0.1	2	Sulfonated Napthalene		3	15
MSP4	CSA	0.1	3	Sulfonated Napthalene		4	17
MSPP	CSA	0.1	0.5	Polycarboxylate Ether		1.75	1
MSP2P	CSA	0.1	1	Polycarboxylate Ether		2.125	5
MSP3P	CSA	0.1	1.5	Polycarboxylate Ether		3	7
MSP4P	CSA	0.1	2	Polycarboxylate Ether		4.25	11
0.25SF	CSA	0.1	2	Sulfonated Napthalene	0.25% 3.6mm Short Steel Fibers	3	15
0.5SF	CSA	0.1	2	Sulfonated Napthalene	0.5% 3.6mm Short Steel Fibers	3	15
1SF	CSA	0.1	2	Sulfonated Napthalene	1% 3.6mm Short Steel Fibers	3	15
2SF	CSA	0.1	2	Sulfonated Napthalene	2% 3.6mm Short Steel Fibers	3	15
3SF	CSA	0.1	2	Sulfonated Napthalene	3% 3.6mm Short Steel Fibers	3	15
5SF	CSA	0.1	2	Sulfonated Napthalene	5% 3.6mm Short Steel Fibers	2.875	15
0.25BF	CSA	0.1	2	Sulfonated Napthalene	0.25% 6mm Brass Coated Steel Fibers	3	15
0.5BF	CSA	0.1	2	Sulfonated Napthalene	0.5% 6mm Brass Coated Steel Fibers	3	15
1BF	CSA	0.1	2	Sulfonated Napthalene	1% 6mm Brass Coated Steel Fibers	3	15
2BF	CSA	0.1	2	Sulfonated Napthalene	2% 6mm Brass Coated Steel Fibers	3	15
3BF	CSA	0.1	2	Sulfonated Napthalene	3% 6mm Brass Coated Steel Fibers	3	15
5BF	CSA	0.1	2	Sulfonated Napthalene	5% 6mm Brass Coated Steel Fibers	2.875	15
0.25LBF	CSA	0.1	2	Sulfonated Napthalene	0.25% 13mm Brass Coated Steel Fibers	3	15
0.5LBF	CSA	0.1	2	Sulfonated Napthalene	0.5% 13mm Brass Coated Steel Fibers	3	15
1LBF	CSA	0.1	2	Sulfonated Napthalene	1% 13mm Brass Coated Steel Fibers	2.875	15
2LBF	CSA	0.1	2	Sulfonated Napthalene	2% 13mm Brass Coated Steel Fibers	2.875	15
3LBF	CSA	0.1	2	Sulfonated Napthalene	3% 13mm Brass Coated Steel Fibers	2.75	15
5LBF	CSA	0.1	2	Sulfonated Napthalene	5% 13mm Brass Coated Steel Fibers	2.625	15

0.25CF	CSA	0.1	2	Sulfonated Napthalene	0.25% 6mm Short Carbon Fibers	3	15
0.5CF	CSA	0.1	2	Sulfonated Napthalene	0.5% 6mm Short Carbon Fibers	2.75	15
1CF	CSA	0.1	2	Sulfonated Napthalene	1% 6mm Short Carbon Fibers	2.5	15
2CF	CSA	0.1	2	Sulfonated Napthalene	2% 6mm Short Carbon Fibers	2.25	15
3CF	CSA	0.1	2	Sulfonated Napthalene	3% 6mm Short Carbon Fibers	1.875	15
5CF	CSA	0.1	2	Sulfonated Napthalene	5% 6mm Short Carbon Fibers	1.5	15
0.25SF2	CSA	0.1	2	Sulfonated Napthalene	0.25% Double Hooked 30mm Steel Fibers - 2% 3.6mm Short Steel Fibers	3	15
0.5SF2	CSA	0.1	2	Sulfonated Napthalene	0.5% Double Hooked 30mm Steel Fibers - 2% 3.6mm Short Steel Fibers	3	15
1SF2	CSA	0.1	2	Sulfonated Napthalene	1% Double Hooked 30mm Steel Fibers - 2% 3.6mm Short Steel Fibers	3	15
2SF2	CSA	0.1	2	Sulfonated Napthalene	2% Double Hooked 30mm Steel Fibers - 2% 3.6mm Short Steel Fibers	3	15
3SF2	CSA	0.1	2	Sulfonated Napthalene	3% Double Hooked 30mm Steel Fibers - 2% 3.6mm Short Steel Fibers	2.75	15
5SF2	CSA	0.1	2	Sulfonated Napthalene	5% Double Hooked 30mm Steel Fibers - 2% 3.6mm Short Steel Fibers	2.5	15
0.25PSF2	CSA	0.1	2	Sulfonated Napthalene	0.25% Straight 50mm Polypropylene Fibers - 2% 3.6mm Short Steel Fibers	3	15
0.5PSF2	CSA	0.1	2	Sulfonated Napthalene	0.5% Straight 50mm Polypropylene Fibers - 2% 3.6mm Short Steel Fibers	2.75	15
1PSF2	CSA	0.1	2	Sulfonated Napthalene	1% Straight 50mm Polypropylene Fibers - 2% 3.6mm Short Steel Fibers	2.75	15
2PSF2	CSA	0.1	2	Sulfonated Napthalene	2% Straight 50mm Polypropylene Fibers - 2% 3.6mm Short Steel Fibers	2.625	15
3PSF2	CSA	0.1	2	Sulfonated Napthalene	3% Straight 50mm Polypropylene Fibers - 2% 3.6mm Short Steel Fibers	2.5	15
5PSF2	CSA	0.1	2	Sulfonated Napthalene	5% Straight 50mm Polypropylene Fibers - 2% 3.6mm Short Steel Fibers	2.5	15
2SF2_25G	CSA	0.1	2	Sulfonated Napthalene	2% Double Hooked 30mm Steel Fibers - 2% 3.6mm Short Steel Fibers - 25% Pea Gravel	2.75	15
2SF2_50G	CSA	0.1	2	Sulfonated Napthalene	2% Double Hooked 30mm Steel Fibers - 2% 3.6mm Short Steel	2.625	15

					Fibers - 50% Pea Gravel		
QM	Modified Portland	0.158	0	N/A	Effective Water to Cement ratio to hydrate and mix cement	1.5	1
QM2	Modified Portland	0.17	0	N/A	Manufacturer Plastic Recommendation	1.5	3
QM3	Modified Portland	0.21	0	N/A	Manufacturer Flowable Recommendation	2	
QM4	Modified Portland	0.24	0	N/A	Manufacturer Fluid Flow Recommendation	4	6
QMSP	Modified Portland	0.158	0.5	Sulfonated Napthalene		1.625	4
QMSP2	Modified Portland	0.158	1	Sulfonated Napthalene		2	6
QMSP3	Modified Portland	0.158	2	Sulfonated Napthalene		3	15
QMSP4	Modified Portland	0.158	3	Sulfonated Napthalene		4.5	16
QMSPPP	Modified Portland	0.158	0.5	Polycarboxylate Ether		1.625	3
QMSP2P	Modified Portland	0.158	1	Polycarboxylate Ether		2.25	5
QMSP3P	Modified Portland	0.158	1.5	Polycarboxylate Ether		3.125	7
QMSP4P	Modified Portland	0.158	2	Polycarboxylate Ether		4.5	11
Q0.25SF	Modified Portland	0.158	2	Sulfonated Napthalene	0.25% 3.6mm Short Steel Fibers	3	15
Q0.5SF	Modified Portland	0.158	2	Sulfonated Napthalene	0.5% 3.6mm Short Steel Fibers	3	15
Q1SF	Modified Portland	0.158	2	Sulfonated Napthalene	1% 3.6mm Short Steel Fibers	3	15
Q2SF	Modified Portland	0.158	2	Sulfonated Napthalene	2% 3.6mm Short Steel Fibers	3	15
Q3SF	Modified Portland	0.158	2	Sulfonated Napthalene	3% 3.6mm Short Steel Fibers	3	15
Q5SF	Modified Portland	0.158	2	Sulfonated Napthalene	5% 3.6mm Short Steel Fibers	3	15
Q0.25BF	Modified Portland	0.158	2	Sulfonated Napthalene	0.25% 6mm Brass Coated Steel Fibers	3	15
Q0.5BF	Modified Portland	0.158	2	Sulfonated Napthalene	0.5% 6mm Brass Coated Steel Fibers	3	15
Q1BF	Modified Portland	0.158	2	Sulfonated Napthalene	1% 6mm Brass Coated Steel Fibers	3	15
Q2BF	Modified Portland	0.158	2	Sulfonated Napthalene	2% 6mm Brass Coated Steel Fibers	3	15
Q3BF	Modified Portland	0.158	2	Sulfonated Napthalene	3% 6mm Brass Coated Steel Fibers	3	15
Q5BF	Modified Portland	0.158	2	Sulfonated Napthalene	5% 6mm Brass Coated Steel Fibers	3	15
Q0.25LBF	Modified Portland	0.158	2	Sulfonated Napthalene	0.25% 13mm Brass Coated Steel Fibers	3	15
Q0.5LBF	Modified Portland	0.158	2	Sulfonated Napthalene	0.5% 13mm Brass Coated Steel Fibers	3	15
Q1LBF	Modified Portland	0.158	2	Sulfonated Napthalene	1% 13mm Brass Coated Steel Fibers	2.875	15
Q2LBF	Modified Portland	0.158	2	Sulfonated Napthalene	2% 13mm Brass Coated Steel Fibers	2.875	15
Q3LBF	Modified Portland	0.158	2	Sulfonated Napthalene	3% 13mm Brass Coated Steel Fibers	2.75	15
Q5LBF	Modified Portland	0.158	2	Sulfonated Napthalene	5% 13mm Brass Coated Steel Fibers	2.75	15
Q0.25CF	Modified Portland	0.158	2	Sulfonated Napthalene	0.25% 6mm Short Carbon Fibers	3	15
Q0.5CF	Modified Portland	0.158	2	Sulfonated Napthalene	0.5% 6mm Short Carbon Fibers	3	15

Q1CF	Modified Portland	0.158	2	Sulfonated Napthalene	1% 6mm Short Carbon Fibers	2.875	15
Q2CF	Modified Portland	0.158	2	Sulfonated Napthalene	2% 6mm Short Carbon Fibers	2.5	15
Q3CF	Modified Portland	0.158	2	Sulfonated Napthalene	3% 6mm Short Carbon Fibers	1.75	15
Q5CF	Modified Portland	0.158	2	Sulfonated Napthalene	5% 6mm Short Carbon Fibers	1.5	15
Q0.25SF2	Modified Portland	0.158	2	Sulfonated Napthalene	0.25% Double Hooked 30mm Steel Fibers - 2% 3.6mm Short Steel Fibers	3	15
Q0.5SF2	Modified Portland	0.158	2	Sulfonated Napthalene	0.5% Double Hooked 30mm Steel Fibers - 2% 3.6mm Short Steel Fibers	3	15
Q1SF2	Modified Portland	0.158	2	Sulfonated Napthalene	1% Double Hooked 30mm Steel Fibers - 2% 3.6mm Short Steel Fibers	3	15
Q2SF2	Modified Portland	0.158	2	Sulfonated Napthalene	2% Double Hooked 30mm Steel Fibers - 2% 3.6mm Short Steel Fibers	3	15
Q3SF2	Modified Portland	0.158	2	Sulfonated Napthalene	3% Double Hooked 30mm Steel Fibers - 2% 3.6mm Short Steel Fibers	3	15
Q5SF2	Modified Portland	0.158	2	Sulfonated Napthalene	5% Double Hooked 30mm Steel Fibers - 2% 3.6mm Short Steel Fibers	3	15
Q0.25PSF2	Modified Portland	0.158	2	Sulfonated Napthalene	0.25% Straight 50mm Polypropylene Fibers - 2% 3.6mm Short Steel Fibers	3	15
Q0.5PSF2	Modified Portland	0.158	2	Sulfonated Napthalene	0.5% Straight 50mm Polypropylene Fibers - 2% 3.6mm Short Steel Fibers	3	15
Q1PSF2	Modified Portland	0.158	2	Sulfonated Napthalene	1% Straight 50mm Polypropylene Fibers - 2% 3.6mm Short Steel Fibers	3	15
Q2PSF2	Modified Portland	0.158	2	Sulfonated Napthalene	2% Straight 50mm Polypropylene Fibers - 2% 3.6mm Short Steel Fibers	2.75	15
Q3PSF2	Modified Portland	0.158	2	Sulfonated Napthalene	3% Straight 50mm Polypropylene Fibers - 2% 3.6mm Short Steel Fibers	2.5	15
Q5PSF2	Modified Portland	0.158	2	Sulfonated Napthalene	5% Straight 50mm Polypropylene Fibers - 2% 3.6mm Short Steel Fibers	2.5	15

Table 3.2 – Flowability and Workability Trial Results

3.2.11 Flowability and Workability Trial Results for CSA Cement Formulations

Initially four different water to cement ratios were tested. The first three were the manufacturers recommendation for fluid flow ($W/c = 0.19$), manufacturers

recommendation for flowable ($W/c = 0.152$) and the manufactures recommendation for plastic ($W/c = 0.11$). To determine if it was possible to reach a water to cement ratio that would still hydrate the CSA rapid set particles, a trial and error process was used to determine the minimum water requirement. It was found that the lowest possible water to cement ratio that could effectively hydrate the CSA cement and still be mixed with a power drill paddle mixer was 0.1. The water to cement ratio of 0.1, produced a very stiff matrix, that was not flowable and had a very short workability, but it satisfactorily hydrated the CSA cement particles. To produce fluidity, both sulfonated naphthalene and polycarboxylate ether super plasticizers were investigated to determine their effects on the composition. The polycarboxylate ether and sulphate naphthalene super plasticizers produce satisfactory flowability results. Polycarboxylate ether based super plasticizer could produce the same flow result as the sulphate naphthalene super plasticizer but at a lower concentration (1.5% by weight for the polycarboxylate ether based super plasticizer as compared to 2% by weight for the sulphate naphthalene based super plasticizer). The main advantage of the sulphate naphthalene based super plasticizer was the longer workability time than the polycarboxylate ether based super plasticizer. From this result it was determined to further pursue the sulphate naphthalene based super plasticizer as it provided a longer flowability and workability interval.

The 3.6 millimeter steel fibers, 6 millimeter brass coated steel fibers, 13 millimeter brass coated fibers seemed to not inhibit the flow of the CSA cement. When mixing the formulations, the 3.6 millimeter steel fibers performed better at being added to the formulation, mixed and maintained the fiber matrix (no segregation). The 6 millimeter carbon fibers were able to be added in concentrations up to one percent by weight, and it

was determined that the carbon fibers needed to be dry mixed into the CSA cement before any addition of water, as once the composition was wet, the carbon fibers would clump together if added after the water. Dry mixing the carbon fibers before the water was added help prevent the clumping. The addition of the 30 millimeter steel double hooked fibers were easily applied and flowable up to a three percent by weight concentration. The five percent by weight concentration of 30 millimeter steel double hooked fibers would clump together and not effectively disperse. The 50 millimeter polypropylene fibers clumped together at the lowest concentrations, and were difficult to disperse. Due to this, the compositions containing polypropylene fibers were determined to not meet the requirements of the research objective and removed from consideration.

The addition of peagravel was determined to produce an effective flowability up to 50 percent by weight and did not have an effect on the workability time. For every 25 percent by weight addition of peagravel, did reduce the flowability measurement by about ½ inch.

3.2.12 Flowability and Workability Trial Results for Modified Portland Cement Formulations

Initially four different water to cement ratios were tested for the modified Portland cement formulations. The first three were the manufacturers recommendation for fluid flow ($W/c = 0.24$), manufacturers recommendation for flowable ($W/c = 0.21$) and the manufactures recommendation for plastic ($W/c = 0.17$). To determine if it was possible to reach a water to cement ratio that would still hydrate the modified portland cement particles, a trial and error process was used to determine the minimum water requirement.

It was found that the lowest possible water to cement ratio that could effectively hydrate the modified portland cement particles and still be mixed with a power drill paddle mixer was 0.158. The water to cement ratio of 0.158, produced a very stiff matrix, that was not flowable and had a very short workability, but it satisfactorily hydrated the modified portland cement particles. To produce fluidity, both sulfonated naphthalene and polycarboxylate ether super plasticizers were investigated to determine their effects on the composition. The polycarboxylate ether and sulphate naphthalene super plasticizers produce satisfactory flowability results. Polycarboxylate ether based super plasticizer could produce the same flow result as the sulphate naphthalene super plasticizer but at a lower concentration (2% by weight for the polycarboxylate ether based super plasticizer as compared to 3% by weight for the sulphate naphthalene based super plasticizer). The main advantage of the sulphate naphthalene based super plasticizer was the longer workability time than the polycarboxylate ether based super plasticizer. From this result it was determined to further pursue the sulphate naphthalene based super plasticizer as it met the required flowability and workability specifications.

The 3.6 millimeter steel fibers, 6 millimeter brass coated steel fibers, 13 millimeter brass coated fibers seemed to not inhibit the flow of the modified portland cement. When mixing the formulations, the 3.6 millimeter steel fibers performed better at being added to the formulation, mixed and maintained the fiber matrix (no segregation). The 6 millimeter carbon fibers were able to be added in concentrations up to one percent by weight, and it was determined that the carbon fibers needed to be dry mixed into the modified portland cement before any addition of water, as once the composition was wet, the carbon fibers would clump together if added after the water. Dry mixing the carbon

fibers before the water was added help prevent the clumping. The addition of the 30 millimeter steel double hooked fibers were easily applied and flowable up to a three percent by weight concentration. The five percent by weight concentration of 30 millimeter steel double hooked fibers would clump together and not effectively disperse. The 50 millimeter polypropylene fibers clumped together at the lowest concentrations, and were difficult to disperse. Due to this, the compositions containing polypropylene fibers were determined to not meet the requirements of the research objective and removed from consideration.

The addition of peagravel was determined to produce an effective flowability up to 50 percent by weight and did not have an effect on the workability time. For every 25 percent by weight addition of peagravel, did reduce the flowability measurement by about $\frac{3}{4}$ inch.

Table 3.3 shows the formulations that passed the initial flowability and workability tests that were then casted into drying free shrinkage samples.

Formulations Meeting Minimum Flowability and Workability Requirements	
CSA Cement	Modified Portland Cement
M4	QMSP3
MSP3	QMSP4
MSP4	Q0.25SF
0.25SF	Q0.5SF
0.5SF	Q1SF
1SF	Q2SF
2SF	Q3SF
3SF	Q5SF
5SF	Q0.25BF

0.25BF	Q0.5BF
0.5BF	Q1BF
1BF	Q2BF
2BF	Q3BF
3BF	Q5BF
5BF	Q0.25LBF
0.25LBF	Q0.5LBF
0.5LBF	Q1LBF
1LBF	Q2LBF
2LBF	Q3LBF
3LBF	Q5LBF
5LBF	Q0.25CF
0.25CF	Q0.5CF
0.5CF	Q1CF
1CF	Q2CF
2CF	Q3CF
3CF	Q5CF
0.25SF2	Q0.25SF2
0.5SF2	Q0.5SF2
1SF2	Q1SF2
2SF2	Q2SF2
3SF2	Q3SF2
5SF2	Q5SF2
2SF2_25G	Q2SF2_25G
2SF2_50G	Q2SF2_50G

Table 3.3 – Passing Rapid Set Formulations

3.2.13 Drying Free Shrinkage Trials

For each formulation that passed the initial flowability and workability requirements, drying free shrinkage specimens were made. Dry free shrinkage specimens were fabricated and shrinkage was determined by following the ASTM C490 Standard Practice

for Use of Apparatus for the Determination of Length Change of Hardened Cement Paste, Mortar, and Concrete. For initial readings each passing formulation was casted into 2 - 1 inch by 1 inch by 11 ¼ inch steel prism free shrinkage molds as per the specification outlined in ASTM C490. The shrinkage recordings were taken on a Humboldt Length Comparator, and were dry cured in the Civil Engineering Laboratory. Shrinkage recordings were taken at 1 day, 3 days, 7 days, 21 days, 28 days. For formulations that remained below 300 microstrains at 28 days were then further investigated. Formulations that surpassed 300 microstrains were discarded. Figure 3.2 to 3.8 present the promising rapid set formulations that have a drying free shrinkage below 300 microstrains at twenty-eight days.

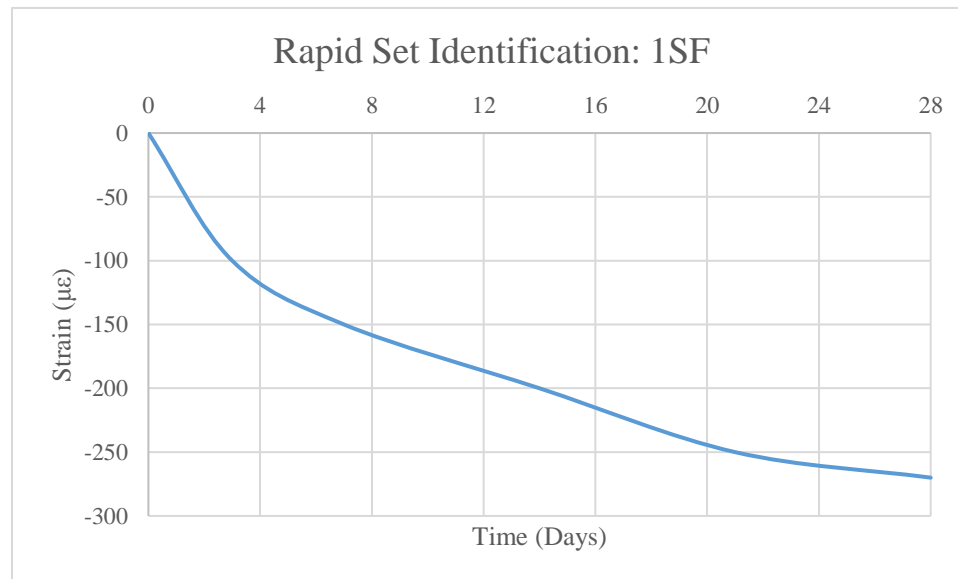


Figure 3.2 – Rapid Set Identification: 1SF

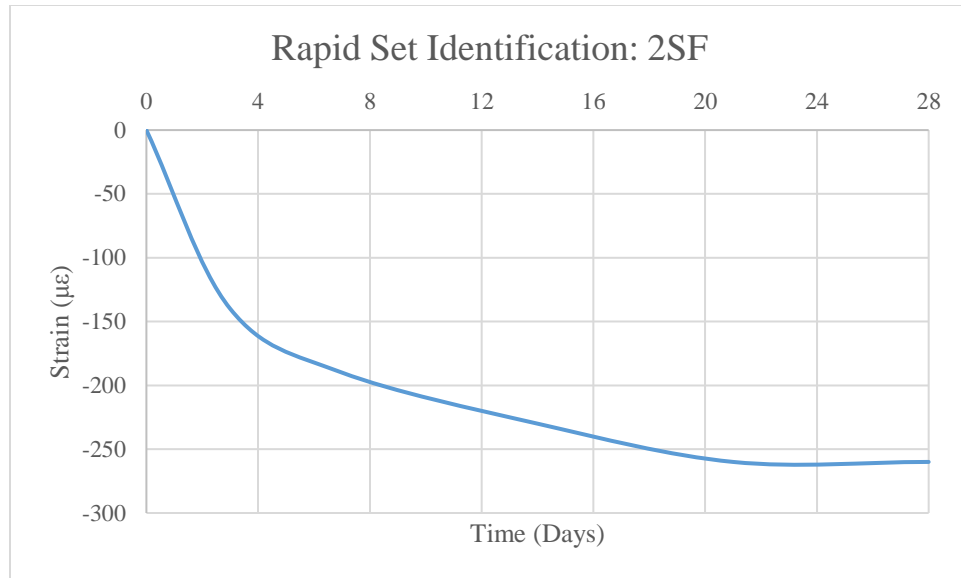


Figure 3.3 - Rapid Set Identification: 2SF

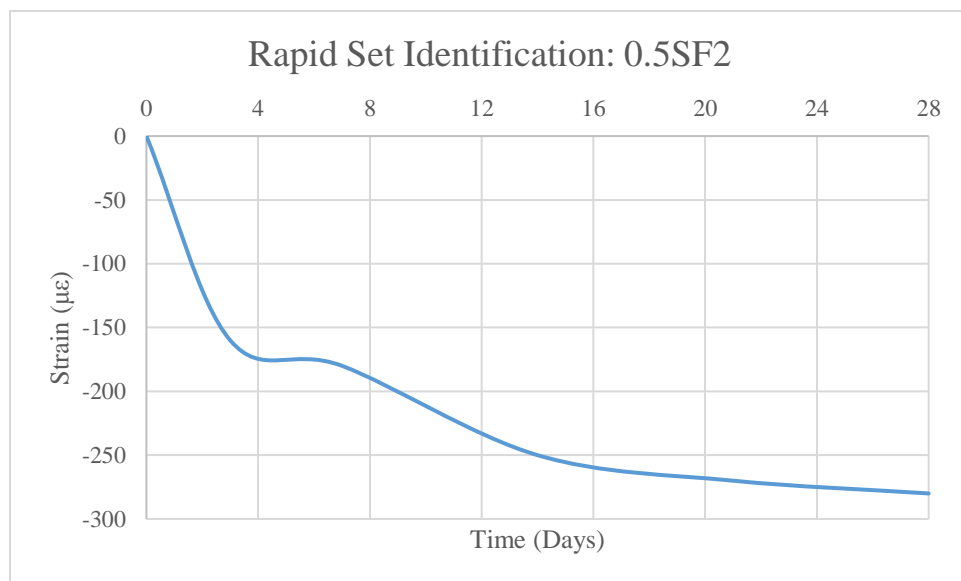


Figure 3.4 - Rapid Set Identification: 0.5SF2

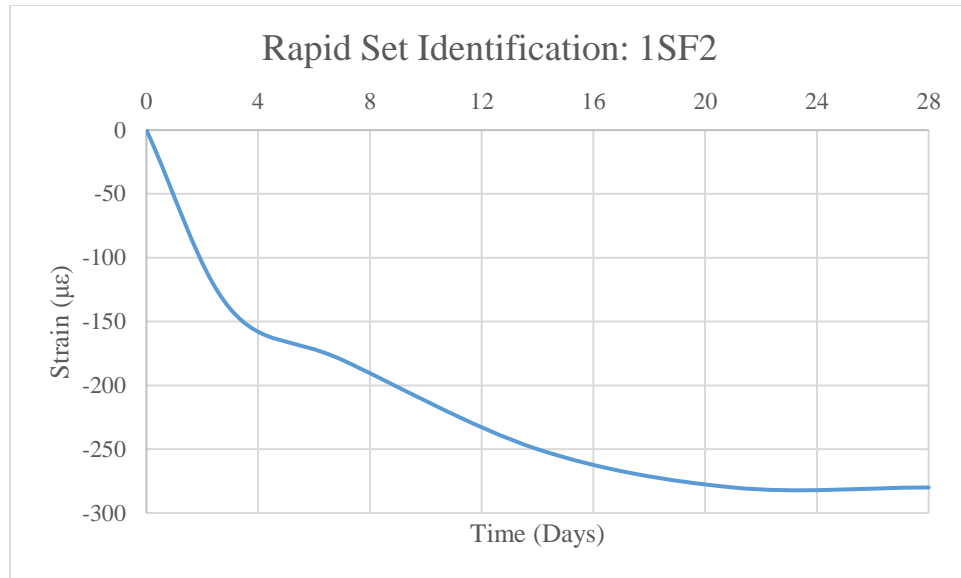


Figure 3.5 - Rapid Set Identification: 1SF2

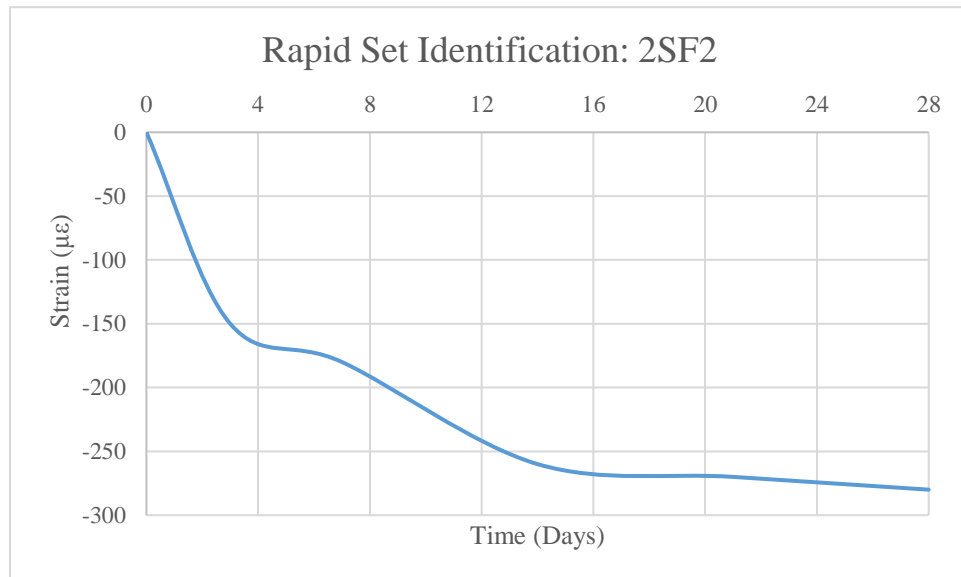


Figure 3.6 - Rapid Set Identification: 2SF2

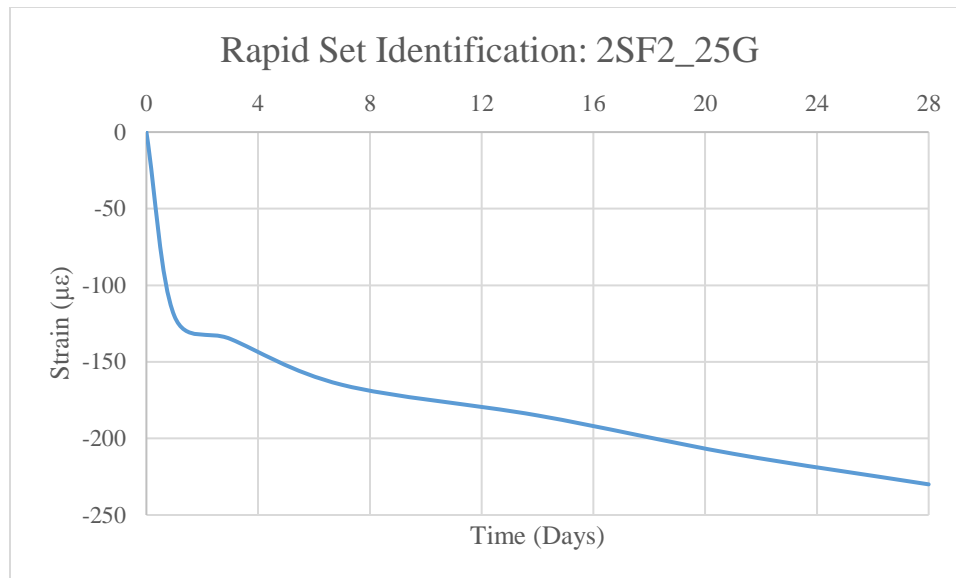


Figure 3.7 - Rapid Set Identification: 2SF_25G

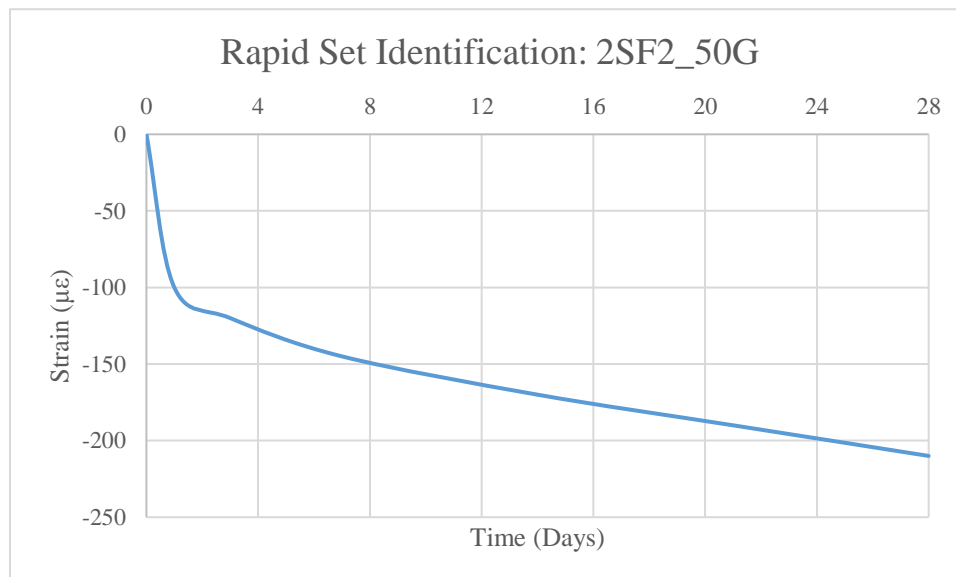


Figure 3.8 - Rapid Set Identification: 2SF2_50G

3.2.14 Drying Free Shrinkage Trial Observations and Analysis

After analyzing the results, the CSA cement performed much better than the modified Portland cement. The CSA cement formulations were able to achieve shrinkage strains as low as 230 microstrains at 28 days. The best performing modified Portland cement formulation achieved a shrinkage strain of 425 microstrains. Based on these initial results it was determined to no longer pursue a modified Portland cement formulation, and instead focus the investigation on further developing a CSA cement formulation.

From the initial drying free shrinkage results for the CSA cement, it can be seen that the addition of the 3.6 millimeter steel fibers with a concentration of 1 percent and 2 percent provided promising shrinkage restraint at 28 days. The addition of the 30 millimeter steel fibers had little differentiation of the shrinkage strains with a concentration below two percent by weight when added with the 3.6 millimeter steel fibers. The addition of 30 millimeter steel fibers at a 3 percent by weight concentration produced a shrinkage strain of 360 microstrains, determining that the maximum concentration of the 30 millimeter fibers is two percent by weight. The addition of the pea gravel further improved the low shrinkage characteristics of the rapid set material, with the addition of 50 percent by weight of pea gravel performing slightly better than the 25 percent by weight addition of pea gravel.

3.2.15 Compressive Strength Trials

For the formulations that passed the initial workability, flowability and drying free shrinkage assessments, the following step was to ensure that the formulations would reach a minimum compressive strength of 3000 psi at 3 hours after placement.

Compressive strength specimens were fabricated following the ASTM C39 Standard Strength of Cylindrical Concrete Specimens. The cylindrical specimens had a 3-inch diameter, 6-inch height and were casted in non-absorbent plastic cylindrical molds. The compressive strength testing was conducted on a Forney 250-kip compression machine at a rate of 250 lbs/s. Three cylinders were tested for each passing rapid set formulation.

3.2.14 Compressive Strength Trial Observations and Analysis

Table 3.4 displays each rapid set formulation and its measured compressive strength at 3 hours. The results show that all of the formulations supersede the minimum 3-hour compressive strength requirement of 3000 psi. Formulations 1SF, 2SF, 0.5SF2, 1SF2 and 2SF2 have very similar averages, with no large difference. Due to the addition of pea gravel formulations 2SF2_25G and 2SF2_50G have approximately a compressive strength increase of 900 psi compared to the other formulations.

Rapid Set Identification	3 Hour Compressive Strength (psi)
1SF	5807
2SF	5890
0.5SF2	5992
1SF2	5823
2SF2	5865
2SF2_25G	6529
2SF2_50G	6661

Table 3.4 – Compressive Strength at 3 Hours

3.2.16 Flexural Strength Trial

To determine the effective flexural strength of the formulations flexural specimens were fabricated by following ASTM standards and testing them to failure. Flexural specimens were fabricated with dimensions of 2 inch by 2 inch by 8 inch. These dimensions are used as they simulate common repair depths as compared to typical fiber reinforced concrete prisms that are 4 inch by 4 inch by 14 inch. Note that specimens with pea gravel; the size of the coarse aggregate in the composition is limited to 0.25 inches. The tests for flexure were executed by following the ASTM C78 Standard Test Method for Flexural Strength of Concrete (Using Simple Beam with Four-Point Loading). The tests were conducted on a 10 kip MTS Criterion Model 43, loaded at a rate of 150 lbs/min. Three flexural specimens were tested at 3 hours after placement.

3.2.17 Flexural Strength Trial Observations and Analysis

In total 21 flexural prisms were tested, three for each passing formulation. Table 3.5 shows the three-hour flexural modulus of rupture for each formulation. For each of the formulations the flexural strength is approximately the same.

Rapid Set Identification	Flexural Strength (psi)
1SF	803
2SF	809
0.5SF2	812
1SF2	818
2SF2	844
2SF2_25G	821
2SF2_50G	834

Table 3.5 – Three Hour Flexural Modulus of Rupture

Figure 3.9 shows the load vs. deflection graphs for each of the passing formulations. Each curve represents the average of three specimens.

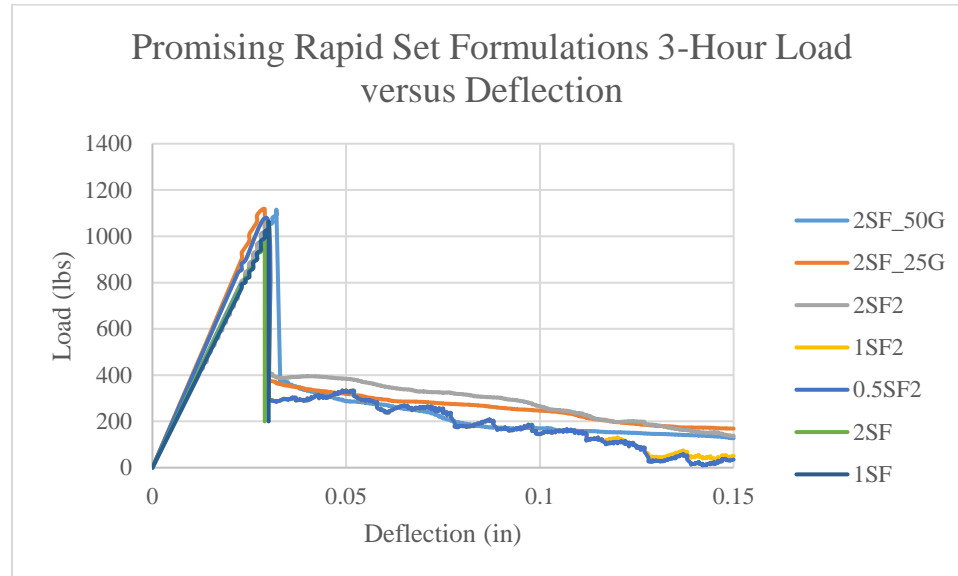


Figure 3.9 – Three Hour Load versus Deflection

From the analysis of Figure 3.9, it can be determined that the formulations with the 30 millimeter double hooked steel fibers provided ductility to the formulations. The formulations with the best performing flexural tests are 2SF2_50G, 2SF2_25G and 2SF2.

3.2.18 Selection of the Promising Rapid Set System (RSHPR)

Two formulations need to be selected as the promising rapid set system. The first system needs to be easily applied in field conditions and the second system must be easily pumped through a pumping apparatus (highly flowable). Based on the analysis of the flowability, workability, drying free shrinkage, compressive strength and flexural strength results, the selection for the promising rapid set system is the 2SF_50G formulation due to the better performing combination of low shrinkage, high early strength, durability and flexural properties. The selection for the promising pumpable

(highly flowable) formulation is 2SF due to the formulations low shrinkage, flowability, and high early strength.

3.3 Part 2: Mechanical Properties of the Promising Rapid Set System (RSHPR)

Compatibility (dimensional, chemical, electrochemical, and permeability) between repair material and existing substrate is one of the most critical components in the repair system (McDonald et. al., 2002). The mechanical properties of the promising Rapid Set High Performance Repair (RSHPR) formulations are tested to provide evidence that RSHPR provides a homogenous compatibility to concrete. The properties to be tested are compressive stress, tensile stress, modulus of elasticity, free drying shrinkage, restrained drying shrinkage and flexural parameters.

To provide uniform material preparation, ASTM standards were consulted and used when possible.

3.3.1 Compressive Strength

Compressive strength specimens were fabricated following the ASTM C39 Standard Strength of Cylindrical Concrete Specimens for both RSHPR and highly flowable RSHPR. The cylindrical specimens had a 3-inch diameter, 6-inch height and were casted in plastic cylindrical molds. The compressive strength testing was conducted on a Forney 250-kip compression machine at a rate of 250 lbs/s. The compressive strength specimens were tested at 3 hours, 24 hours, 1 day, 3 days, 7 days, 28 days, 56 days and 100 days after placement, six samples tested at each interval. The compressive stress was computed using the equation:

$$f'_c = \frac{P}{A} \quad (3.1)$$

Where:

f'_c = compressive stress of RSHPR (psi)

P = maximum compressive load on RSHPR (psi)

A = average cross sectional area of RSHPR cylinder (in²)

3.3.2 Compressive Strength Observations and Analysis

It is already known that the compressive strength surpasses the required 3000 psi within 3 hours. Figure 3.10 shows the compressive strength over time for RSHPR and highly flowable RSHPR. Figures 3.11 displays the compressive strength gain over time for RSHPR and very flowable RSHPR.

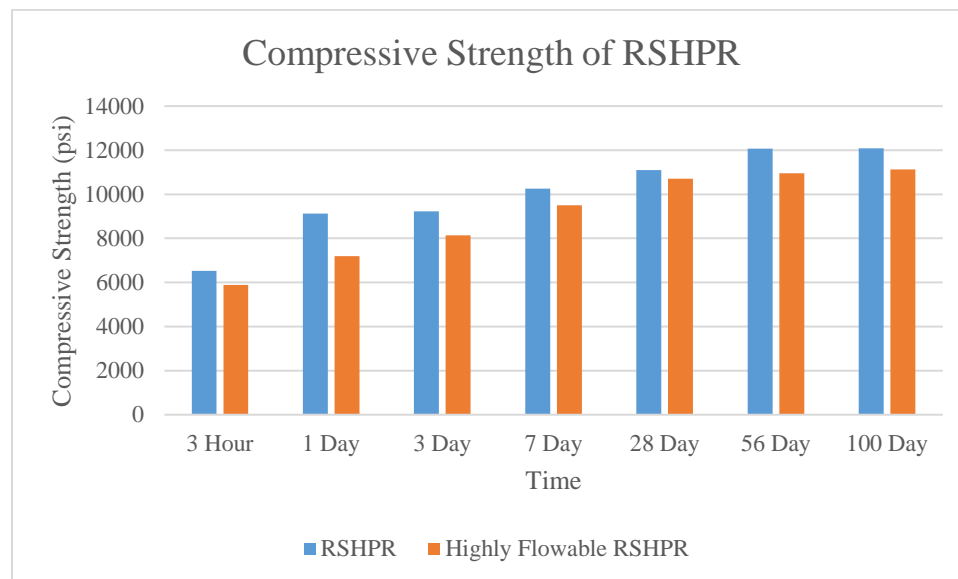


Figure 3.10 – Compressive Strength of the Promising Rapids Set Formulations

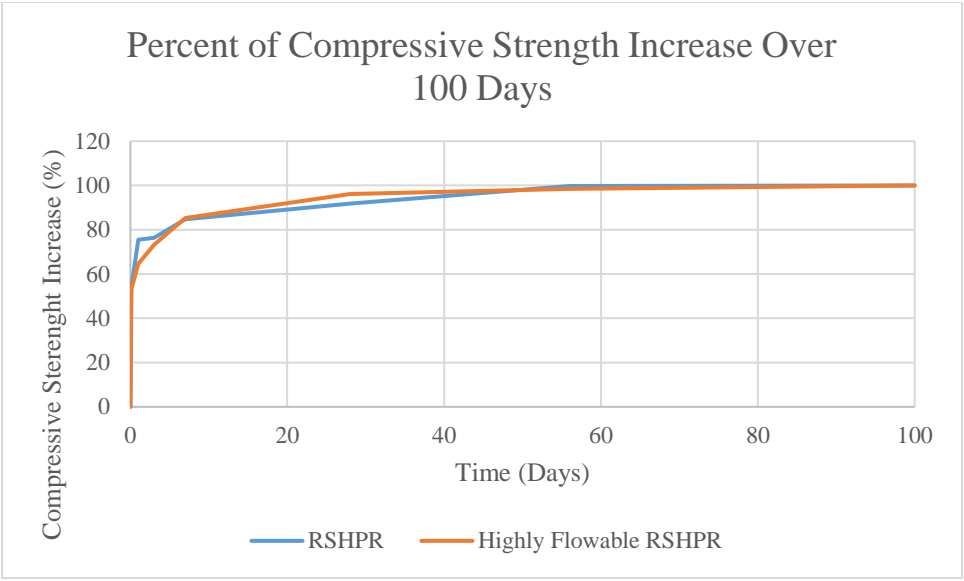


Figure 3.11 – Percent of Compressive Strength Increase Over 100 Days

The results show that RSHPR reaches a higher ultimate strength as compared to the highly flowable RSHPR. The two formulations have approximately the same compressive strength increase over time, interpreting that the pea gravel and fibers in RSHPR contribute to the higher compressive strength but does not affect the strength gain over time.



Figure 3.12 – RSHPR Compressive Specimen in the Forney 250-Kip Compression Machine

3.3.3 Free Drying Shrinkage

Dry free shrinkage specimens were fabricated and shrinkage was determined by following the ASTM C490 Standard Practice for Use of Apparatus for the Determination of Length Change of Hardened Cement Paste, Mortar, and Concrete. RSHPR was casted into 6 - 1 inch by 1 inch by 11 ¼ inch steel prism free shrinkage molds as per the specification outlined in ASTM C490. The shrinkage recordings were taken on a Humboldt Length Comparator, and were dry cured in the Civil Engineering Laboratory. Shrinkage recordings were taken at 1 day, 3 days, 7 days, 21 days, 28 days, 56 days, and 100 days.

For each reading, a steel reference bar reading was taken first. The reference bar is placed into the Humboldt Length Comparator, then rotated slowly through at least one

complete revolution while the gauge reading is being taken. The shortest gauge reading is recorded. The reference bar is then removed and the specimen is carefully placed into the Humboldt Length Comparator. The specimen is slowly rotated while the comparator readings is being taken. The minimum reading of the gauge is recorded. Specimens for comparator readings were placed into the measuring instrument with the same end up each time.

3.3.4 Free Drying Shrinkage Observations and Analysis

The shrinkage results show that it is possible to achieve and maintain a stabilized drying shrinkage strain less than 300 micro strains over a period of 100 days.

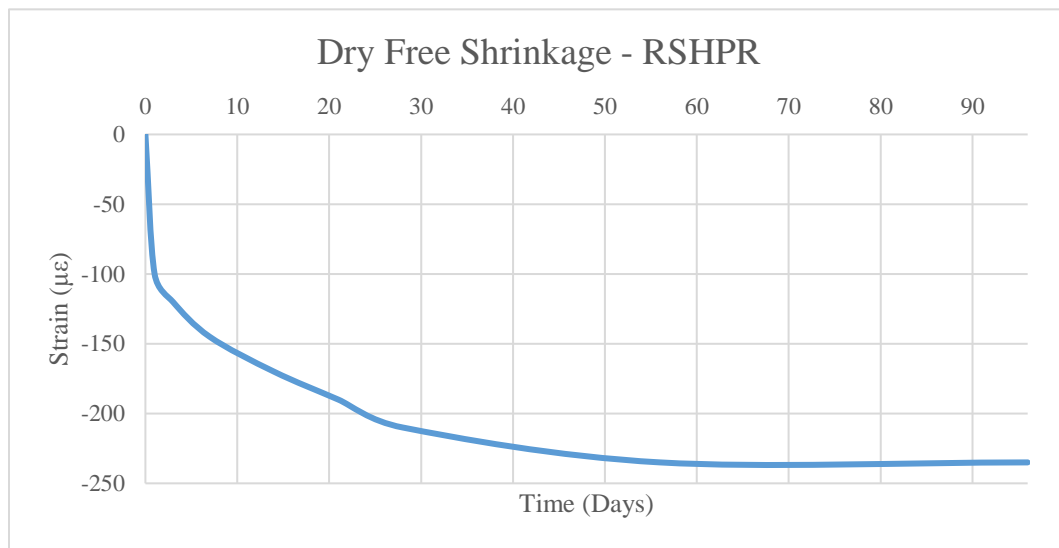


Figure 3.13 – RSHPR Dry Free Shrinkage

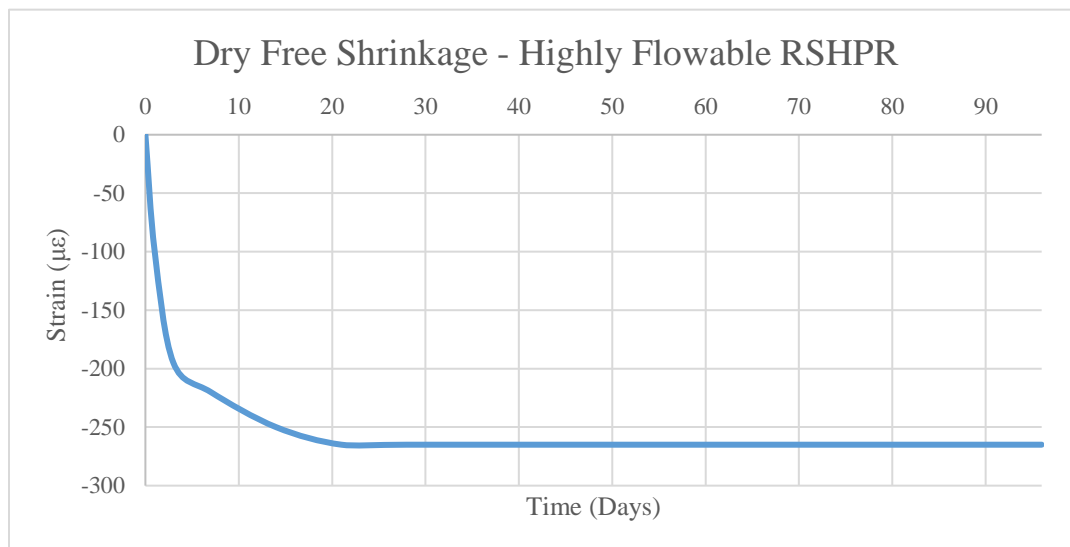


Figure 3.14 – Highly Flowable RSHPR Dry Free Shrinkage

RSHPR reaches its ultimate shrinkage strain of $-230\mu\epsilon$ at approximately 28 days. The highly flowable RSHPR reaches its ultimate shrinkage of $-260\mu\epsilon$ strain at approximately 28 days. Analysis of Figure 13 and 14 appears that the addition of pea gravel assisted the formulation to achieving an ultimate lower shrinkage strain. As shown in section 3.3.4, the compressive strength continually increased after 28 days, but shrinkage stabilized after 28 days. The interpretation is that the RSHPR had continually gained strength without shrinkage.

3.3.5 Splitting Tensile

RSHPR splitting tensile capacity specimens were fabricated and tested following ASTM C496 Splitting Tensile Strength of Cylindrical Concrete Specimens. The tests were performed on cylindrical specimens with a 3-inch diameter, 6-inch height using a Forney 1,000-kip compression machine at a rate of 700 lbs/min. The maximum applied load

indicated by the testing machine is recorded. Three splitting tensile test recordings were taken at 3 hours, 1 day, 3 days, 7 days, and 28 days after cylinder placement.

First the specimen was properly seated between the two loading plates. The load was then gradually increased until failure occurred. Figure GRAPH shows the average splitting tensile strength over 28 days for both RSHPR and highly flowable RSHPR. The splitting tensile strength was computed using the following equation:

$$f_t = \frac{2P}{3.14ld} \quad (3.2)$$

Where:

f_t = splitting tensile strength (psi)

P = maximum applied tensile load on the specimen (lbf)

l = length of RSHPR specimen (in)

d = diameter of concrete specimen (in)

3.3.6 Splitting Tensile Observations and Analysis

As the load continued to increase, the RSHPR specimens at some point would have a hairline fracture propagate, extending to both the upper and lower loading plates. At this point the load would drop, and at some point the load would again continue to increase until it reached its maximum load capacity. This is an indication of a strong bond and end anchorage between the macro fibers and the rapid set matrix. The splitting tensile

strength capacity increased by 43% from 3-hours to 28-days for both the RSHPR and highly flowable RSHPR.

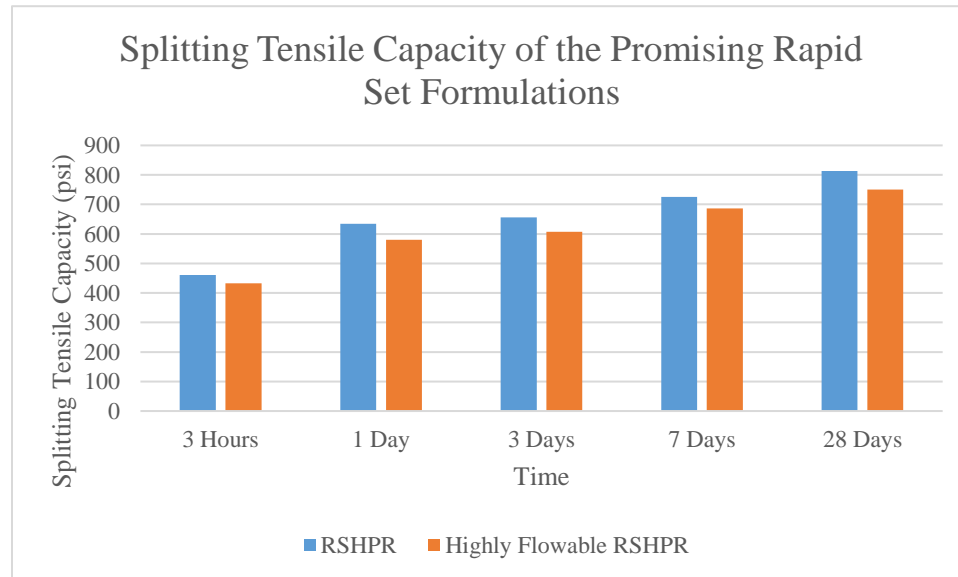


Figure 3.15 – Average Splitting Tensile Capacity

3.3.8 Modulus of Elasticity

Modulus of elasticity specimens were fabricated following ASTM C469 Static Elastic Modulus of Elasticity and Poisson's ratio of Concrete in Compression. A total of 15 – 4-inch diameter by 8 inch height concrete cylinders were fabricated for RSHPR and highly flowable RSHPR. A cage with a compressometer was attached to the cylinder which was then placed into a Forney 250 kip compression machine, loaded at a rate of 450 lb/sec, taking deflection recordings every 2000 lbs until reaching 40 percent of the compressive strength capacity of the concrete cylinder. Three cylinders were tested at 3 hours, 1 day, 3 days, 7 days, and 28 days after placement of the repair material. The deflection from the compressometer was computed using the following equation:

$$d = \frac{ge_r}{e_r + e_g} \quad (3.3)$$

Where:

d = total deformation of the specimen throughout the effective gauge length (μin)

g = gauge reading (μin)

e_r = the perpendicular distance measured to the nearest 0.01 in. from the pivot rod to the vertical plane passing through the two support points of the rotating yoke

e_g = the perpendicular distance, measured to the nearest 0.01 in. from the gauge to the vertical plane passing through the two support points of the rotating yoke

The modulus of elasticity was computed by graphing the stress versus strain curve, then calculating the slope.

The RSHPR and highly flowable RSHPR compressive modulus of elasticity results are presented in Figure 3.16.

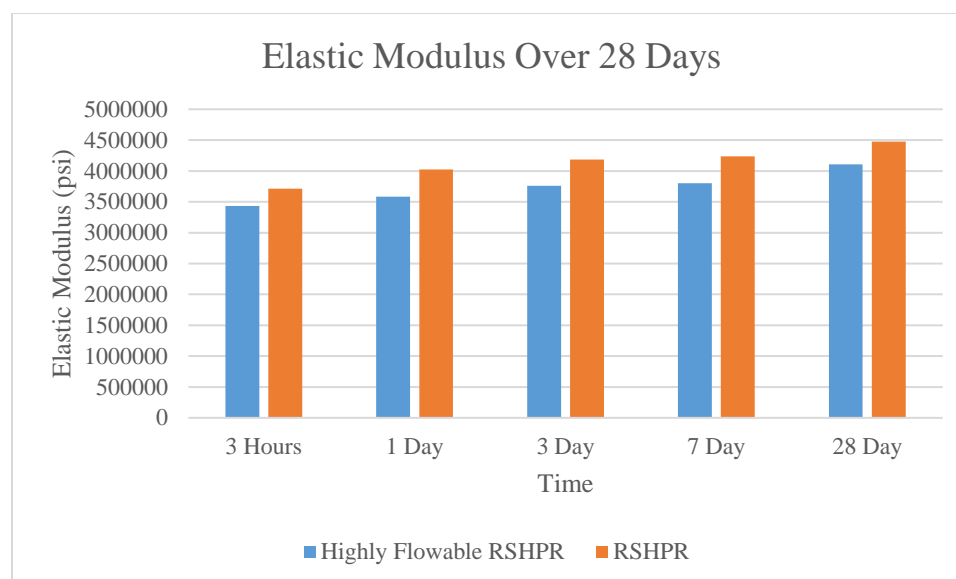


Figure 3.16 – Modulus of Elasticity

3.3.9 Modulus of Elasticity Observations and Analysis

It can be observed that RSHPR has a modulus of elasticity approximately 8.2% greater than the modulus of elasticity for the highly flowable RSHPR at 28 days. For both the modulus of elasticities are below 5000 ksi, providing evidence of RSHPR and highly flowable RSHPR low shrinkage characteristics.

3.3.10 Restrained Drying Shrinkage

Three RSHPR 14-inch inner diameter by 18-inch outer diameter by 2-inch-deep restrained drying shrinkage specimens were fabricated outside of 14-inch diameter, 6-inch-tall, ½ inch thick steel tube on top of a ¾ inch plywood base on February 13th, 2017. After 3 hours of the initial curing, the specimens were removed from their formwork, identified and were dry cured in the Civil Engineering Laboratory. The specimens are visually monitored daily to record any crack formation and propagation. Figure 3.17 shows the specimen when it was 3 hours after casting.



Figure 3.17 – Restrained Shrinkage Ring Sample

3.3.11 Restrained Drying Shrinkage Observations and Analysis

It is observed that there are no visible cracks in any of the specimens observed over a year after casting on Monday April 2nd, 2018. This can be interpreted that no significant shrinkage occurred to create a tensile stress large enough to cause visible cracking within the specimens.

3.3.12 Flexural Strength

Flexural specimens were fabricated by following ASTM standards and testing them to failure. Flexural specimens were fabricated with dimensions of 2 inch by 2 inch by 8 inch. These dimensions are used as they simulate common repair depths as compared to typical fiber reinforced concrete prisms that are 4 inch by 4 inch by 14 inch. Note that the size of the coarse aggregate in the composition is limited to 0.25 inches.

All 48 flexural specimens fabricated are self-compacting and did not require the use of a vibrator to consolidate the concrete. After 3 hours of the initial curing, the specimens

were removed from their formwork, identified and were dry cured in the Civil Engineering Laboratory.

The tests for flexure were executed by following the ASTM C78 Standard Test Method for Flexural Strength of Concrete (Using Simple Beam with Four-Point Loading). The tests were conducted on a 10 kip MTS Criterion Model 43, loaded at a rate of 150 lbs/min. The flexural specimens were tested at 3 hours, 24 hours, 1 day, 3 days, 7 days, 28 days, 56 days and 100 days after placement, six specimens at each interval.

To determine the flexural strength for each specimen, the following equation was used as follows:

$$f_r = \frac{PL}{bd^2} \quad (3.4)$$

Where:

f_r = Flexural Strength (psi)

P = maximum applied load indicated by the testing machine (lbf)

L = span length = 6 in

b = average width of specimen at the fracture = 2 in

d = average depth of specimen (in) at the fracture = 2 in

Table 3.6 shows the flexural strength for the specimens and figure 3.18 displays the load-deflection curve for RSHPR. Each curve represents the average of six specimens. Table 3.7 displays the flexural strength for the highly flowable RSHPR specimens and figure 3.19 displays the load-deflection curve for highly flowable RSHPR.

RSHPR Flexural Strength		
3 - Hour	Maximum Load (lbs):	Flexural Strength, f_r (psi)
Sample 1	1063	797
Sample 2	1079	809
Sample 3	1198	899
Sample 4	1113	835
Sample 5	1057	793
Sample 6	1094	821
	Average:	826
	Standard Deviation:	36
1 - Day	Maximum Load (lbs):	Flexural Strength, f_r (psi)
Sample 1	1115	836
Sample 2	1180	885
Sample 3	1704	1278
Sample 4	1165	874
Sample 5	1350	1013
Sample 6	1447	1085
	Average:	995
	Standard Deviation:	153
3 - Day	Maximum Load (lbs):	Flexural Strength, f_r (psi)
Sample 1	1349	1012
Sample 2	1514	1136
Sample 3	1442	1082
Sample 4	1654	1241
Sample 5	1592	1194
Sample 6	1433	1075
	Average:	1123
	Standard Deviation:	77
7 - Day	Maximum Load (lbs):	Flexural Strength, f_r (psi)
Sample 1	1474	1106
Sample 2	1380	1035
Sample 3	1317	988
Sample 4	1751	1313
Sample 5	1693	1270
Sample 6	1571	1178
	Average:	1148
	Standard Deviation:	118

28 - Day	Maximum Load (lbs):	Flexural Strength, f_r (psi)
Sample 1	1505	1129
Sample 2	1582	1187
Sample 3	1648	1236
Sample 4	1573	1180
Sample 5	1627	1220
Sample 6	1645	1234
	Average:	1198
	Standard Deviation:	38
56 - Day	Maximum Load (lbs):	Flexural Strength, f_r (psi)
Sample 1	1755	1316
Sample 2	1748	1311
Sample 3	1694	1271
Sample 4	1731	1298
Sample 5	1766	1325
Sample 6	1657	1243
	Average:	1294
	Standard Deviation:	29
100 - Day	Maximum Load (lbs):	Flexural Strength, f_r (psi)
Sample 1	1801	1351
Sample 2	1862	1397
Sample 3	1745	1309
Sample 4	1766	1325
Sample 5	1798	1349
Sample 6	1732	1299
	Average:	1338
	Standard Deviation:	32

Table 3.6 – RSHPR Specimen Flexural Strength

Highly Flowable RSHPR Flexural Strength		
3 - Hour	Maximum Load (lbs):	Flexural Strength, fr (psi)
Sample 1	1006	755
Sample 2	1108	831
Sample 3	1030	773
Sample 4	1061	796
Sample 5	1071	803
Sample 6	1075	806
	Average:	794
	Standard Deviation:	25
1 - Day	Maximum Load (lbs):	Flexural Strength, fr (psi)
Sample 1	1305	979
Sample 2	1215	911
Sample 3	1412	1059
Sample 4	1046	785
Sample 5	1395	1046
Sample 6	1496	1122
	Average:	984
	Standard Deviation:	111
3 - Day	Maximum Load (lbs):	Flexural Strength, fr (psi)
Sample 1	1414	1061
Sample 2	1494	1121
Sample 3	1463	1097
Sample 4	1516	1137
Sample 5	1432	1074
Sample 6	1521	1141
	Average:	1105
	Standard Deviation:	30
7 - Day	Maximum Load (lbs):	Flexural Strength, fr (psi)
Sample 1	1427	1070
Sample 2	1666	1250
Sample 3	1400	1050
Sample 4	1484	1113
Sample 5	1416	1062
Sample 6	1607	1205
	Average:	1125
	Standard Deviation:	76

28 - Day	Maximum Load (lbs):	Flexural Strength, fr (psi)
Sample 1	1446	1085
Sample 2	1518	1139
Sample 3	1560	1170
Sample 4	1551	1163
Sample 5	1611	1208
Sample 6	1599	1199
	Average:	1161
	Standard Deviation:	41
56 - Day	Maximum Load (lbs):	Flexural Strength, fr (psi)
Sample 1	1763	1322
Sample 2	1629	1222
Sample 3	1721	1291
Sample 4	1691	1268
Sample 5	1668	1251
Sample 6	1628	1221
	Average:	1263
	Standard Deviation:	36
100 - Day	Maximum Load (lbs):	Flexural Strength, fr (psi)
Sample 1	1783	1337
Sample 2	1751	1313
Sample 3	1714	1286
Sample 4	1759	1319
Sample 5	1775	1331
Sample 6	1709	1282
	Average:	1311
	Standard Deviation:	21

Table 3.7 – Highly Flowable RSHPR Specimen Flexural Strength

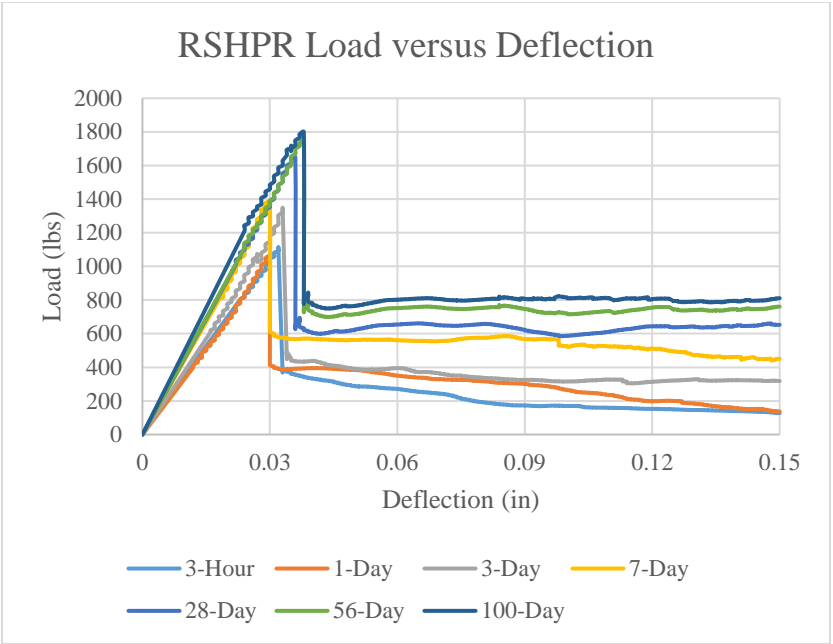


Figure 3.18 – RSHPR Load versus Deflection

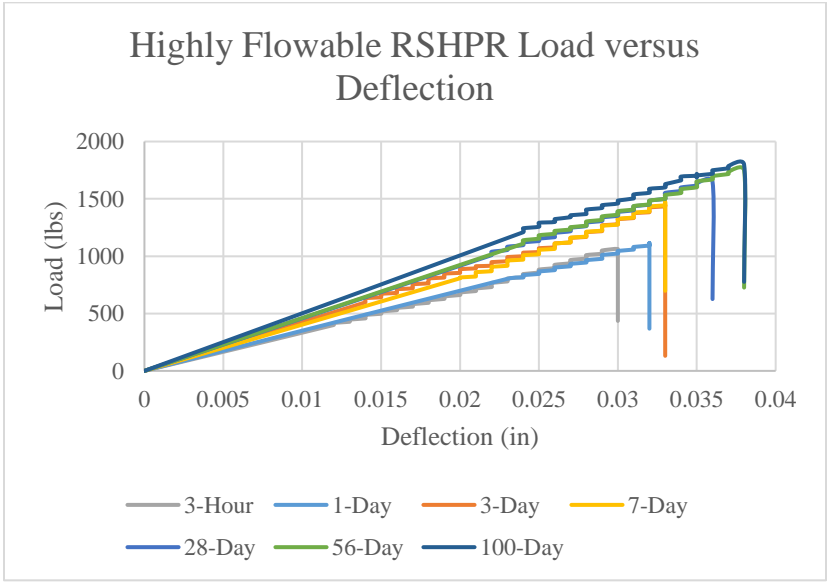


Figure 3.19 – Highly Flowable RSHPR Load versus Deflection

3.3.13 Flexural Strength Analysis and Observations

RSHPR specimens first cracked at the weakest section, rupture occurred and further curvature became concentrated at the failure plane in the fashion of a plastic hinge as shown in figure 3.20, with the steel fibers holding the two fractured pieces together although the concrete interface has completely disintegrated. This is an indication of good bond and end anchorage between the fibers and rapid set matrix. Fibers breaking in tension indicate that the bond of the fibers to the rapid set matrix is higher than the tensile strength of the fibers. The flexural strength increased by 38% from 3-hours to 100-days. Load at first crack was also the maximum load, since the specimens ruptured at first crack.



Figure 3.20 – Flexural Strength Fractured Specimen

The load continued to increase until a maximum was reached, usually the absolute maximum. The descending branch then began. The significance of an increase in

ductility over time can be seen from the load-deflection curves, indicating an increase in the absorption energy as described by the descending portion of the curve.

3.4 Tensile Strain Capacity of Fiber Reinforced Rapid Set Concrete

In the design of flexural concrete elements, it is commonly assumed that the compressive static modulus of elasticity is the same as the flexural elastic modulus of elasticity. This is apparent when calculating the curvature of an elastic concrete beam element using the Euler-Bernoulli Beam Theory, equation 3.5.

$$\frac{M}{\phi} = EI \quad (3.5)$$

Where:

M = Moment (in-kip)

ϕ = Curvature

E = Compressive Static Modulus of Elasticity

I = Moment of Inertia

In this equation, the assumption is that the compressive static modulus of elasticity is effectively the same as the flexural modulus of elasticity. After the beam passes its elastic region, the modulus of elasticity value remains the same, the standard calculation involves calculating a new moment of inertia based on the cracked section. This chapter investigates if the compressive modulus of elasticity is the same as the flexural modulus of elasticity of RSHPR, and determines the RSHPR cracking flexural strain capacity.

3.4.1 Test Set-Up

To determine the flexural modulus of elasticity, and cracking flexural strain capacity, four RSHPR flexural specimens were fabricated with dimensions of 2 inch by 2 inch by 8 inch. These dimensions are used as they simulate common repair depths as compared to typical fiber reinforced concrete prisms that are 4 inch by 4 inch by 14 inch. Note that the size of the coarse aggregate in the composition is limited to 0.25 inches.

All four flexural specimens fabricated are self-compacting and did not require the use of a vibrator to consolidate the concrete. After 3 hours of the initial curing, the specimens were removed from their formwork, identified and were dry cured in the Civil Engineering Laboratory. After 27 days of curing, a micro-measurement C2A-06-125LW-120 strain gauge was attached with M-Bond 200 adhesive to the maximum tensile fiber at mid span (Figure 3.21). The epoxy was given the manufacturers required time to cure.

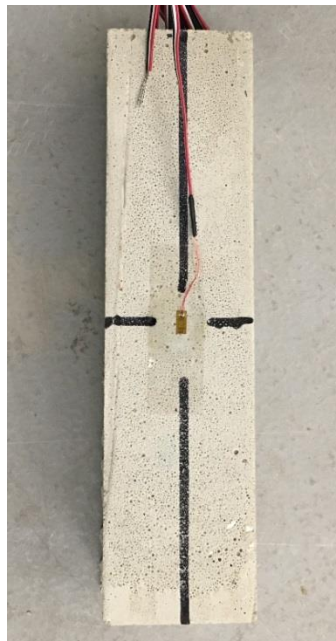


Figure 3.21 - C2A-06-125LW-120 Strain Gauge Attached to RSHPR Flexural Sample

The tests for flexure were executed by following the ASTM C78 Standard Test Method for Flexural Strength of Concrete (Using Simple Beam with Four-Point Loading). The tests were conducted on a 10 kip MTS Criterion Model 43, loaded at a rate of 150 lbs/min. Strain readings were recorded on a Vishay P3 Strain Indicator and Recorder box. The flexural specimens were tested at 28 days after placement. The specimens were loaded until they reached 1000 lbs, recording the strain at every 100 lbs.

To determine the flexural strength at each recorded interval for each specimen, the following equation was used as follows:

$$f_r = \frac{PL}{bd^2} \quad (3.6)$$

Where:

f_r = Flexural Strength (psi)

P = load indicated by the testing machine (lbf)

L = span length = 6 in

b = average width of specimen at the fracture = 2 in

d = average depth of specimen (in) at the fracture = 2 in

3.4.2 Test Results

Table 3.8, 3.9, 3.10, 3.11 show the corresponding load, deflection and strain recording for each sample. Table 3.12 shows the calculated flexural modulus of elasticity for each sample. Figures 3.22, 3.23, 3.24 and 3.25 show the flexural stress versus strain curves. Figures 3.26, 3.27, 3.28, 3.29 show the load versus deflection curves.

Sample 1		
Load (lbs):	Deflection (in):	Strain ($\mu\epsilon$):
0	0	0
100	0.001	25
200	0.002	45
300	0.006	98
400	0.008	129
500	0.01	153
600	0.013	183
700	0.015	206
800	0.017	236
900	0.019	262
1000	0.022	283

Table 3.8 - Sample 1 Load, Deflection & Strain Results

Sample 2		
Load (lbs):	Deflection (in):	Strain ($\mu\epsilon$):
0	0	0
100	0.001	25
200	0.002	43
300	0.006	99
400	0.008	124
500	0.01	149
600	0.013	177
700	0.015	207
800	0.017	231
900	0.018	243
1000	0.021	269

Table 3.9 – Sample 2 Load, Deflection & Strain Results

Sample 3		
Load (lbs):	Deflection (in):	Strain ($\mu\epsilon$):
0	0	0
100	0.001	26
200	0.003	48
300	0.007	103
400	0.009	128
500	0.011	154
600	0.013	186
700	0.015	208
800	0.017	223
900	0.019	234
1000	0.02	243

Table 3.10 – Sample 3 Load, Deflection & Strain Results

Sample 4		
Load (lbs):	Deflection (in):	Strain ($\mu\epsilon$):
0	0	0
100	0.001	18
200	0.003	45
300	0.005	69
400	0.008	98
500	0.01	123
600	0.014	158
700	0.017	190
800	0.019	212
900	0.021	262
1000	0.024	263

Table 3.11 – Sample 4 Load, Deflection & Strain Results

Sample:	Flexural Modulus of Elasticity (psi):
1	2549078
2	2643759
3	2510985
4	2780040
Average:	2620966
SD:	103788
COV:	0.0396

Table 3.12 – Flexural Modulus of Elasticity Results

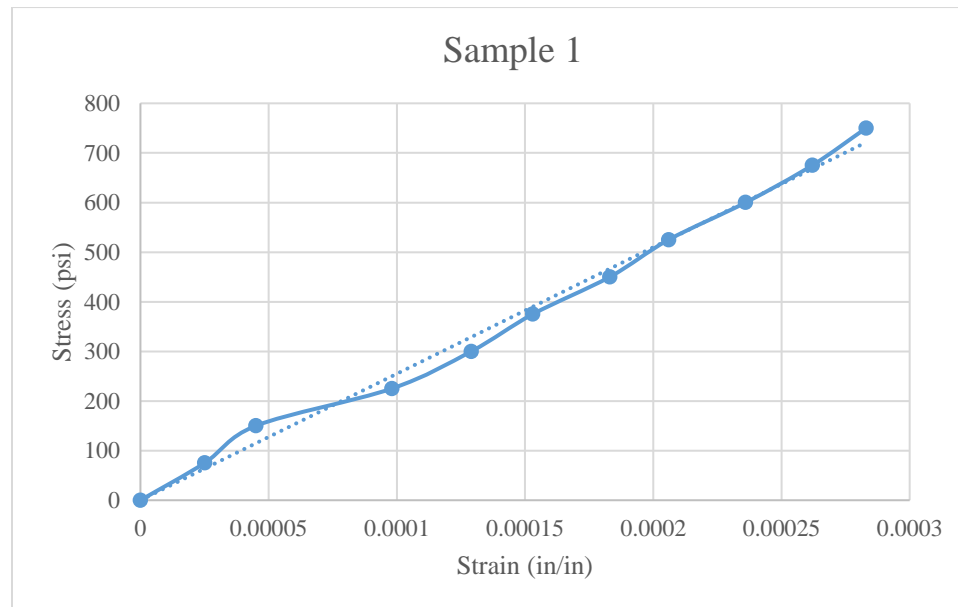


Figure 3.22 – Sample 1 Flexural Stress versus Strain

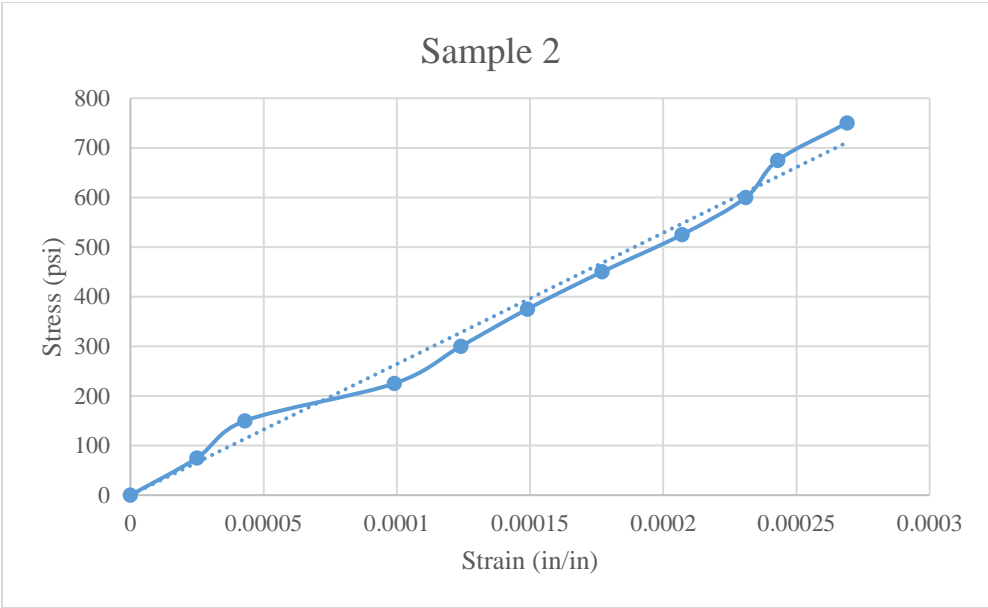


Figure 3.23 – Sample 2 Flexural Stress versus Strain

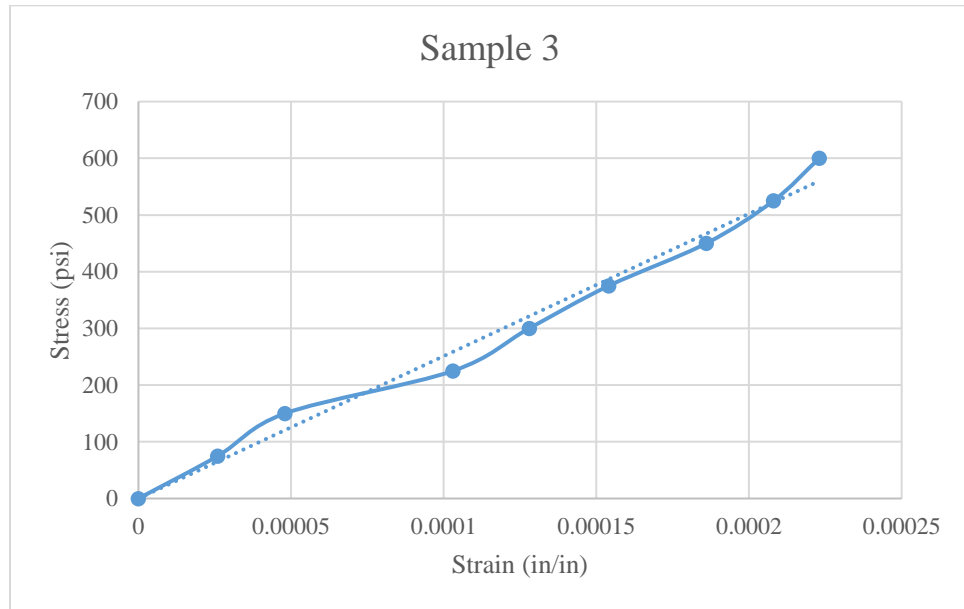


Figure 3.24 – Sample 3 Flexural Stress versus Strain

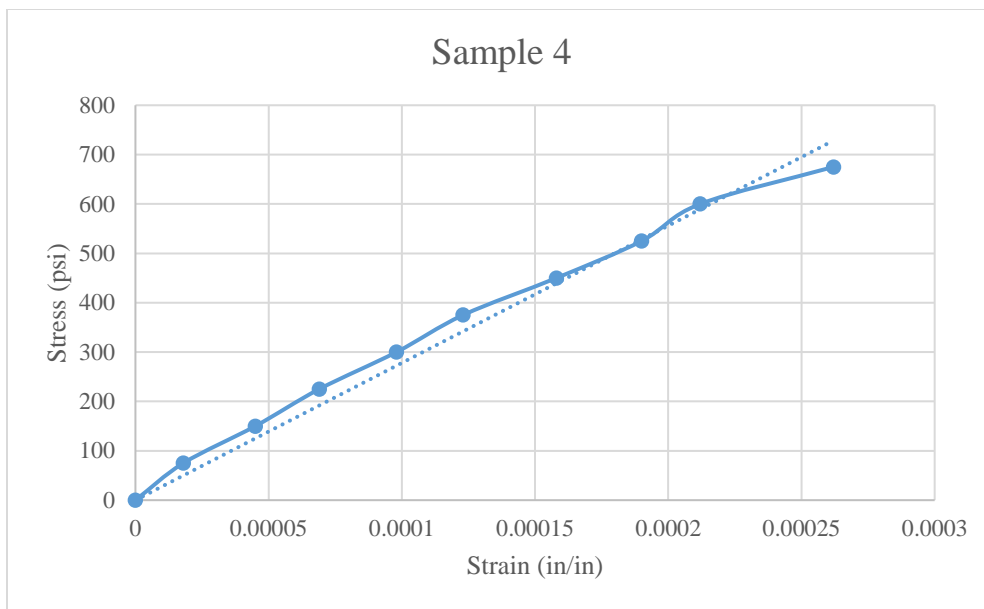


Figure 3.25 – Sample 4 Flexural Stress versus Strain

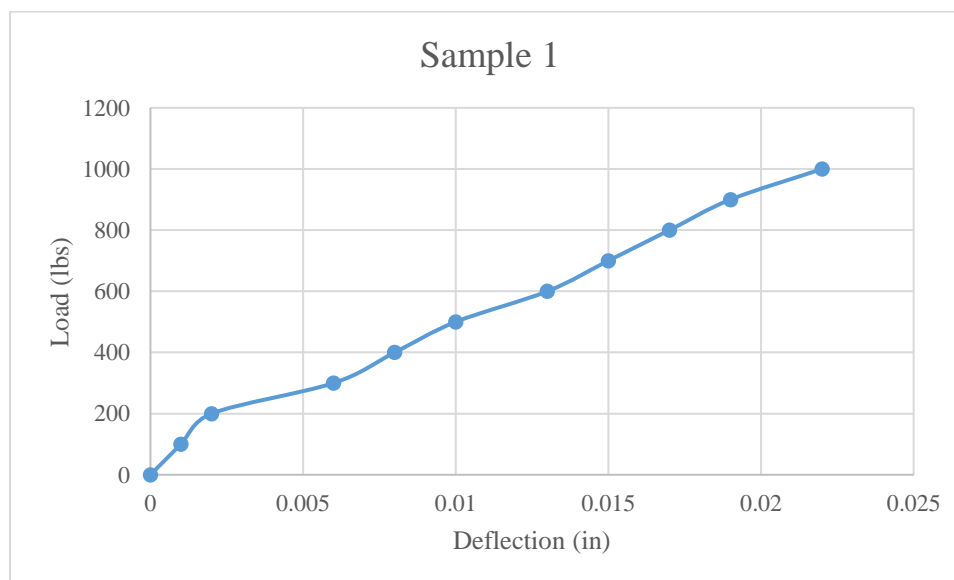


Figure 3.26 – Sample 1 Load versus Deflection Curve

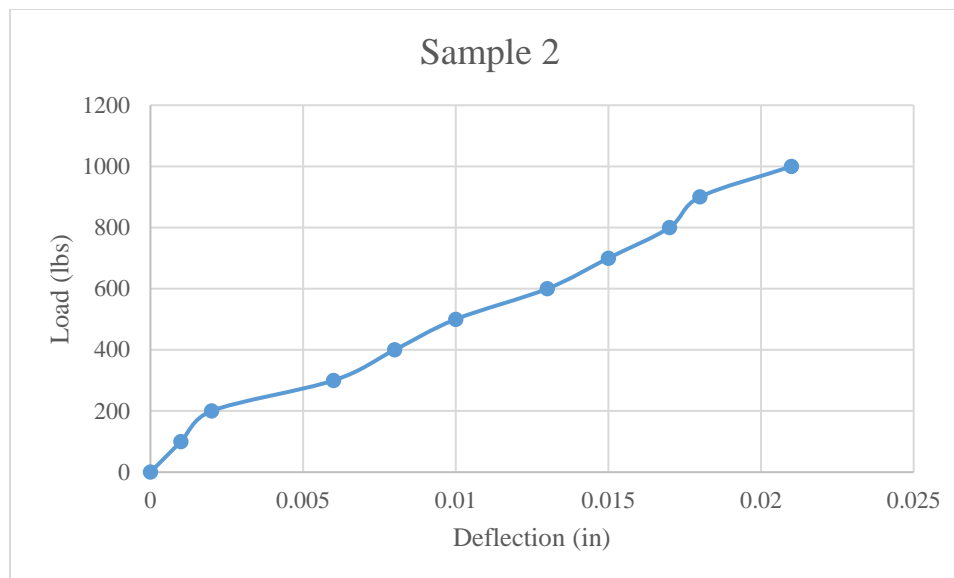


Figure 3.27 – Sample 2 Load versus Deflection Curve

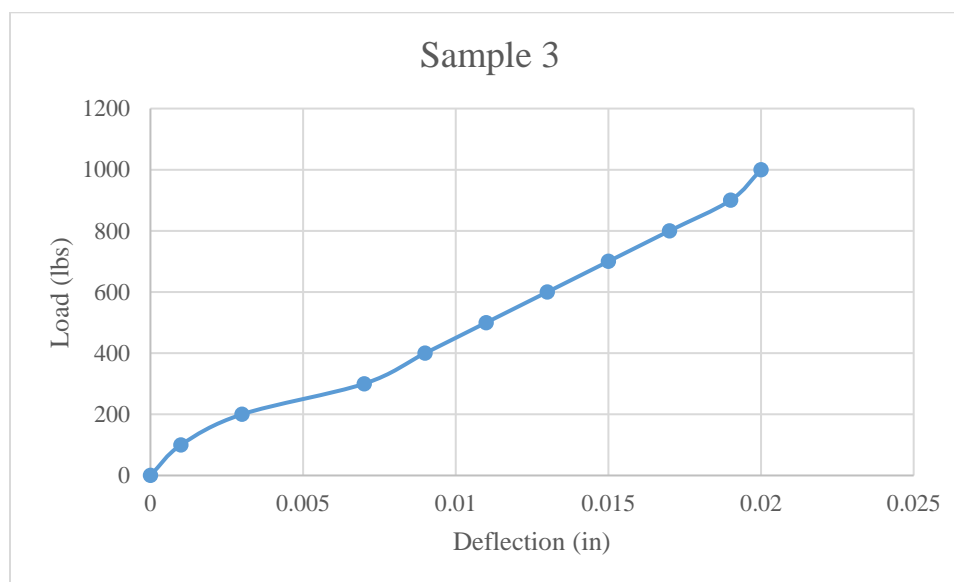


Figure 3.28 – Sample 3 Load versus Deflection Curve

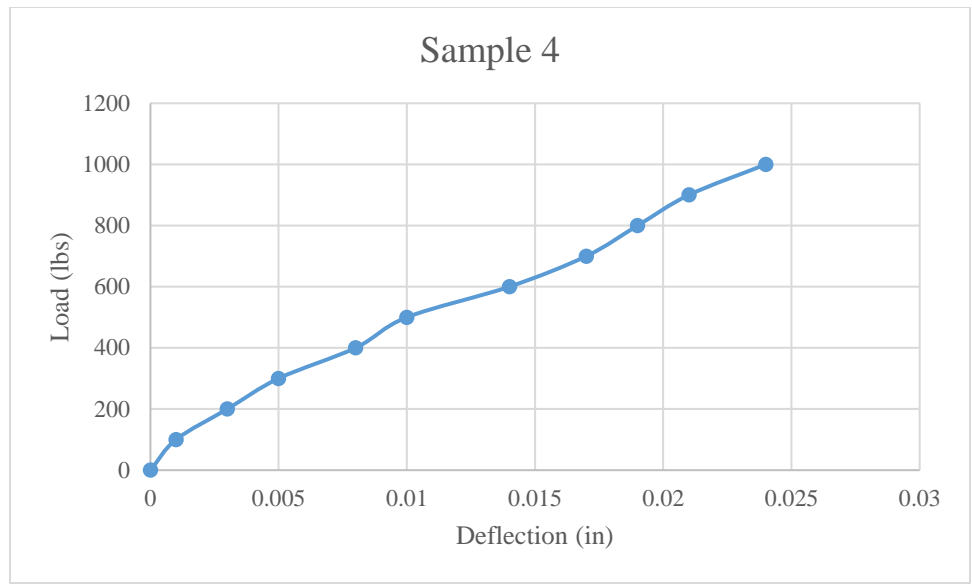


Figure 3.29 – Sample 4 Load versus Deflection Curve

3.4.3 Flexural Modulus of Elasticity Analysis and Observations

From the results it can be concluded that the average flexural modulus of elasticity is 2,620,966 psi, with a coefficient of variation of 0.0396. From chapter 3, the 28-day compressive modulus of elasticity is 4,473,539 psi, Figure 3.30 displays the results.

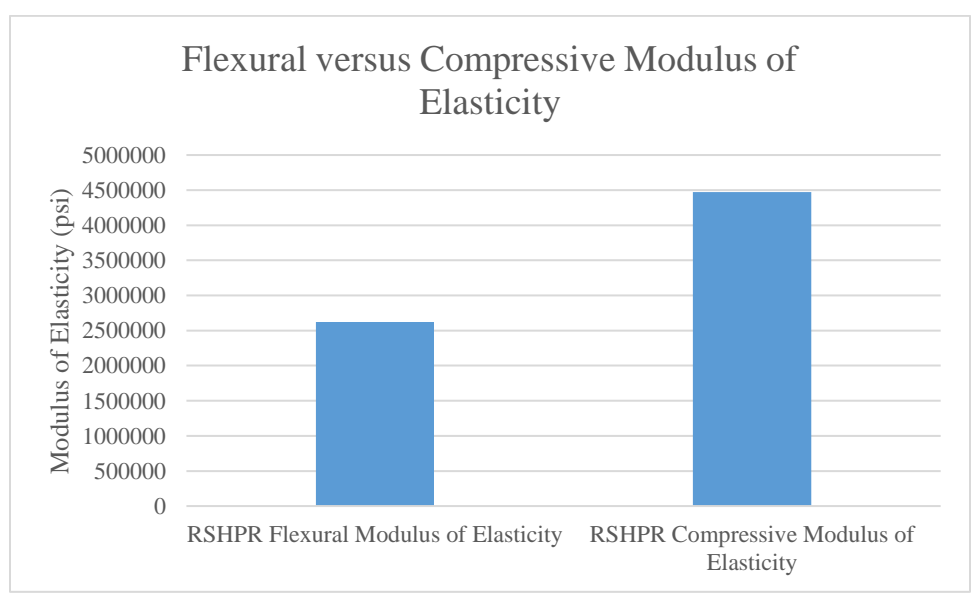


Figure 3.30 – Flexural Modulus of Elasticity versus Compressive Modulus of Elasticity

The results show that the flexural modulus of elasticity is 41% less than the compressive modulus of elasticity. This provides evidence that the modulus of elasticity in bending is not the same as in direct uniaxial loading. Note in the compression test, the entire cylinder is in uniform compression, as in the flexural specimen part of the beam is in tension. In addition, there is a strain gradient in the flexural specimen.

To determine the strain at first crack for flexure, the calculated flexural modulus was used to determine the strain point from the modulus of rupture from the results presented in this chapter. Equation 3.7 was used to calculate the strain. Table 3.13 shows the results of the analysis.

$$\varepsilon = \frac{f_r}{E_f} \quad (3.7)$$

Where:

ε = strain at first crack (in/in)

f_r = Modulus of Rupture at 28 days (psi)

E_f = Flexural Modulus of Elasticity (psi)

Sample	f_r (psi)	Estimated Flexural Tensile Strain (in/in)
1	1128.75	0.000430662
2	1186.50	0.000452696
3	1236.00	0.000471582
4	1179.75	0.00045012
5	1220.25	0.000465573
6	1233.75	0.000470723
	Average:	0.000456893
	SD:	0.000014

Table 3.13 – Estimated Flexural Tensile Strain Capacity of RSHPR

It is calculated that the average cracking flexural tensile strain in the samples is 457 $\mu\epsilon$. The drying shrinkage results discussed previously provided an ultimate drying shrinkage of 230 $\mu\epsilon$. Therefore, subtracting the effects of shrinkage from the strain at first crack provides a shrinkage strain resistance of 227 $\mu\epsilon$. The additional shrinkage strain resistance which provides extra allowance for thermal strains and strains caused by vehicular traffic loadings. Hence, providing more evidence of the materials crack resistant properties.

3.5 Physical Property Relationships

This section presents a study on the relationship between the compressive strength versus modulus of elasticity, splitting tensile strength, flexural strength and the relationship between flexural strength and flexural strength.

3.5.1 Compressive Strength versus Modulus of Elasticity

Figure 3.31 and 3.32 plot the values of modulus of elasticity versus the square root of compressive strength for the results obtained in this investigation. It can be seen that the relationship between the modulus of elasticity and square root of compressive strength is almost linear.

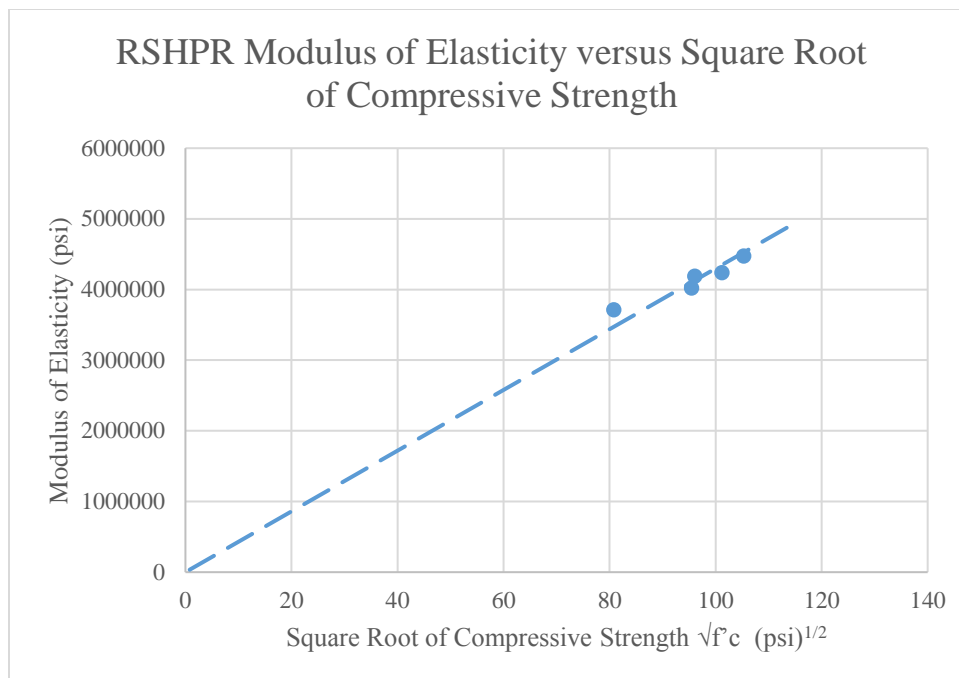


Figure 3.31 – Correlation between RSHPR Modulus of Elasticity and Square Root of Compressive Strength

Applying a graphical approach, a relationship between the modulus of elasticity and square root of compressive strength of the RSHPR is explained by the following equation:

$$E_{\text{RSHPR}} \approx 42970 * \sqrt{f'_c} \quad (3.8)$$

Where:

E_{RSHPR} is the Modulus of Elasticity of RSHPR (psi)

f'_c is the compressive strength of RSHPR (psi)

Similarly, the same graphical approach is applied to the modulus of elasticity and square root of compressive strength of the highly flowable RSHPR (Figure 3.33), is explained by the following equation:

$$E_{\text{Flowable RSHPR}} \approx 41080 * \sqrt{f'_c} \tag{3.9}$$

Where:

$E_{\text{Flowable RSHPR}}$ is the Modulus of Elasticity of the Highly Flowable RSHPR (psi)

f'_c is the compressive strength of RSHPR in (psi)

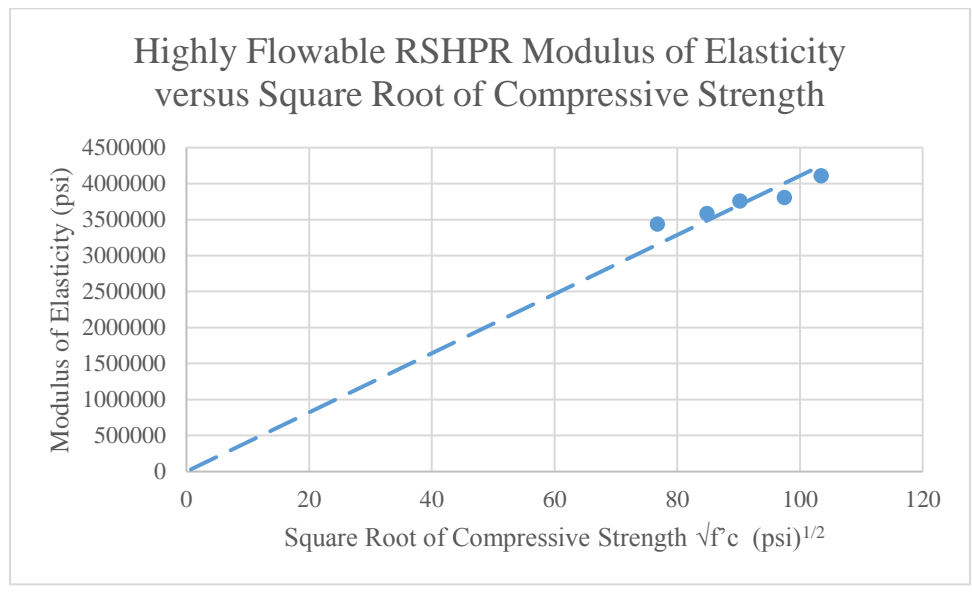


Figure 3.32 – Correlation between Highly Flowable RSHPR Modulus of Elasticity and Square Root of Compressive Strength

The ACI 318-14 code equation: $E = w_c^{1.5} 33 \sqrt{f'_c}$; where w_c is between 90 and 155 lb/ft³, f'_c is in psi and E is in psi x 10⁶, is found to be unconservative for the ranges of physical properties found in this investigation. The modulus of elasticity found by experiment is less than the modulus of elasticity found using the ACI equation.

3.5.1 Compressive Strength versus Splitting Tensile Strength

Figure 3.33 and 3.34 presents a plot of the splitting tensile strength versus the square root of compressive strength for the results obtained in this investigation. It can be seen that

the relationship between the splitting tensile strength and the compressive strength is almost linear.

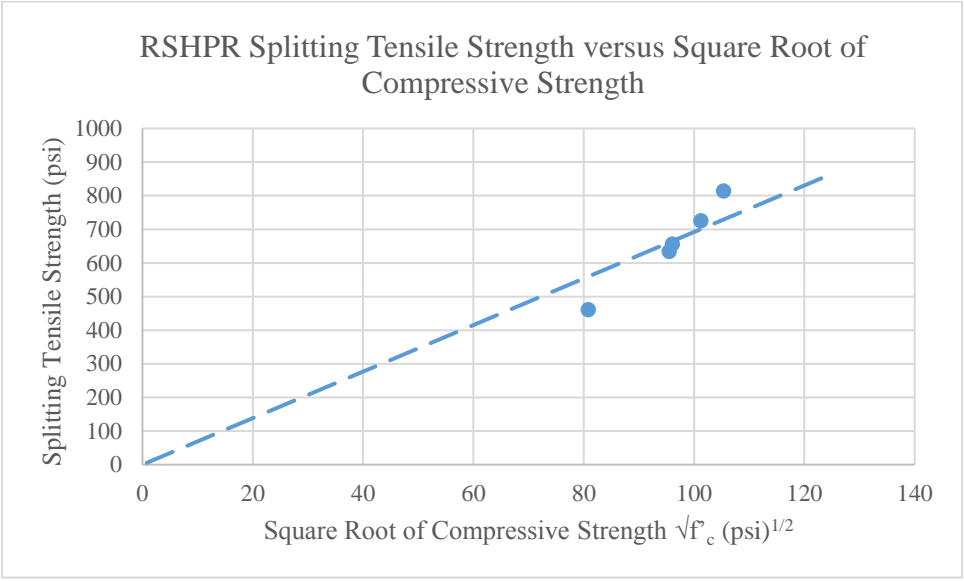


Figure 3.33 – Correlation Between RSHPR Splitting Tensile Strength and Square Root of Compressive Strength

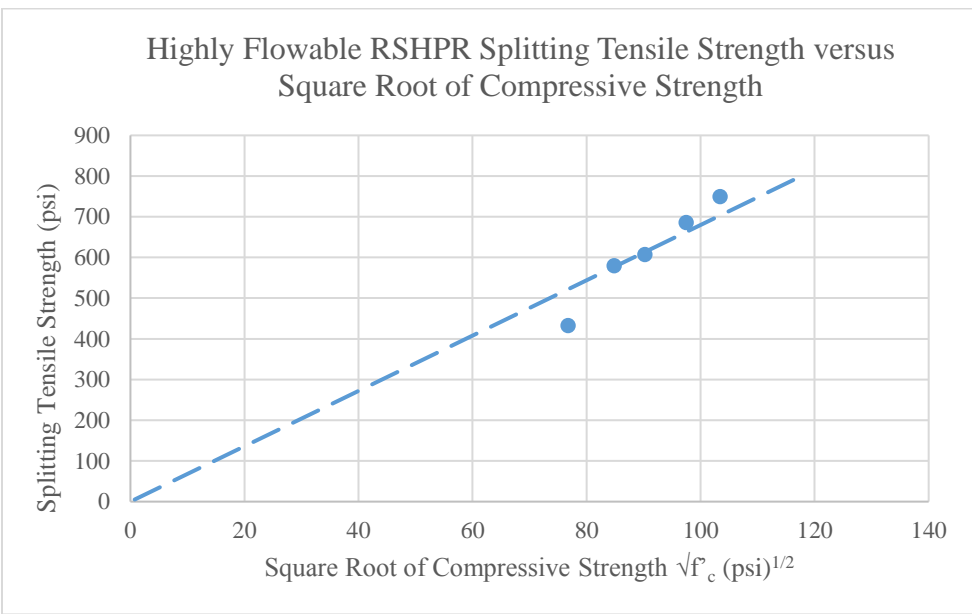


Figure 3.34 – Correlation Between Highly Flowable RSHPR Splitting Tensile Strength and Square Root of Compressive Strength

Applying a graphical interpretation, a relationship between the splitting tensile strength and square root of compressive strength of the RSHPR is explained by the following equation:

$$f_{t_RSHPR} \approx 6.9 * \sqrt{f'_c} \quad (3.10)$$

Where:

f_{t_RSHPR} is the splitting tensile strength of RSHPR (psi)

f'_c is the compressive strength of RSHPR (psi)

Similarly, the same approach is applied to the modulus of elasticity and square root of compressive strength of the highly flowable RSHPR (Figure 3.35), is explained by the following equation:

$$f_{t_HFRSHPR} \approx 6.8 * \sqrt{f'_c} \quad (3.11)$$

Where:

$f_{t_HFRSHPR}$ is the splitting tensile strength of the Highly Flowable RSHPR (psi)

f'_c is the compressive strength of RSHPR in (psi)

Comparing the relationship for normal weight concrete from ACI 318-14 code: $f_t = 6.7\sqrt{f'_c}$, where f'_c is expressed in psi, it was found to be slightly conservative.

3.5.2 Compressive Strength versus Flexural Strength

Figure 3.35 and 3.36 present the plots of the flexural strength versus the square root of the compressive strength.

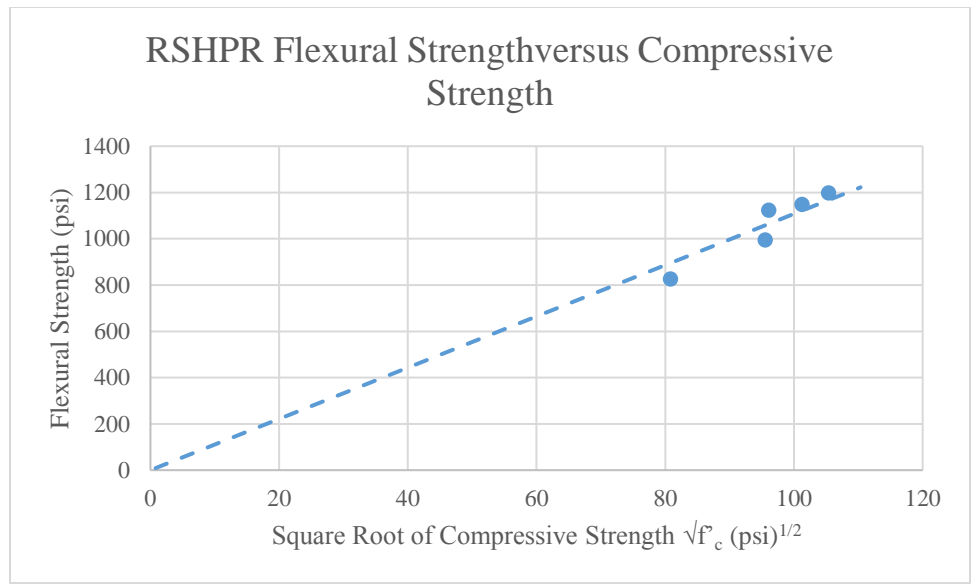


Figure 3.35 – Correlation Between RSHPR Flexural Strength and the Square Root of Compressive Strength

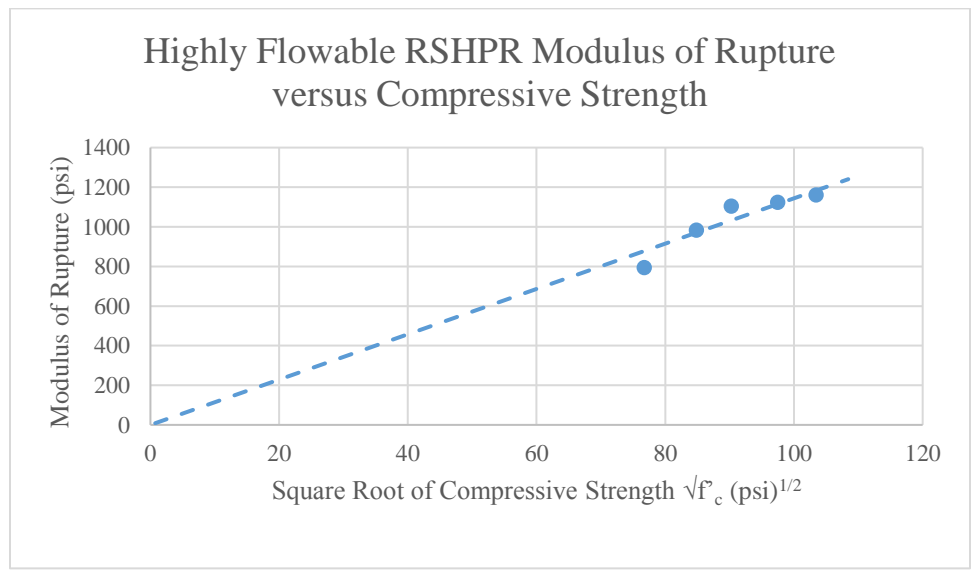


Figure 3.36 – Correlation Between Highly Flowable RSHPR and the Square Root of Compressive Strength

Applying a linear interpretation, a relationship between the flexural strength and square root of compressive strength of the RSHPR is explained by the following equation:

$$f_{r_RSHPR} \approx 11.1 * \sqrt{f'_c} \quad (3.12)$$

Where:

f_{r_RSHPR} is the Flexural Strength of RSHPR (psi)

f'_c is the compressive strength of RSHPR (psi)

Similarly, the same analytical approach is applied to the flexural strength and square root of compressive strength of the highly flowable RSHPR (Figure 3.37), is explained by the following equation:

$$f_{r_HFRSHPR} \approx 11.4 * \sqrt{f'_c} \quad (3.13)$$

Where:

$f_{r_HFRSHPR}$ is the Splitting Tensile Strength of the Highly Flowable RSHPR (psi)

f'_c is the compressive strength of RSHPR in (psi)

The relationship for normal weight concrete using ACI 318-14 code equation: $f_r = 7.5\sqrt{f'_c}$; where f'_c is expressed in psi, was found to be conservative for both RSHPR and highly flowable RSHPR formulations for ranges of results found in this investigation (f_r experimental is higher than calculated f_r). This indicates that the fiber content had a greater influence on the flexural strength than on the compressive strength.

3.5.3 Flexural Strength versus Splitting Tensile Strength

Figure 3.37 and 3.38 shows the plot of the flexural strength versus the splitting tensile strength capacity.

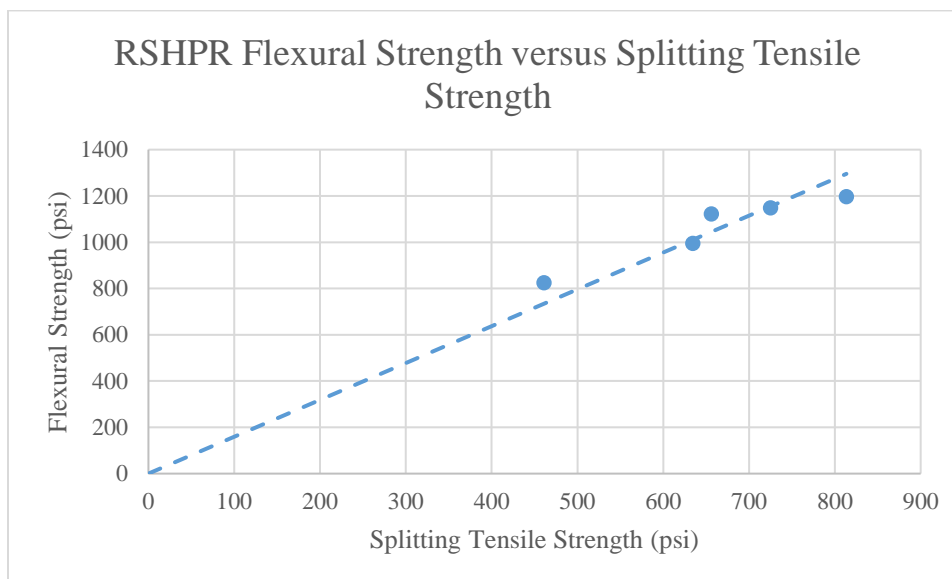


Figure 3.37 – Correlation Between RSHPR Flexural Strength and Splitting Tensile Strength

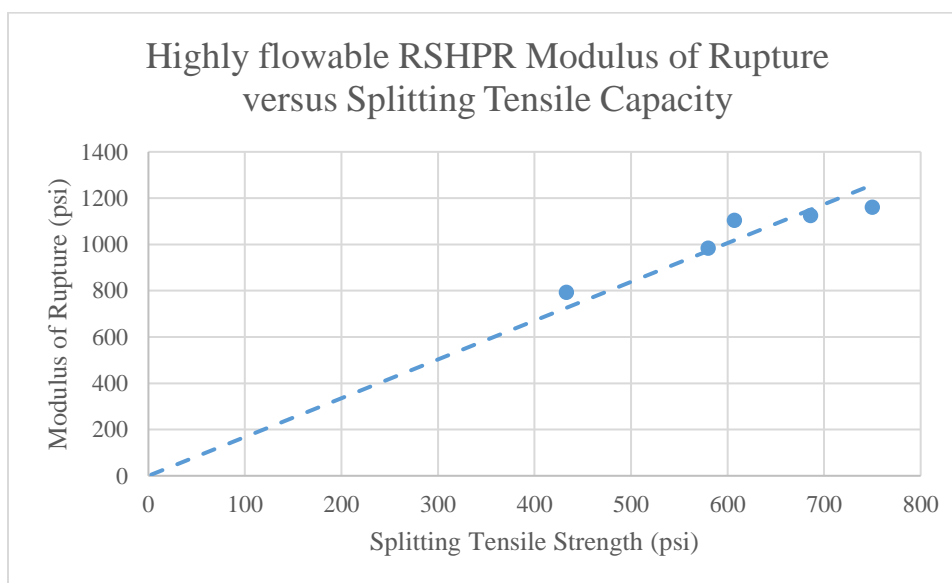


Figure 3.38 – Correlation Between Highly Flowable RSHPR Flexural Strength and Splitting Tensile Strength

The linear relationship between the flexural strength and splitting tensile strength of the RSHPR is explained by the following equation:

$$\frac{f_r}{f_t} = 1.6 \quad (3.14)$$

Where:

f_r is the flexural strength of RSHPR (psi)

f_t is the splitting tensile strength of RSHPR (psi)

Similarly, the same approach is applied to the flexural strength and splitting tensile strength of the highly flowable RSHPR (Figure 3.39), is explained by the following equation:

$$\frac{f_{r,hf}}{f_{t,hf}} = 1.7 \quad (3.15)$$

Where:

$f_{r,hf}$ is the flexural strength of the highly flowable RSHPR (psi)

$f_{t,hf}$ is the splitting tensile strength of the highly flowable RSHPR in (psi)

Figure 3.39 shows the plot of the flexural strength versus the splitting tensile strength capacity from the material properties for the CSA cement.

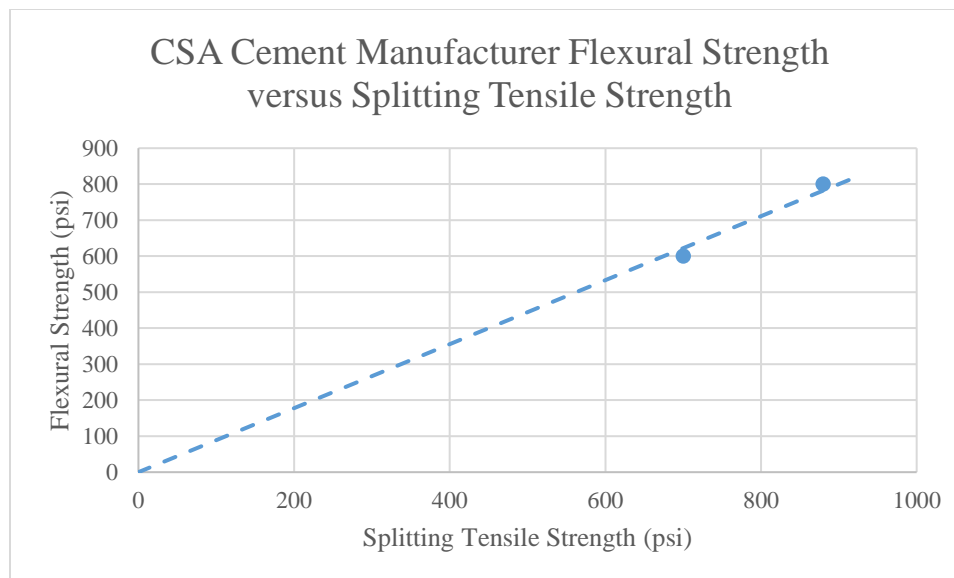


Figure 3.39 – Correlation Between CSA Cement Manufacturer Flexural Strength and Splitting Tensile Strength

Determining the relationship between the flexural strength and splitting tensile strength of the Manufacturer provided data is explained by the following equation:

$$\frac{f_{rm}}{f_{tm}} = 0.9 \quad (3.16)$$

Where:

f_{rm} is the flexural strength of the manufacturer CSA cement (psi)

f_{tm} is the splitting tensile strength of the manufacturer CSA cement (psi)

The relationship for the manufacturers CSA cement has a lower bending capacity than both RSHPR and highly flowable RSHPR. This indicates that RSHPR and Highly Flowable RSHPR have a higher resistance to bending.

Forming a relationship between ACI 318-14 equations for flexural strength ($f_r = 7.5\sqrt{f'_c}$) and splitting tensile strength ($f_t = 6.7\sqrt{f'_c}$) is explained by the following ratio:

$$\frac{f_{rACI}}{f_{tACI}} = 1.11 \quad (3.17)$$

Where:

f_{rACI} is the flexural strength of normal weight concrete (psi)

f_{tACI} is the splitting tensile strength of normal weight concrete (psi)

The relationship for the ACI 318-14 equations for flexural strength and splitting tensile strength for normal weight concrete has a lower bending capacity than both RSHPR and highly flowable RSHPR. This indicates that RSHPR and Highly Flowable RSHPR have a higher resistance to bending.

3.6 Summary

- The CSA cement formulations provided the best mechanical properties for repairs.
- It is possible to formulate fiber reinforced concrete with fiber volume fractions of 2 percent that is highly flowable.
- Using admixtures, the water to cement ratio can be reduced further than the manufacturers recommendation. Reduction in water to cement ratio further reduced shrinkage as compared to data provided by the manufacturer.
- The limiting factor for lowering the water to cement ratio is the amount of water needed to uniformly mix the rapid set formulation before the addition of the high range water reducer.
- In the case of water reducing admixtures, sulphate naphthalene formaldehyde based high range water reducers provided a longer workability time than the

polycarboxylic ether based high range water reducer for the promising rapid set formulation.

- The addition of fibers reduces the shrinkage strains by 54 percent.
- By providing shrinkage strains less than 300 micro strains, it is possible to fabricate crack free repairs leading to durable repairs and structures.
- Shrinkage had no longer increased after 28 days, but the compressive strength continued to increase. Therefore, strength gain is not related to shrinkage.
- The promising rapid set formulations have a higher resistance to bending by 33 percent than the original manufacturer composition.
- The modulus of elasticity measured using the flexural test samples (in flexural mode) is 59% of the modulus of elasticity measured during compression strength testing.
- RSHPR has a cracking flexural tensile strain limit $227 \mu\epsilon$ greater than the shrinkage strains for RSHPR. This allows for additional resistance from other loads.

CHAPTER 4 – FIELD EVALUATION AND REPAIR OF NON-HORIZONTAL SURFACES

4.1 Introduction

With an aging infrastructure, an increasing concern is the deterioration of concrete bridge decks and substructures over time. Complete deck replacement, although often the best solution for bridges, is not the most economical solution (Cervo & Schokker, 2010). The next economical solution is to repair the bridge deck at areas of deterioration. The application of the selected rapid set formulation (RSHPR) is applied to repair horizontal structural patches on an active Route 18, County Road 516 overpass bridge deck located in Old Bridge, New Jersey and to repair a non-horizontal patch conducted outside of the CAIT laboratory on Rutgers Livingston campus in Piscataway, New Jersey.

4.2 Horizontal Structural Patch Repair

4.2.1 Laboratory Horizontal Structural Patch Repair Test Overview

Two 12 inch by 12 inch by 1-inch simulated patch repair RSHPR slabs were fabricated in the Civil Engineering Laboratory on Busch Campus at Rutgers University, Piscataway, NJ to determine the ultimate effective direct tensile capacity of RSHPR. The RSHPR slabs were casted in molds fabricated from $\frac{3}{4}$ inch thick plywood supplied by Tulnoy lumber in Carteret, New Jersey.

Three 4-inch diameter bridge deck concrete cylinders were extracted with the use of a wet core drill and core bit from Ramp A over US 202, Route 23 in Wayne, New Jersey on October 3rd, 2016. The cylinders were placed into non-absorbent, plastic 4 inch by 8 inch cylindrical molds, making sure to not remove any of the dust or debris from the

extracted cylinders. RSHPR is then casted on top of the unprepared surface to determine the lower effective tensile bond capacity of RSHPR of an unprepared surface.

4.2.2 Horizontal Structural Patch Repair Field Test Overview

The New Jersey Department of Transportation (NJDOT) were replacing the Route 18, County Road 516 overpass bridge deck and allowed for experimental testing to be conducted on the old deck before replacement. The age of the parent concrete is 57 years old (bridge was constructed in 1959 as per NJDOT) at the time of experimental testing, conducted in September 2016. From observation the surface of the parent concrete was worn down to the aggregate. As per NJDOT engineers there never was any over coating placed on the parent concrete, just occasional patch work for exposed pot holes. The specimens for the surface patch rehabilitation were 1 square foot by ½ inch deep patches located on the west bound lane of the Route 18, County Road 516 overpass bridge (Figure 4.1). It should be noted that this was an active construction site, where access was limited due too allowable workable location with time constraints.

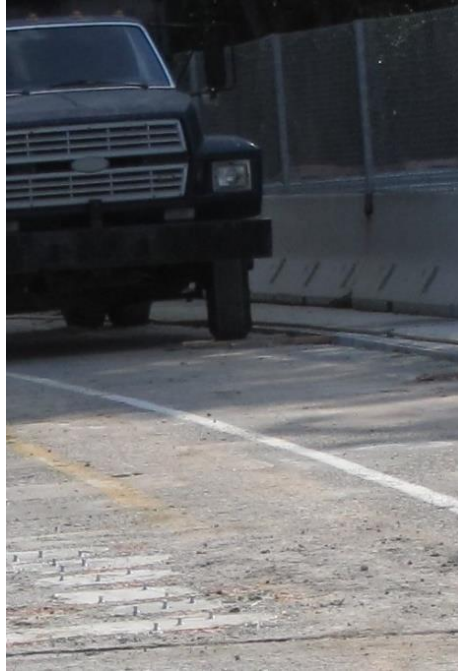


Figure 4.1 - Route 18, County Road 516 overpass bridge repaired with RSHPR

4.2.3 Horizontal Structural Patch Repair Laboratory Test Preparation

After the simulated patch repair RSHPR slabs had been given three hours to air cure in the Civil Engineering Laboratory at Rutgers University, six circular cuts equivalent to the outside diameter of the pull off dollies were drilled $\frac{1}{2}$ inch through each RSHPR slab using a wet core drill press and a core bit. The RSHPR slabs were then dried using compressed air. Once the RSHPR slabs were dried, 20 millimeter pull off test dollies were epoxied onto each cut (Figure 4.2). The epoxy was given 24 hours to fully cure as per manufacturer specification before pull off testing.

To create the formwork for casting the RSHPR on the extracted bridge cylinders, a non-absorbent plastic 4-inch diameter ring was placed around each cylinder. A $\frac{1}{2}$ inch thick layer of RSHPR was then casted on top of the cylinder. Note that no cleaning or preparation was conducted on the interface between the extracted cylinder and RSHPR.

This is to simulate the bond strength capacity of the interface between RSHPR and an unprepared surface. Once the RSHPR had three hours to cure, one circular cut equivalent to the outside diameter of the pull off dollies were drilled through the RSHPR layer and $\frac{1}{2}$ inch through the extracted concrete cylinder using a wet core drill press and a core bit. The RSHPR tops were then were dried using compressed air (to allow for pull off dolly placement). Then 20 millimeter pull off test dollies were epoxied onto each cut (Figure 4.3). The epoxy was given 24 hours to fully cure as per manufacturer specification before pull off testing.



Figure 4.2 - Laboratory RSHPR Slab with attached Pull Off Dollies



Figure 4.3 - 20-Millimeter Pull Off Dolly Attached to RSHPR Casted on Un-prepared Surface

4.2.4 Horizontal Structural Patch Repair Field Test Preparation

In total there were six horizontal repairs conducted. For each patch repair, compressed air was used to clean the placement area. Each patch was then uniformly lightly dampened with a spray of water before the rapid set material was placed. RSHPR and highly flowable RSHPR were each casted into three patches. Due to the patch repair location being an active construction site, casting of the patches needed to be conducted and hardened within 30 minutes to allow for the passing of construction equipment. After the rapid set formulations had three hours to cure, 20 millimeter pull off test dollies (Figure 4.4) were epoxied onto each rehabilitated repair (Figure 4.5), three per hole. Following the placement of the dollies, 20-millimeter-wide hole were drilled around each dolly, penetrating approximately 36 millimeters to go through both the RSHPR and parent bridge deck concrete. The epoxy was given 24 hours to fully cure as per manufacturer specification before pull off testing.



Figure 4.4 – 20-millimeter Pull Off Test Dolly



Figure 4.5 - Attached Pull Off Dollies on RSHPR Patch Repair

4.2.5 Test Procedure

Twenty-four hours after the epoxy has cured, pull off testing was conducted on the specimens following the guidelines of ASTM C1583, Standard Test Method for Tensile Strength of Concrete surfaces and the Bond Strength of Tensile Strength of Concrete Repair by Direct Tension, to conduct the pull off test (Figure 4.6). The pull off tester used was a PosiTest® AT-M Manual Adhesion Tester. The tensile load was applied at a constant rate of 5 ± 2 psi/s. After each failure, the tensile stress and failure mode was recorded. Epoxy failures were disregarded.



Figure 4.6 - PosiTest® AT-M Manual Adhesion Tester

Figure 4.7 shows the different types of failures for the pull off test. Figure 4.7 (a) shows a failure in the substrate concrete, signifying that the bond strength between the repair material and substrate is stronger than the tensile capacity of the substrate concrete. Figure 4.7 (b) shows bond failure at concrete/overlay interface, signifying the bond strength between the repair material and substrate concrete is less than both the tensile

capacity of the repair material and of the substrate concrete. Figure 4.7 (c) display a failure in the repair material, displaying that that repair material tensile capacity is less than the substrate concretes tensile capacity. Figure 4.7 (d) displays a bond failure in the epoxy interface, any results with a type-d failure were omitted from the results.

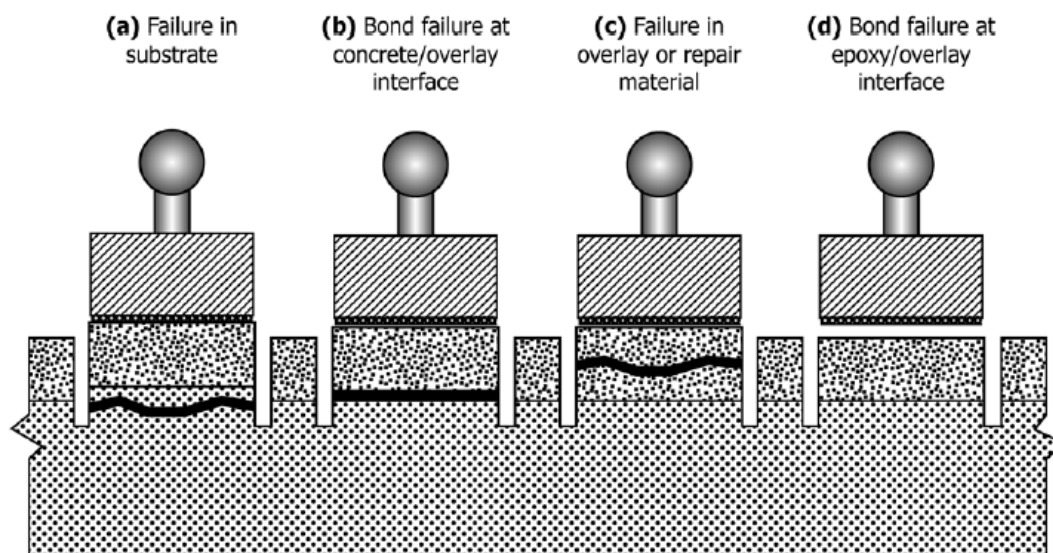


Figure 4.7 – Schematic of Failure Modes (ASTM C1583, 2016)

4.2.6 Laboratory Horizontal Structural Repair Test Results

Table 4.1 presents the pull off test results for the RSHPR simulated slabs and table 4.2 presents the pull off test results for the simulated unprepared surface.

RSHPR Simulated Patch Repair Tensile Capacity - Laboratory Testing		
Dolly I.D.	Tensile Stress (psi)	Comments
1	998	
2	1124	
3	957	
4	N/A	Epoxy Failure
5	N/A	Epoxy Failure
6	N/A	Epoxy Failure
7	N/A	Epoxy Failure
8	967	
9	998	
10	979	
11	1021	
12	994	
Average:	1005	
S.D.	49	

Table 4.1 - RSHPR Simulated Slab Pull Off Test Results

RSHPR Lower Effective Tensile Bond Capacity		
Dolly I.D.	Tensile Stress (psi)	Comments
1	309	Failed at bond interface
2	374	Failed at bond interface
3	302	Failed at bond interface
Average:	328	
S.D:	32	

Table 4.2 - Simulated Unprepared Surface Pull Off Test Results

4.2.7 Field Horizontal Structural Repair Test Results

Table 4.3 presents the pull off test results for the RSHPR and highly flowable RSHPR horizontal patch repairs. Table 4.4 presents the failure location for the pull off test results.

Field Horizontal Structural Patch Repair Test Results				
Hole ID	Dolly ID	Mix Identification	Tensile Stress (psi)	Comments
1	1	Highly Flowable RSHPR	300	
1	2	Highly Flowable RSHPR	352	
1	3	Highly Flowable RSHPR	469	
2	4	Highly Flowable RSHPR	369	
2	5	Highly Flowable RSHPR	N/A	Epoxy Failure
2	6	Highly Flowable RSHPR	429	
3	7	Highly Flowable RSHPR	556	
3	8	Highly Flowable RSHPR	539	
3	9	Highly Flowable RSHPR	540	
4	10	RSHPR	542	
4	11	RSHPR	418	
4	12	RSHPR	433	
5	13	RSHPR	530	
5	14	RSHPR	271	
5	15	RSHPR	530	
6	16	RSHPR	N/A	Epoxy Failure
6	17	RSHPR	485	
6	18	RSHPR	462	
		Average:	452	
		Standard Deviation:	88	

Table 4.3 - Route 18, County Road 516 Bridge Pull Off Test Results

Pull Off Test Failure Location		
	Highly Flowable RSHPR	RSHPR
Failed In Substrate	56%	67%
75% Failed In Substrate	44%	33%

Table 4.4 - Pull Off Test Failure Location

4.2.8 Horizontal Structural Patch Repair Observations and Analysis

Application of RSHPR and highly flowable RSHPR into the horizontal slab patches was conducted with no issue in an active construction environment, where there was working area and time constraints. It can be concluded that the selected repair material can be easily mixed and applied in an active construction environment.

The average tensile capacity for the laboratory slabs is 1005 psi; this value is interpreted as the ultimate bond capacity of RSHPR. The average tensile capacity strength of the extracted bridge cylinders is 328 psi; this is interpreted as the minimum effective bond strength of RSHPR. All of the pull off tests conducted on the Route 18, County Road 516 overpass bridge failed within the substrate concrete for both RSHPR and highly flowable RSHPR. The average tensile strength for these tests is 452 psi. Therefore, the bond strength capacity of the RSHPR to the substrate concrete is larger than the tensile capacity of the substrate concrete by 55 percent.

Preparation of the substrate surface before application of RSHPR is a significant factor in bond strength. Based on the results found, preparation of the surface before application of RSHPR produced no bond interface failures (type c failures), and all of the failures

occurred in the substrate concrete. An unprepared surface causes approximately a 27% reduction in bond strength, and caused bond failures at the repair material interface.

4.3 Patching Repairs of Non-Horizontal Surfaces

4.3.1 Test Overview

A non-horizontal surface patch repair was conducted outside of the CAIT laboratory on Rutgers Livingston campus in Piscataway, NJ using a highly flowable RSHPR. The purpose of the test is to provide evidence that the material can be successfully pumped through a RSHPR pumping apparatus to conduct a patching repair of non-horizontal surfaces in a short time span.

A non-horizontal surface RSHPR pumping apparatus was developed to achieve non-horizontal pumping. The assembly consists of a grout pump, a modified quick connection hose, and a 12 inch by 12-inch, ¼ inch thick applicator plate made out of an acrylic sheet that was installed with a backflow valve (to allow for one flow direction) steel plates for easier attachment to a non-horizontal surface, plastic ribbing to create a seal with the wall, and a quick connect valve for the grout pump hose. Figure 4.8 and Figure 4.9 depicts the set up. The use of an acrylic plate is beneficial due to its flexibility to form to uneven surfaces, and that it is transparent, allowing easy visualization of the repair process.

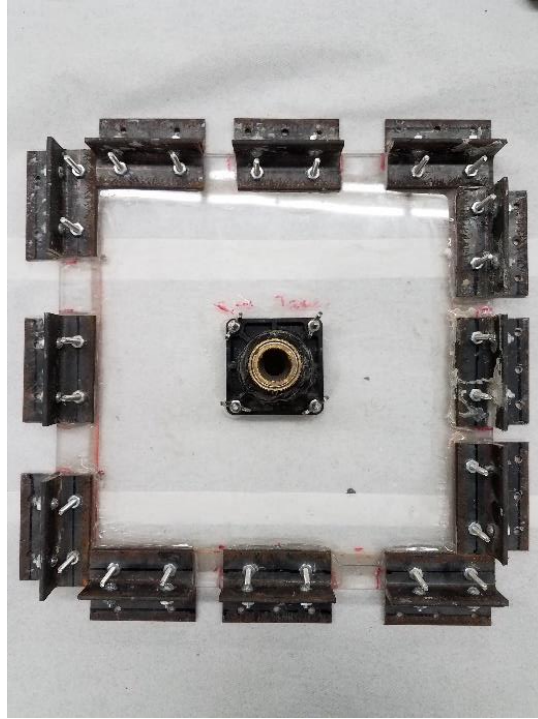


Figure 4.8 – Non-Horizontal Surface Patch Repair Applicator Plate



Figure 4.9 – Non-Horizontal Surface Patch Repair Application System

4.3.2 Non-Horizontal Patch Preparation

The patch to be repaired was first rock hammered to simulate a typical non-horizontal structural surface patch needing repair. The area to be repaired is approximately 9 inches long by 9 inches wide and 1-inch-deep (Figure 4.10). Before application of the repair material, the repair area was cleaned using compressed air to remove any dust or loose debris, then lightly uniformly dampened with water.



Figure 4.10 – Non-Horizontal Surface: Before Repair

4.3.3 Non-Horizontal Patch Test Set Up

The first part of the vertical repair is to attach a plastic LDPE film with a thin silicon epoxy on the face of contact on the applicator plate. This allows for easier removal of the applicator plate and a smooth finish on the repair material. The following step is to

attach the applicator plate that has been rigged with a backflow valve, quick hose adapter, and steel plates for attachment over the hole. Initially ½ inch long concrete screws with a 6 gauge (3.5-millimeter-wide) was installed every 4 inches around the perimeter of the applicator plate. During initial testing this set up allowed to much leaking, and was difficult to keep attached to the non-horizontal surface during pumping. This was then rectified by using 1-inch-long concrete screws with an 8 gauge (4mm wide) every 2 inches around the perimeter of the acrylic plate. This produced a total of 24 concrete screws installed around the 12-inch by 12-inch acrylic plate shown in Figure 4.11 with an installation time of 4 minutes and 50 seconds.



Figure 4.11 – Non-Horizontal Surface Repair: Patch Repair Test Set Up

The highly flowable RSHPR was used for the non-horizontal structural patch repair. The repair material was made flowable with the addition of a super plasticizer. It should be

noted that it is possible to pump pea gravel (gravel with a diameter less than ¼ inch) as well.

Once the applicator plate is attached, the repair material was mixed for application. The repair material is then poured into the grout pump hopper, the grout pump hose is connected to the applicator plate, then manually pumped into the hole. Once it is visibly seen that the hole has been filled, the grout pump hose is disconnected from the applicator plate and the grout pump is cleaned. After a 10-minute wait period, the applicator plate is removed from the wall, the left over repair material is then used to fill the applicator plate attachment holes and any necessary finishing procedures can be conducted on the repair.

4.3.4 Non-Horizontal Patch Repair Test Result

There was minimal leaking around the seal of the applicator plate. After waiting the 10-minute period the applicator plate was removed with ease and had a smooth clean finish, flush with the original surface. Figure 4.12 shows the result. The approximate volume of the void is 81 in³ was filled in approximately 10 seconds. This equates to a flow rate of 2.8 cubic feet per minute. The maximum pressure for the pump was not exceeded during the test. Figure 4.13 shows the non-horizontal patch repair two years after application. It can be determined that no pop outs, spalling or cracking has occurred on the repair.



Figure 4.12 – Non-Horizontal Surface Repair: After Completion of Repair



Figure 4.13 – Non-Horizontal Surface Repair: Two Years After Completion of Repair

4.3.5 Non-Horizontal Patch Observations and Analysis

The developed procedure and special formwork can be used for rapid repair of non-horizontal surfaces. The end result was a smooth finished patch repair. The total time from installation of the applicator plate, injecting the highly repair material and removing the applicator plate was approximately 20 minutes, which resulted in a complete repair, with no follow up required. This process eliminates the need to remove formwork at a later time frame, allowing for more effective and rapid application of labor forces and resources.

4.4 Summary

- RSHPR was effectively placed in an active construction zone, with little operating room and time constraints. It was displayed that a horizontal patch repair could be effectively conducted and completed within 30 minutes.
- After 24 hours, the tensile strength capacity of RSHPR was higher than the substrate concrete. Therefore, the tensile capacity of the substrate concrete is the limiting factor for the bond strength of the repair schematic.
- Surface preparation before the application of RSHPR is an important factor for an effective repair. Based on this investigation, an unprepared surface can reduce the bond strength of RSHPR to a substrate surface by 27 percent.
- The procedure developed can be used for rapid repair of non-horizontal surfaces.
- Special formwork can be constructed for non-horizontal structural patch RSHPR placement.

- It is possible to pump fiber reinforced concrete volume fractions of 2 percent that is highly flowable, and effectively place in a non-horizontal structural patch.
- It is possible repair a damaged part of a structural member even in a non-horizontal position. The system provides a mean for a quick one-step repair. There is no need for multiple work-day schedule for placing and removal of formwork.

CHAPTER 5 – MECHANICAL ANCHORS TO PREVENT DE-BONDING OF REPAIR MATERIALS

5.1 Introduction

The adhesive performance is one of the most important issues for applying repair materials to existing reinforced concrete structures. There are two ways already known for enhancing the interfacial performance: one is the surface roughness to be repaired and the other is the performance of the repair material (Satoh et al., 2015). If there is shrinkage or de-bonding of the repair layer it can lead to premature repair failure by allowing ingress of water, air, chlorides, and other contaminants into the concrete. Hence, if the surface bond or performance of the repair material is inadequate it can lead to further deterioration of a concrete structure by spalling and/or pop outs.

Common current repair practices for achieving a stronger adhesion to the substrate concrete for horizontal patch repairs is the application of polymer concretes. Polymer concretes are popular due to their high early compressive strengths, fast curing, high specific strength, adhesion capabilities and resistance to chemical attacks (Bedi et al., 2013). According to Vaysburd (2014) disadvantages of polymer concrete are:

- Polymer-based materials cover an extremely broad range of chemical/physical types;
- Their physical properties are uniquely different to those of concrete (i.e., there is a basic mismatch);
- To use them in intimate contact with an existing concrete substrate, the response of the composite repair system (not the isolated repair material) needs to be assessed;

- The material properties are sensitive to the effects of relatively small temperature changes and are also time dependent;
- Hardened properties can be markedly affected by the environment in which the material is applied and cured.

An integral part of this method is the assessment of the likely consequences of any “mismatch” of properties (e.g., thermal coefficient of expansion, modulus of elasticity, creep, etc.). For many applications, success depends on recognizing and overcoming a potentially damaging mismatch, either by use of an appropriate polymer type or by appropriate application procedures. The primary importance of dimensional compatibility properties such as shrinkage, creep, and elastic modulus in concrete repair is whether or not their interaction would lead to cracking and/or de-bonding (Vaysburd, A. M. et al., 2014). There is a strong importance on selecting the correct type of polymer concrete to apply, and a wrong selection can reduce longer-term structural efficiency. This requires an extra precaution and potential for error when applying polymer concrete to ensure that it is compatible with the substrate concrete.

There is a requirement of having a repair material with the ability to adhere to the substrate concrete when repairing a concrete structure with Fiber Reinforced Polymers (FRP). As Ray (2011) mentions, concrete patching and repair is a necessary step before the application of FRP reinforcement. Many issues exist with FRP repairs when the repair patch material and the substrate concrete de-bond due to poor adhesion between the surfaces. This can lead to a decrease in the structures strength capacity, and pop outs. Providing a method to add an increase in the adhesion capacity between the substrate

concrete and repair material before the application of FRP, adds an additional system of support.

To enhance the effectiveness of the adhesion between the repair material and substrate concrete, mechanical anchors were implemented in patch repairs to determine if there is an increase in adhesive strength. Outside of the CAIT laboratory on Rutgers Livingston campus, a horizontal mechanical anchored patch repair was conducted using RSHPR and mechanical anchors on a Route 18, County Road 516 overpass bridge deck donated by the New Jersey Department of Transportation. The use of a PosiTest[®] AT-M Manual Adhesion Tester and pull off dollies were applied to determine the tensile strength capacity.

5.2 Specimen Preparation

Four 12-inch-wide by 12-inch length by 1-inch-deep patches were cut into the parent concrete of the Route 18, County Road 516 overpass bridge deck (Figure 5.1) which was placed by the CAIT laboratory on Livingston Campus and donated by the New Jersey Department of Transportation. Two of the patches were repaired with the RSHPR, the other two patches were repaired with mechanical anchors and RSHPR. For the two patches repaired with structural anchors, each patch will have a different anchor system. The first anchor system was a 2 ¼ inch long by ¼ inch diameter screw in anchor (Figure 5.2), the second system was a 1 ¾ inch long by ¼ inch diameter hammer in place anchor (Figure 5.3). The first anchor system will be classified as Anchor Type 1 and the second anchor system will be classified as Anchor Type 2 for this thesis. For both anchor systems, an anchor will be placed every 2 to 4 square inches inside the patch. For both

anchor systems a ¼ inch diameter hole was drilled into the parent concrete using a rotary hammer drill and carbide tip ¼ inch SDS rotary hammer drill bit. After drilling, the patch was cleaned by using compressed air, then lightly dampened with water. The anchors were then installed following manufacturer guidelines (if applicable) as shown in figures 5.4 and 5.5. After installation of the anchors the RSHPR was placed.



Figure 5.1 – Typical Simulated Patch



Figure 5.2 – Type 1 Mechanical Anchor

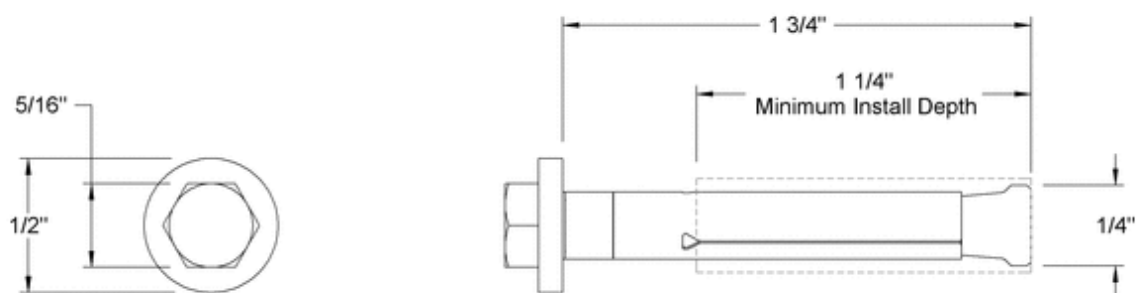


Figure 5.3 – Type 2 Mechanical Anchor



Figure 5.4 – Type 1 Mechanical Anchor Installation



Figure 5.5 – Type 2 Mechanical Anchor Installation

5.3 Horizontal Patch Repair Test Set Up

After the RSHPR had set, circular cuts equivalent to the outside diameter of the pull off dollies were drilled through the RSHPR and a minimum of ½ inch into the substrate concrete using a wet core drill press and a core bit (Figure 5.6). For the patch repairs with the anchors, the circular cuts were drilled about the center of the anchor, making the anchor aligned directly with the center of the pull off dolly. This was done to ensure that the recorded tensile strength capacity increase was due to the anchors. Following the core drilling, the repair area was then cleaned and dried. Once the patch repairs were dried, 20 millimeter pull off dollies were adhered to the circular cut areas using a two-part manufacturer supplied epoxy and were required to have a minimum of 24 hours to cure (Figure 5.7). Twenty-four hours after the epoxy has cured, pull off testing were conducted on the specimens following the guidelines of ASTM C1583, Standard Test Method for Tensile Strength of Concrete surfaces and the Bond Strength of Tensile Strength of Concrete Repair by Direct Tension (Figure 5.8). The pull off tester used was a PosiTest® AT-M Manual Adhesion Tester. The tensile load was applied at a constant rate of 15 to 20 psi/s. After each failure, the tensile stress and failure mode were recorded. Failure holes were labeled and if the failure plane included any irregularities such as epoxy failures or voids; it was omitted from the results.



Figure 5.6 – Core Drill and Wet Core Bit Used to Make Circular Cuts

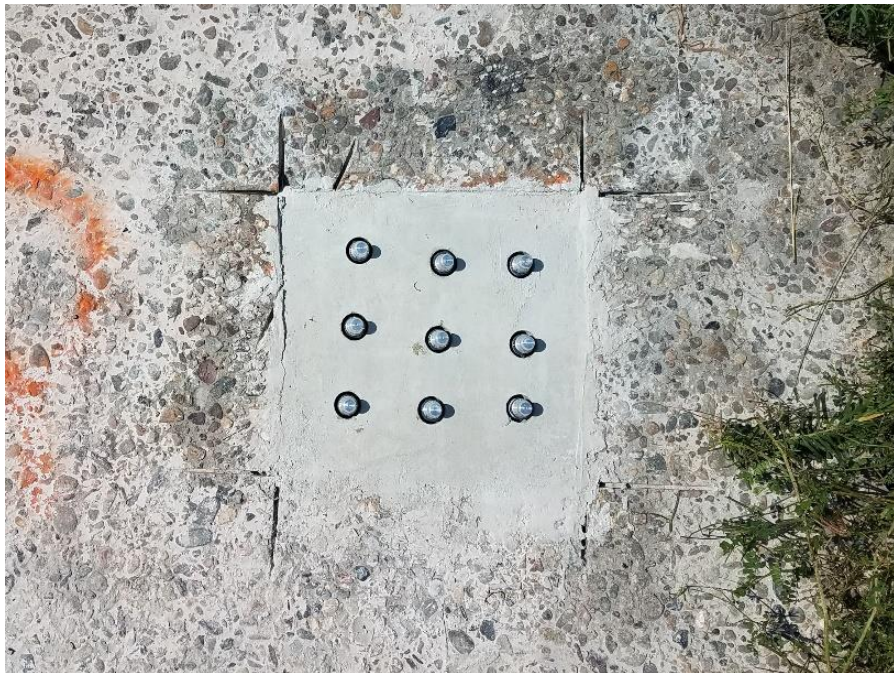


Figure 5.7 - Pull Off Test Dollies Attached to Repaired Patch



Figure 5.8 - Pull Off Test Conducted on Repaired Patch with a PosiTest® AT-M Manual Adhesion Tester

To determine the actual tensile capacity of the substrate concrete, ten circular cuts equivalent to the outside diameter of the pull off dollies were drilled through the parent concrete a minimum depth of a ½ inch into the substrate concrete using a wet core drill press and a core bit. The surface was then made smooth with an angle grinder equipped with a diamond tip masonry wheel. After cleaning the area with water and compressed air, 20 millimeter pull off dollies were adhered to the circular cut areas using a two-part manufacturer supplied epoxy and were required to have a minimum of 24 hours to cure. Twenty-four hours after the epoxy has cured, pull off testing were conducted on the specimens following the guidelines of ASTM C1583. The pull off tester used was a PosiTest® AT-M Manual Adhesion Tester. The tensile load was applied at a constant rate of 15 to 20 psi/s. After each failure, the tensile stress and failure mode were recorded. Failure holes were labeled and if the failure plane included any irregularities such as epoxy failures or voids; it was omitted from the results.

Figure 5.9 shows the different types of failures for the pull off test. Figure 5.9 (a) shows a failure in the substrate concrete, signifying that the bond strength between the repair material and substrate is stronger than the tensile capacity of the substrate concrete. Figure 5.9 (b) shows bond failure at concrete/overlay interface, signifying the bond strength between the repair material and substrate concrete is less than both the tensile capacity of the repair material and of the substrate concrete. Figure 5.9 (c) display a failure in the repair material, displaying that that repair material tensile capacity is less than the substrate concretes tensile capacity. Figure 5.9 (d) displays a bond failure in the epoxy interface, any results with a type-d failure were omitted from the results.

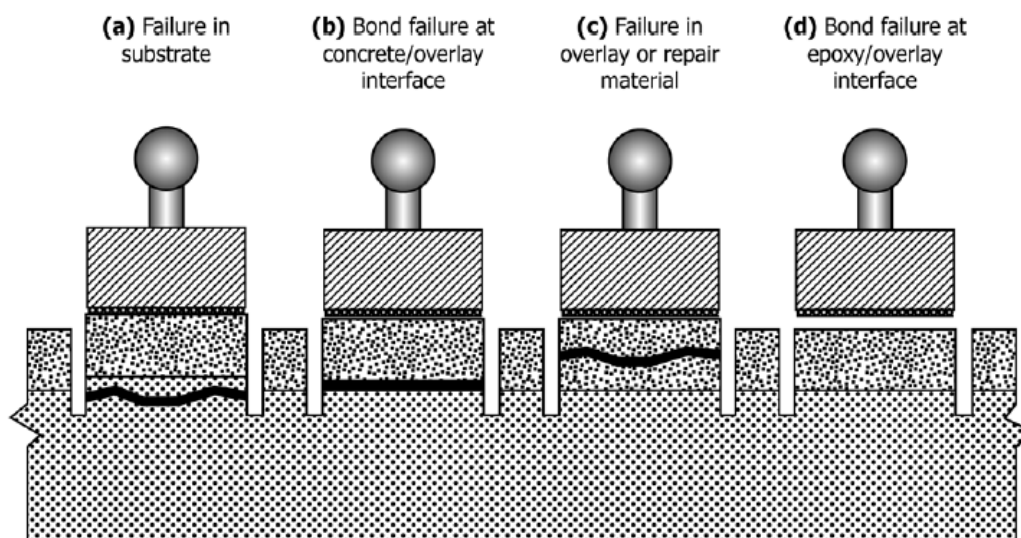


Figure 5.9 - Schematic of Failure Modes (ASTM C1583, 2016)

5.4 Horizontal Patch Repair Test Results

A total of 15 dollies were placed on the RSHPR and substrate, 10 dollies placed over Type 1 mechanical anchors and RSHPR, 10 dollies placed over Type 2 mechanical anchors and RSHPR, and 10 dollies placed directly on the substrate concrete. The RSHPR and substrate dollies had five epoxy failures, the Type 1 and Type 2 mechanical

anchors each had one epoxy failure, and the substrate had one epoxy failure. The data from the epoxy failures were omitted from the results. Figure 5.10 shows the average tensile capacity for each patch repair. Table 5.1 shows the amount of failures that occurred completely in the substrate concrete, and failures that occurred approximately 75 percent in substrate concrete. Figure 5.11 shows a typical pull out core from the RSHPR and substrate concrete patch repair. Figure 5.12 displays a typical Mechanical Anchor pull out core. Tables 5.2, 5.3, 5.4 and 5.5 lists each pull off test result and failure mode. To further investigate the interface between the substrate concrete and RSHPR, a Veho VMS-004 microscopic camera was used to capture the bond interface (Figure 5.13).

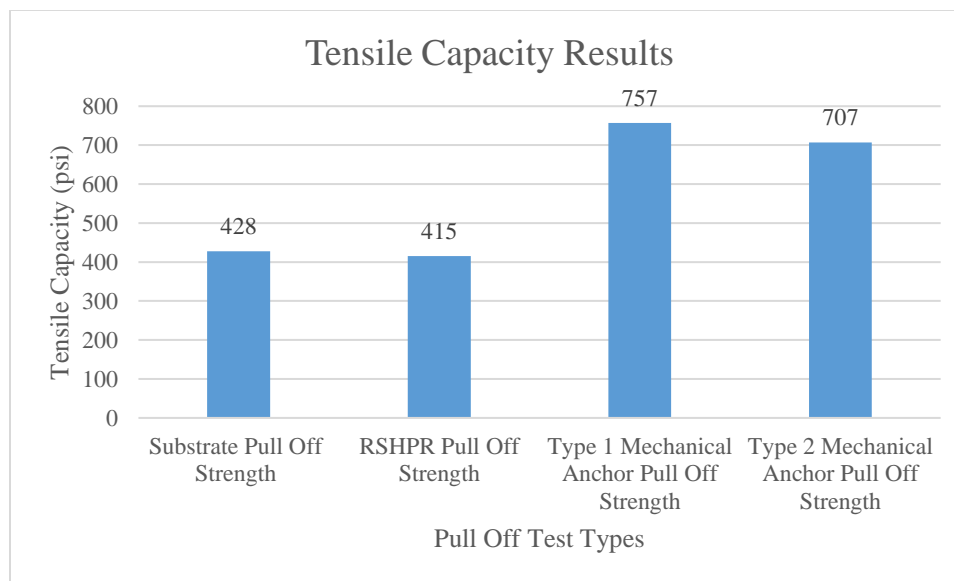


Figure 5.10 – Average Tensile Capacity

	No - Anchorage	Type 1 Mechanical Anchorage	Type 2 Mechanical Anchorage
Failed In Substrate	60%	78%	67%
75% Failed in Substrate	40%	22%	33%
Total	100%	100%	100%

Table 5.1 – Failure Location Percentage from Tensile Test



Figure 5.11 – Typical RSHPR & Substrate Pull Off Result



Figure 5.12 – Typical Anchor Pull Out

Substrate Tensile Capacity	
Failure Strength (psi)	Failure Mode
434	Substrate
300	Substrate
513	Substrate
350	Substrate
535	Substrate
566	Substrate
436	Substrate
344	Substrate
373	Substrate
N/A	Epoxy

Table 5.2 – Substrate Tensile Capacity & Failure Mode

RSHPR & Substrate Tensile Capacity Results	
Failure Strength (psi)	Failure Mode
484	Substrate
322	75% Substrate
339	Substrate
306	75% Substrate
453	Substrate
334	75% Substrate
323	75% Substrate
509	Substrate
573	Substrate
510	Substrate
N/A	Epoxy

Table 5.3 – RSHPR & Tensile Capacity Results

Type 1 Mechanical Anchor Results	
Failure Strength (psi)	Failure Mode
762	Substrate
692	Substrate
546	75% Substrate
749	Substrate
860	Substrate
893	Substrate
868	Substrate
769	Substrate
670	75% Substrate
N/A	Epoxy

Table 5.4 – Type 1 Mechanical Anchor Tensile Capacity & Failure Mode Results

Type 2 Mechanical Anchor Results	
Failure Strength (psi)	Failure Mode
514	75% Substrate
781	Substrate
730	Substrate
797	Substrate
712	Substrate
769	Substrate
689	75% Substrate
722	Substrate
652	75% Substrate
N/A	Epoxy

Table 5.5 – Type 2 Mechanical Anchor Tensile Capacity & Failure Mode Results



Figure 5.13 – Magnified x25 Interface of RSHPR and Substrate Concrete

Pull Off Test Results Distribution				
	Type 1 Mechanical Anchor	Type 2 Mechanical Anchor	Substrate	RSHPR
Average (\bar{x}):	757	707	428	415
Standard Deviation (σ):	104	81	88	95
Coefficient of Variation:	0.138	0.114	0.207	0.229
Max Value:	893	797	566	573
Min Value:	546	514	300	306
$\bar{x} - \sigma =$	652	627	339	320
$\bar{x} - 2\sigma =$	548	546	251	225
$\bar{x} - 3\sigma =$	444	465	163	130

Table 5.6 – Pull Off Test Results Distribution

5.5 Mechanical Anchors Observations and Analysis

Overall the pull off test results provided evidence that the structural anchors increased the average tensile capacity of the bond strength by 44 percent for Type 1 mechanical anchors and an increase of 40 percent for Type 2 mechanical anchors compared to the substrate tensile capacity. Figure 5.13 shows the interface between RSHPR and the substrate concrete, and it is observed that RSHPR appears to penetrate into the substrate concrete.

Using the data from Table 5.4, 5.5, and 5.6, the probability of the stress capacity from both types of anchors to fall below two standard deviations of the mean anchorage tensile stress capacity is calculated using equation 5.1.

$$Z = \frac{X - \mu}{\sigma} \quad (5.1)$$

Where:

Z = Normal Random Variable (Z-Score)

X = Tensile Capacity for Anchor (psi)

μ = Average Tensile Capacity of Each Respective Anchor (psi)

σ = Standard Deviation for Each Respective Anchor (psi)

Equation 5.1 transforms all the observations of any normal random variable X into a new set of observations of a normal random variable, Z , with mean 0 and variance 1.

Whenever X assumes a value x (in this case, x is the value of two standard deviations below the mean tensile capacity of the anchors), the corresponding value of Z is given.

From this value of Z , Z -tables are utilized to determine the probability (area underneath the normal probability curve) of the mean tensile capacity falling two standard deviations below the mean tensile capacity.

The results determined that there is a 2.22% chance of the Type 1 Mechanical Anchors tensile stress capacity falls below two standard deviations from the mean tensile stress capacity, and a 2.33% chance of the Type 2 Mechanical Anchors tensile stress capacity falling two standard deviations below the mean tensile stress capacity. For Type 1 Mechanical Anchors at a 2.22% probability of the tensile capacity falling two standard deviations below from the mean tensile stress capacity, is a larger tensile capacity than the average capacity of the substrate by 120 psi. For a 2.33% probability of the tensile capacity of the Type 2 Mechanical Anchors falling two standard deviations below the mean tensile stress capacity, is a larger tensile capacity than the average tensile stress capacity of the substrate by 118 psi. With low probabilities of falling below two standard

deviations from the average anchorage tensile capacity, both Type 1 Mechanical Anchors and Type 2 Mechanical Anchors contribute additional strength to the substrate.

Based on the results, and to ensure a factor of safety it is recommended to install mechanical anchors in patch repairs as a form of added insurance. To ensure that the anchors will provide a 40% to 44% increase in tensile capacity, the geometry of the anchor installation in the patch was analyzed to determine spacing. It is assumed that the effective area of the anchor is in relation to the depth of the RSHPR (Figure 5.14). Equation 5.2 was developed to determine the effective installation pattern for the mechanical anchors.

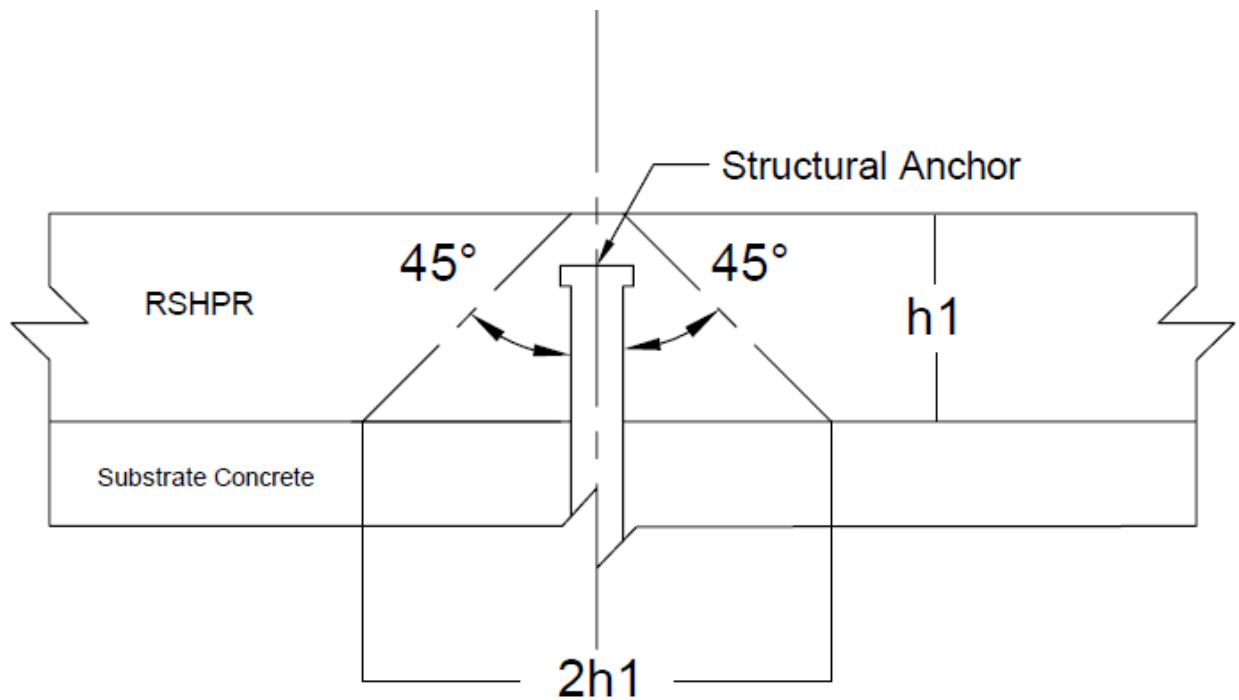


Figure 5.14 – Diagram of Mechanical Anchor in Patch Repair

$$D = d_{Anchor} + 2h_1 \quad (5.2)$$

Where:

D = Effective Installation Length (inches)

d_{Anchor} = diameter of the Anchor (inches)

h_1 = Depth of the RSHPR (inches)

5.6 Summary

- Providing Anchorage in patch repairs provides improvement in the substrate concrete by increasing the tensile strength capacity by 44 percent.
- RSHPR does not react or reduce the tensile capacity of the substrate concrete.
- Providing Anchorage in patch repairs decreases the amount of partial pull outs by 18 percent.
- Type 1 mechanical anchors and Type 2 mechanical anchors provide approximately the same increase in tensile capacity.
- At a 97.5% confidence interval, the strength of the repair system for both type 1 and type 2 mechanical anchors is 118 psi higher than parent material.
- It is recommended that anchors are provided at a spacing of two times the depth of the repair plus the diameter of the anchor.

CHAPTER 6 – TEST CRITERIA FOR ACCELERATED CORROSION TESTING

6.1 Selection of Criteria

For all construction materials, durability plays an important role as it dictates the longevity and effectiveness of the material. Many outdoor structures, such as bridges, are exposed to freeze and thaw cycles, ultra violet (UV) radiation, wetting and drying and salt exposure. This is due to the fact that bridges are outdoor structures, exposed to air on all four sides. These exposure environments can accelerate deterioration and ultimately the longevity of the structures life span by providing an environment for corrosion to propagate.

The objective of this study is to develop an accelerated corrosion testing method to simulate real life deterioration on steel thin coating paints. It is important to properly evaluate the condition of the existing coating to determine suitability for thin coating paints. It is common practice for transportation agencies to apply a protective coating to the steel (Chong, 2004), hence the importance in evaluation of the thin coating paints. The transportation authorities in the United States use ASTM B117, and ASTM D5894 for performance test protocol of protective thin coating paints. The fundamental weakness of the current testing is that the tests do not provide the estimate of service life in actual field conditions. The tests are intended only for comparative evaluations. A successful test should correlate with actual field exposure for predicting all modes of failure. Listed are accelerated test methods the new accelerated corrosion testing of thin coating paints conducts to better simulate field conditions.

- Cyclical Corrosion
- Degradation of thin coating due to wetting and drying exposure

- Degradation of thin coating due to ultra violet exposure
- Degradation of thin coating due to temperature changes including freezing and higher ambient temperatures during summers

A new chamber for accelerated corrosion testing was developed to provide a more realistic simulation of the interaction of these factors than is found in current accepted tests.

6.2 Description of Criteria

There are many standards developed by the American Society of Testing Materials to test the durability of materials. The motivation of these standards is to produce a system where different products can be compared, and variations allowed for user acceptance. For this investigation, the most commonly used and accepted standards are investigated further.

Outdoor structures are exposed to the environment and cyclical weather events. ASTM D5894-16 – Alternating Exposure: Fog/Dry Cabinet and UV/Condensation Cabinet simulates a specimen being exposed to a cyclic salt fog spray and cyclic UV radiation. ASTM D5894 also includes guidelines from ASTM B117-Standard Practice for Operating Salt Spray (Fog) Apparatus, and ASTM G154 – Standard Practice for Operating Fluorescent Ultraviolet (UV) Lamp Apparatus for Exposure of Nonmetallic Materials for construction and operation of the testing cabinet.

The test specimens for ASTM D5894 are exposed to alternating periods of one week in a fluorescent UV/condensation chamber followed by one week in a cyclic salt fog/dry chamber. The fluorescent UV/condensation cycle is 4 hour UV at $0.89 \text{ W}/(\text{m}^2 \cdot \text{nm})$ at

340 nm at 60°C followed by 4 hour condensation at 50°C, using UVA-340 lamps. The fog/dry chamber runs a cycle of 1-hour fog at ambient temperature and 1 hour dry-off at 35°C. The fog electrolyte is a relatively dilute solution, with 0.05 % sodium chloride and 0.35 % ammonium sulfate. The sodium chloride at a 5 percent concentration keeps the corroded metal ions in solution so they can act as conductors to enhance the corrosive effect (Blakeley, 2016). The specimens will be repositioned periodically to ensure even amount of exposure. Compressed air is used to remove moisture from the specimens. The intent of this test is to provide an environment of corrosive atmosphere, rain, condensed dew, UV light, wet/dry cycling, and temperature cycling; simulating common weathering events.

All of the interactions are not in one cycle, as each interaction rotates over a span of multiple weeks. This test involves one week in a cyclical salt fog/dry chamber, followed by another week in a fluorescent UV/condensation chamber. The cyclical salt fog and UV irradiation are not included in the same cycle. This test does not include the effects of freeze and thaw, a common weather event for exposed construction materials.

Freeze-thaw damage occurs by the penetration of water into a material and the continuous repetition of water expansion when it freezes and contraction when it thaws. Over time this process deteriorates the material. Freeze-thaw damage occurs in elements exposed to the environment, where there are temperature gradients below and above freezing. For the purpose of this investigation, freeze-thaw interactions are a critical factor when analyzing thin coating paints.

Thin coating paint resistance to freeze-thaw interactions are analyzed by ASTM D6944 – Standard Practice for Determining the Resistance of Cured Coatings to Thermal Cycling.

This practice determines the resistance of cured coatings or coating systems to repeated thermal cycles and is designed to assess the effect of thermal cycling on the properties of a coating or coating system. These properties may include adhesion, resistance to checking, cracking, blistering, or others. It is important to mention that the procedure is not intended to provide a quantitative measure of the service life that can be expected from a specific coating system on a given substrate. The specimens undergo a heating cycle of 8 hours in $122 \pm 5^{\circ}\text{F}$ ($50 \pm 3^{\circ}\text{C}$) air, then 16 hours of a freezing temperature of $-20 \pm 5^{\circ}\text{F}$ ($-29 \pm 3^{\circ}\text{C}$) in air, constituting 1 cycle. This process will then repeat for 30 cycles, or other agreed upon number of cycles. Evaluation of specimens take place either every 5 cycles, or at the end of 30 cycles.

An objective of this investigation was to include all of these alternating events into one cycle, that can better represent actual service life of the material.

6.3 Description of Test Set Up

For the alternating exposure cabinet in ASTM D5894, ASTM B117 – Standard Practice for Operating Salt Spray (Fog) Apparatus, dictates the specification of the salt fog sprayers, position of samples, salt solution reservoir and preparation of the salt solution. The apparatus required for salt spray (fog) exposure consists of a fog chamber, a salt solution reservoir, a supply of suitably conditioned compressed air (for drying specimens), one or more atomizing nozzles, specimen supports, provision for heating the chamber, and necessary means of control. The size and detailed construction of the apparatus are optional, provided the conditions are met. The salt solution reservoir must be designed so that the salt solution can be recycled during each cycle. The specimens

placed into the cabinet must be supported at an angle between 15° and 30° from the vertical and preferably parallel to the principal direction of flow of fog through the chamber, based upon the dominant surface being tested. Specimens shall not contact each other, or be in contact with any material with the ability to act as a wick. According to ASTM B117 the salt solution shall be prepared by dissolving 5 ± 1 parts by mass of sodium chloride in 95 parts of water conforming to Type IV water (reagent grade water) in Specification D1193 (except that for this practice limits for chlorides and sodium may be ignored). Careful attention should be given to the chemical content of the salt. The salt used shall be sodium chloride with not more than 0.3 % by mass of total impurities. Halides (Bromide, Fluoride, and Iodide) other than Chloride shall constitute less than 0.1 % by mass of the salt content. Copper content shall be less than 0.3 ppm by mass. Sodium chloride that has had anti-caking agents added shall not be used because such agents may act as corrosion inhibitors.

For the alternating UV exposure exposed to repetitive cycles in ASTM D5894 follows the guidelines outlined in ASTM G154 – Standard Practice for Operating Fluorescent Ultraviolet (UV) Lamp Apparatus for Exposure of Nonmetallic Materials. The specification does not allow for the mixing of different UV lamp types, as it may produce major inconsistencies in the light falling on the specimens. Standard fluorescent UV lamps are allowed to be used, as long as the power supply and irradiance requirements are met for the lamps. The light source should be located with respect to the specimens receives uniform irradiance. To determine if a specific fluorescent UV lamp for a fluorescent UV device meets the required spectral band pass wavelength, the relative

irradiance percentage can be calculated using equation 6.1 then compared to a relative spectral power distribution chart.

$$I_R = \frac{\sum_{\lambda_i=A}^{\lambda_i=B} E_{\lambda_i}}{\sum_{\lambda_i=C}^{\lambda_i=400} E_{\lambda_i}} \times 100 \quad (6.1)$$

Where:

I_R = relative irradiance in percent

E = irradiance at wavelength λ_i

A = lower wavelength of wavelength bandpass

B = upper wavelength of wavelength bandpass

C = lower wavelength of total UV bandpass used for calculating relative spectral irradiance

λ_i = wavelength at which irradiance was measured

For ASTM D6944 the required freeze-thaw apparatus must be a chamber suitable with the necessary refrigerating and heating equipment controls to achieve the specified temperature requirements (-20°F to 122°F). It is also allowed to use multiple chambers if it is not possible to achieve both temperatures in one apparatus.

6.4 Development of the Chamber for Accelerated Testing

The current practice for evaluating a materials durability in environmental conditions involves multiple tests and analysis, as previously discussed. Based on literature discussed in chapter 2 and current ASTM standards, a chamber for accelerated corrosion

testing was developed to encompass these standards in a cyclic process of wetting, drying, and freezing.

A recycling salt spray is utilized in the newly developed system based from ASTM D5894. Instead of a fog spray, the system uses a flat spray. The motivation of this decision is to better simulate rain and water-run off exposure that occurs with exterior structures, as a fog spray does not simulate typical rain and water run-off conditions. The developed chamber ensures that an even coverage is maintained with a flat spray, as it would be with a fog spray. The sodium chloride used in the system is typical roadway de-icing salt used by transportation authorities, to closer simulate field conditions. The motivation in ASTM D5894 is to use sodium chloride as a conductor to expedite corrosion. For this developed chamber, the sodium chloride to expedite corrosion is the same as the road de-icing salt, as this is a typical factor in the degradation of bridges (Houska, 2007).

A holding rack for specimens is part of the chamber for accelerated testing, and its construction will follow the guidelines of ASTM D5894 and ASTM B117. The holding rack supports specimens at an angle between 15° and 30° from the vertical, constructed from a non-corrosive/conductive material capable of resisting deterioration from the components of the chamber and will be placed preferably parallel to the principal direction of the salt spray through the chamber.

Ultraviolet irradiation is included in the new system, and follow many of the guidelines established in ASTM D5894 and ASTM G154. The type of UV light and placement of UV light will follow the guidelines discussed. Instead of being in a separate

UV/condensation cabinet, the UV lights will be part of the main chamber, and included in every cycle.

To provide a deep freeze environment for the chamber for accelerated testing, an apparatus suitable with the necessary refrigeration to achieve the specified temperature requirements of $-20 \pm 5^{\circ}\text{F}$ ($-29 \pm 3^{\circ}\text{C}$) is used, following the specification in ASTM D6944. To provide a thawing environment for the chamber for accelerated testing, a heating system capable of achieving and maintaining a temperature of $122 \pm 5^{\circ}\text{F}$ ($50 \pm 3^{\circ}\text{C}$) within an hour is applied following the guidelines in ASTM D6944. For the developed heating system in the chamber for accelerated testing also acts as the drying system, differentiating from ASTM D5894 where the drying system is compressed air.

The chamber for accelerated testing will be a semi-automatic operation, where the operation of the salt sprayers, UV lights, freezing and heating system is an automatic system. The only manual requirements for the developed system are the movement of the specimens, and replenishment of the salt solution.

6.5 Testing Scheme for the Chamber for Accelerated Testing

The developed chamber for accelerated testing experimental schedule is based on current ASTM standards. For ASTM D5894 the UV exposure cycle is 4-hours followed by 4-hours condensation at 50°C , using UVA-340 lamps; this cycle repeats for seven days. Following the UV/condensation cycle, specimens are placed into the fog/dry chamber for seven days, which operates a cycle of 1-hour fog at ambient temperature and 1 hour dry-off at 35°C . To simulate freeze/thaw interactions, ASTM D6944 dictates that specimens undergo a heating cycle of 8 hours in air, then 16 hours of a freezing temperature in air,

constituting 1 cycle. This process will then repeat for 30 cycles, or other agreed upon number of cycles. The motive of this investigation is to combine all of these testing standards into one cycle.

For the developed chamber for accelerated testing, the experimental schedule emphasizes the effect of the creep of corrosion, therefore there will be more focus on the wetting and drying, the processes that accelerates corrosion. Similar to ASTM D5894, there will be a rotational wetting and drying period. Instead of a rotating 4-hour wetting and a 4-hour drying period, the developed experimental system applies a 1-hour wetting period followed by a 1-hour drying period to further accelerate the creep of corrosion. The wetting and drying periods will rotate one after another for 8 cycles each, over a 16-hour period. This produces four times more exposure to wetting and drying sequences in 1 cycle than ASTM D5894. During the drying period the specimens will be exposed to UV irradiation as well, therefore having a total of 8-hours of irradiation exposure. This increases the UV exposure from ASTM D5894 by 4-hours per cycle. To further accelerate the creeping of corrosion, the specimens are placed into a chamber capable of maintaining a deep freeze for 8 hours after the 16-hours of wetting, drying and UV exposure. Combined these sequences produce a 24-hour period, and will constitute 1-master cycle. When the specimens are removed from the freezer cabinet and placed into the chamber for accelerated testing, this is considered the beginning of the next master cycle. The beginning of the cycle begins with exposure to heat and UV radiation for 1 hour to thaw the specimens as well as dry off any moisture on the specimens from the freezer. The samples at the end of the wetting/drying rotation end on the wetting process,

leaving the specimens saturated with salt solution. Therefore, when the specimens are placed into the freezer cabinet, ice will form and further accelerate the rate of corrosion.

6.6 Summary

- Many outdoor structures, such as bridges, are exposed to freeze and thaw cycles, ultra violet (UV) radiation, wetting and drying and salt exposure. There are multiple ASTM tests applied to test the durability of materials exposed to these environments.
- The fundamental weakness of the current testing standards is that the tests do not provide the estimate of service life in actual field conditions. The tests are intended only for comparative evaluations.
- It is important to properly evaluate the durability of thin coatings to determine application suitability.
- The test chamber for accelerated corrosion increases UV exposure by 4-hours, as well as increases the number of wetting and drying rotations by 8-hours from the commonly used standard ASTM D5894. The increase of UV exposure, and number of wetting and drying rotations will help increase the creep of corrosion.
- The test chamber designed and built for this investigation combines wetting, drying, UV exposure, freezing and thawing in 1 master cycle. The existing standards separate these degradation mechanisms. For example, UV exposure is done after the exposure to a saline solution spray. This current process better simulates actual field conditions by combining response variables and can help provide a better estimate of service life in actual field conditions.

- The newly developed chamber for accelerated testing places specimens in an environment of 16-hours wetting/drying rotation (8-hours each), 8 hours of UV exposure, and 8 hours of deep freeze. The length of these combined events to occur takes 24 hours, and constitutes 1 master cycle.

CHAPTER 7 – EXPERIMENTAL SETUP: ACCELERATED TESTING

7.1 Introduction

A chamber for accelerated testing was developed to create a cyclic process of wetting, drying and freezing. The chamber developed is fully automatic except for the manual replacement of salt water and placement of the specimens from the deep freezer to the chamber. To prevent any negative effects such as material creep or corrosion, the chamber had to be created out of strong durable materials. A recirculating salt water system is utilized for the chamber to effectively recycle and distribute the salt water. A system for the freezing, thawing and UV exposure was also developed and installed to ensure the required temperature and UV exposure metrics are achieved.

7.2 Salt Water Spray System

To ensure that the Chamber for Accelerated Testing itself does not creep nor corrode, a 5/16-inch-thick, 150-gallon polyethylene plastic tub was selected as the main body for the chamber. The tank being made out of polyethylene has no corrosion risk, and the substantial thickness of the polyethylene removes any doubt about the tank deforming due to creep. On one outer wall, at the bottom center of the tank there is a drain, where a polyethylene tube was connected to it to direct the water flow directly into the 10-gallon salt solution reservoir (Figure 7.1). Connected to the salt solution reservoir, there is a 120/240V AC, 1/3 Horsepower Stainless Steel Circulation Pump designed for pumping caustic fluids. A pump designed for caustic fluids was chosen to ensure that the salt water solution does not corrode the internal elements of the pump and potentially risk pump failure. The pump is connected to the salt solution reservoir by a cam and groove

connection (Figure 7.2), to allow easy removal of the salt water storage tank for maintenance.



Figure 7.1 - 150 Gallon Polyethylene Plastic Tub and Salt Water Solution Reservoir

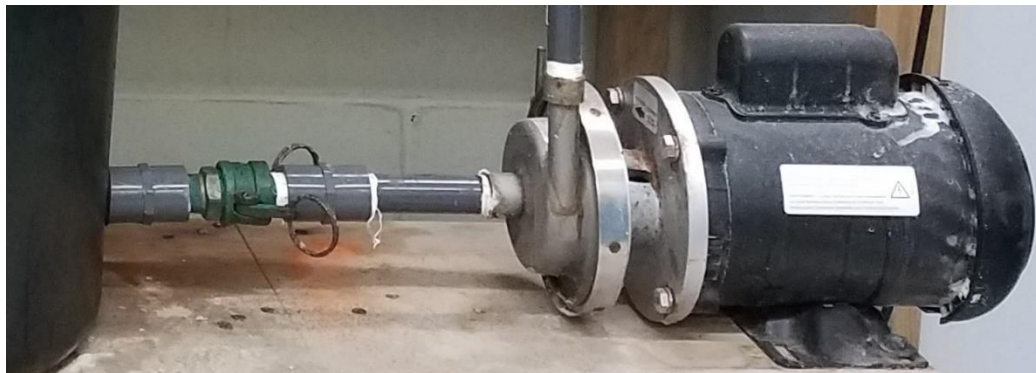


Figure 7.2 - Salt Water Solution Reservoir Connection to the Pump

From the pump there is a ½ inch inner diameter high pressure PVC clear tubing, that reduces to a ¼ inch inner diameter high pressure PVC clear tubing, leading back to the 150-gallon polyethylene plastic tub. The high pressure PVC tubing was selected to reduce the risk of potential tube rupture from the pumping pressure. Along the top edge of the tub there are 10 spaced flat spray nozzles, and on the lower edge of the tank there are 4 spray nozzles connected by a ¼ inch inner diameter high pressure PVC clear tube to ensure an even salt spray coverage of the specimens in the chamber (Figure 7.3).



Figure 7.3 - Salt Sprayer Layout



Figure 7.4 - PVDF Flat Spray Nozzles



Figure 7.5 - Salt Water Sprayer Assembly

The flat spray nozzles are made out of polyvinylidene fluoride (PVDF), and have ¼ inch NPT male threads (Figure 7.4). The flat spray nozzles are then connected into ¼ inch NPT bronze adapters, connected to a nylon inline tee adapter with a ¼ inch male thread (Figure 7.5). Adjustable clamping hangers were epoxied to the tanks walls to hold the PVC tubes in place. As the salt water is sprayed, the water drips off of the specimens, and then flows back into the salt solution reservoir through the polyethylene tube, where the salt water solution is then recirculated. To function automatically, the pump is connected to a time activated on/off switch that operates seven days a week. The schedule for the pump to turn on every day at 6pm for one hour, then shut off for the following hour. This on/off cycle will continue every hour until 9am, resulting in a total of 8 hours of salt water solution spray exposure.

7.3 Salt Water Solution Preparation

The salt used for Chamber for Accelerated Testing is New Jersey Department of Transportation de-icing road salt from the Trenton, NJ headquarters. As discussed previously, the required salinity content of the salt water solution is 5 percent by weight. To ensure that the de-icing road salt is able to be uniformly mixed, and can flow thru the pump without issue, the salt is ground down to a composition of approximately 1180 microns with a high-speed blade blender. Buckets are then filled with water and weighed on a calibrated scale. The weight of each bucket of water is recorded, then the required amount of salt (5 percent by weight) is weighed out for each bucket. Once the salt is added the water, it is then agitated with a paddle mixer connected to a power drill able to produce 1500 rpm for a minimum of 90 seconds to ensure a homogenous solution. If there is still a significant amount of salt particles resting on the bottom of the bucket, the

solution is agitated for longer until homogeneous. After the salt water solution is made homogenous, it is then poured into the salt solution reservoir. Each batch of salt water solution is used for one master cycle of testing (24 hours). Upon completion of a master cycle, the salt water is removed from the salt solution reservoir, any leftover debris is cleaned out of the reservoir and new salt water solution is produced.

7.4 Specimen Holding Rack

A specimen holding rack was constructed to guarantee a uniform salt-water spray application, infrared heat and UV exposure to each specimen. Due to the concern of deterioration from the salt water, heat and UV exposure, the specimen holding rack was constructed out of high density polyethylene (HDPE) synthetic wood and connected by galvanized wood screws to prevent degradation. The holding rack was constructed to have two layers, each with an elevation angle of 17 degrees. At this elevation the specimens can be evenly coated by the salt water spray without salt water excessively collecting on the specimens. The overall size of the holding rack was constructed to optimize the space inside the chamber for accelerated testing. Figure 7.6 displays the holding rack inside the chamber for accelerated testing.



Figure 7.6 – Specimen Holding Rack

To reduce the effects of sagging and relaxation of the HDPE synthetic wood from creep, the elements on the holding rack were doubly reinforced. Every four inches along the support beams where the specimens are to be placed, a $\frac{1}{4}$ inch diameter, $\frac{1}{2}$ inch long nylon shoulder screws were installed to prevent the specimens from slipping off the holding rack (Figure 7.7). The nylon shoulder screws were selected due to their chemical resistant, non-conductive, and light weight properties.



Figure 7.7 - Shoulder Screws Installed on the Specimen Holding Rack

7.5 Heat and UV Exposure System

As discussed in the previous chapter, the temperature required for the drying process to occur was determined to be 120 degrees Fahrenheit. To reach the required temperature, three 5-inch diameter infrared light bulbs were selected. To meet the UV exposure requirements, two A19 UV light, 120 volts 60 Hz 365 nanometer wavelength were selected. To position the heat and UV sources directly over the specimens, a frame was constructed out of pressure treated lumber. Pressure treated lumber was chosen due to its strong water damage resistant properties and ease of constructing a custom fit that appropriately fits around the 150-gallon polyethylene plastic tub. Figure 7.8 displays the frame used to support the infrared and UV light bulbs.



Figure 7.8 - Infrared and UV Light Frame

The frames columns are 4x4 posts, and the cross beams are 2x4 studs which were constructed to fit over the 150-gallon polyethylene plastic tub, and rest on the table. The frame is connected by galvanized wood screws to reduce any possible deterioration issues from corrosion. The infrared and UV lights were placed at a height on the frame were the

salt water sprayers would not accidentally hit the lights, but the lights would still provide the required infrared heat and UV exposure requirements. The lights are set at a height of 14 inches above the 150-gallon polyethylene plastic tub. To function automatically, the infrared heat and UV lights are connected to a time activated on/off switch that operates seven days a week. The schedule for the infrared and UV lights is to turn on every day at 5pm for one hour, then shut off for the following hour. This on/off cycle will continue every hour until 8am, resulting in a total of 8 hours of infrared and UV light exposure.

7.6 Deep Freezer

As the previous chapter discussed, the samples need to undergo a cycle of 8 hours' deep freeze at a temperature of 0 degrees Fahrenheit. A 7.0 cubic foot compact chest freezer was selected to provide the required deep freeze for the specimens. To utilize the maximum amount of space in the freezer, a series of removable shelves were constructed out of 1-inch x 1-inch steel angles and HDPE synthetic wood (Figure 7.9). The specimens are placed into the compact chest freezer at 9am daily, and removed from the freezer to be placed into the chamber at 5pm daily. Figure 7.9 shows the specimens being stored in the compact chest freezer.



Figure 7.9 - Removable Shelf for the Freezer

7.7 Chamber for Accelerated Testing Maintenance

After every 7 master cycles the Chamber for Accelerated testing is cleaned and thoroughly inspected to prevent any performance issues while the specimens are in the chest freezer. The 150-gallon polyethylene plastic tub is first flushed with clean potable water, and scrubbed to remove any residue from the salt or specimens. Next, the salt water is removed from the salt solution reservoir, which is then filled with clean potable water. The pump is then turned on for a minimum of 15 minutes but no longer than an hour, to flush any debris out of the PVC tubes, pump, and flat nozzle sprayers. The following step is to inspect the infrared lights, UV lights, pump, flat nozzle sprayers, tubes, supporting components and overall tank for any possible issues. If an issue is identified, the part is repaired or replaced.

7.8 Summary

- The Chamber for Accelerated Testing is a functioning automatic system for accelerated corrosion testing.
- Corrosion and creep resistant materials were selected as the chambers components to prevent possible deterioration and performance issues.
- Once cycle constitutes 24 hours, which involves 8 hours of deep freeze at 0 degrees Fahrenheit, 8 hours of drying and UV exposure, and 8 hours of 5 percent salt solution spray exposure.
- The salt water solution is recirculated during each cycle, and replaced with fresh salt water solution after each cycle.
- Regular preventative maintenance on the Chamber for Accelerated Testing ensures a well performing automatic system.

CHAPTER 8 – DURABILITY TESTS: THIN COATINGS

8.1 Introduction

The outdoor corrosion of painted metals is influenced by many factors, including: corrosive atmospheres, rain, condensed dew, UV light, wet/dry cycling, and temperature cycling. These factors frequently have a synergistic effect on one another (ASTM D5894, 2016). As discussed in previous chapters, a new testing procedure has been developed to better simulate actual field deterioration conditions on thin coating paints with all of these factors combined. Unfortunately, current over coating performance evaluations do not provide an indicator of actual field performance for over coating paints. This chapter discusses the new procedure for specimen preparation, evaluation and result interpretation for the developed accelerated testing system.

8.2 Thin Coating Specimen Preparation

For this developed evaluation, 2 inch by 2 inch by 12 inch (long) thin coated steel angle specimens were used to simulate typical steel bridge components. Two ½ inch diameter holes were drilled thru one leg of the angle, and on the other leg there were 1-inch long line welds (Figure 8.1 and 8.2). The line welds help accelerate corrosion due to chemical changes, and the holes simulate any possible pitting corrosion. The surface of the steel angle conformed to the paint manufacturers required surface preparation prior to painting by the use of an Aurand hand held steel toothed cleaning machine (figure 8.4). For each face of the angle, five plastic O-rings were attached using a water-soluble glue (figure 8.3). The dimensions of the O-rings are an inner diameter of 20.6 millimeter, and an outer diameter of 23.8 millimeters. The plastic O-rings are removed after painting to

create the scribe for the salt solution penetration. The painted circle area within the scribe formed in the specimen will be the location where a 20 millimeter pull off dolly will be attached for tensile strength testing, without the requirement to remove or damage any painted area for the evaluation.



Figure 8.1 – Typical ½ inch diameter holes in steel specimens



Figure 8.2 - Typical 1-inch-long welds on steel specimens



Figure 8.3 – O-rings attached to steel specimen



Figure 8.4 - Aurand hand held steel toothed cleaning machine

After the water-soluble glue has cured, the specimens were sprayed with New Jersey Department of Transportation approved thin coat paint systems for bridges. The paint systems were applied on the steel specimens by the use of a low-pressure sprayer (figure 8.5). A low-pressure sprayer for paint application has the advantage of providing easy thickness control for achieving uniform application along the specimen (figure 8.6). To provide quality assurance for spray coverage and that the specimens meet the paint manufacturers application specifications, a PosiTest[®] DFT – dry film thickness gage was used. The gage determines if the thickness of the over coated specimen conforms to the manufacturers specifications as well as uniformity of application (for all layers) along the specimen (figure 8.7).

After the over coating paint layers have cured (as per manufacturer specification), the O-Rings are then removed, leaving approximately a 3-millimeter-wide exposed steel scribe

around painted circles with 20 millimeter diameters. This simulates possible damages that may be caused in the field. Any residue from the water soluble glue is carefully rinsed with water and scrubbed off. Figure 8.8 is an example of a painted steel specimen with the O-rings removed. The over coated steel specimen is then prepared to begin testing.



Figure 8.5 – Low Pressure Spray Apparatus



Figure 8.6 – Spray Painting Specimens



Figure 8.7 – Thickness gage used for measuring the thickness of paint layers

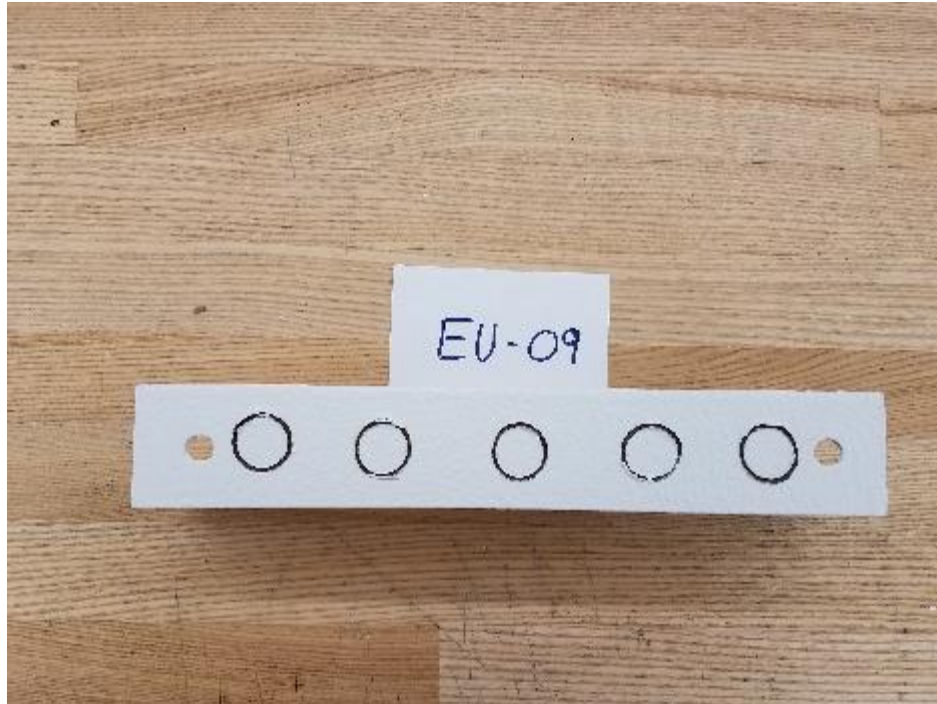


Figure 8.8 – Painted steel specimen with O-rings removed

8.3 Test Procedure

The thin coated specimens after the required curing time (as specified by the manufacturer), are placed into the chamber for accelerated testing; undergoing the cyclical wetting, drying, and freezing procedure outlined in chapter 6. The response variables for this evaluation are:

- Pull off testing
- Color change
- Thickness change
- Visual inspection

8.3.1 Response Variable: Pull Off Testing

Before placement of the specimens in the chamber for accelerated testing, the virgin over coated specimen pull off strength must be determined. To conduct the pull off testing, 20 millimeter pull off dollies are adhered to the circular painted areas within the scribe using a two-part manufacturer supplied epoxy and are required to have a minimum of 24 hours to cure (figure 8.12). The standard requires the use of a scoring tool (circular hole cutter), to score through the over coating paint to ensure that the pull off dolly is placed on a surface area equivalent to the dolly surface area. Since the surface area within the scribe is equal to the surface area of the dolly, the scoring tool is not needed. Hence no damage to the paint or corroded areas has to take place, and potentially disrupt the pull off result. Twenty-four hours after the epoxy has cured, pull off testing is then conducted on the specimens following the guidelines of ASTM D4541, Standard Test Method for Pull-Off Strength of Coatings Using Portable Adhesion Testers. The pull off tester used is a PosiTest[®] AT-M Manual Adhesion Tester. The tensile load is then applied at a constant rate of 150 psi/s (1 MPa/s) or less, but finishing the test within 100 seconds. After each failure, the tensile stress and failure mode are recorded. The pull off dollies are then labeled and kept for comparison. Once testing has been completed, the over coated steel specimens are then placed into the chamber for accelerated testing to begin evaluation.

After the required number of master cycles in the chamber for accelerated testing, the over coated steel specimens are then removed from the chamber. The specimens are rinsed with clean water to remove any debris or residue, then gently dried with compressed air. Following the cleaning, 20 millimeter pull off dollies are then adhered to

the circular painted areas within the scribe using a two-part manufacturer supplied epoxy and are required to have a minimum of 24 hours to cure (figure 8.9). Twenty-four hours after the epoxy has cured, pull off testing is then conducted on the specimens following the guidelines of ASTM D 4541, Standard Test Method for Pull-Off Strength of Coatings Using Portable Adhesion Testers. The pull off tester used is a PosiTest[®] AT-M Manual Adhesion Tester. The tensile load is then applied at a constant rate of 150 psi/s (1 MPa/s) or less, but finishing the test within 100 seconds. After each failure, the tensile stress and failure mode are recorded. The pull off dollies are then labeled and kept for comparison. Once testing has been completed, the over coated steel specimens are then placed into the chamber for accelerated testing for continued experimentation.



Figure 8.9 – 20 Millimeter Pull Off Dolly: Epoxied to Thin Coated Steel Specimen

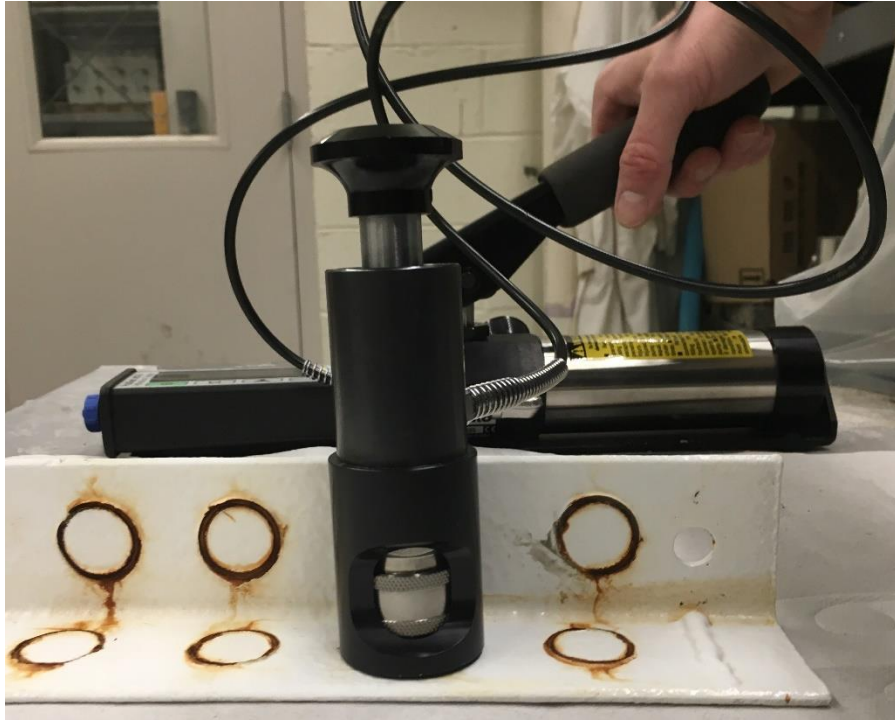


Figure 8.10 – Typical Pull Test

8.3.2 Interpretation of Pull off Test Result

The pull off strengths from the over coated steel specimens are converted to corrosion (rust) creep using equivalent diameter calculations. As the pull off strength goes down as the contact area decreases, it is assumed that the pull off strength determined from the virgin sample is retained in the un-corroded areas. Therefore, the un-corroded area can be converted to the radius of a circle that is not corroded. Hence corrosion creep can be estimated by subtracting this radius from the original radius (10 millimeter). The following example further explains the calculation.

1. Pull-off strength for the virgin sample = 800 psi or 400 lb (area of 20 mm circle is 0.5 Sq inch)
2. Pull-off strength at a given exposure, 400 psi or 200 lb

3. Assuming the original adhesive strength is same in un-corroded areas, un-corroded area = $200/800$ Sq. inch.
4. Radius of un-corroded area = Square root of $(200/\{800 \times 3.14\}) = 0.28$ in or 7.2 mm
5. Corrosion Creep = original radius of 10 mm- radius after corrosion
6. Corrosion Creep = $10 - 7.2 = 2.8$ mm
 - Note: this provides an average of the corrosion growth around the diameter of 20 mm

8.3.3 Response Variable: Color Change

To determine the color change for the over coating steel paints a colorimeter was used to determine the, a^* , b^* , and L^* coordinates. Defined by the Commission Internationale de l'Eclairage (CIE), the L^* , a^* , b^* color space was modeled after a color-opponent theory stating that two colors cannot be red and green at the same time or yellow and blue at the same time. L^* indicates lightness, a^* is the red/green coordinate, and b^* is the yellow/blue coordinate. For each over coated steel specimen, a Konica Minolta CR-10 Plus color reader (colorimeter) is used to analyze the a^* , b^* , and L^* coordinates on three non-corroded sections. The values from the three readings are recorded and averaged together. Colorimeter recordings are taken at cycle 0 (virgin specimens), and cycle 100, when the specimens have completed the accelerated corrosion testing. At master cycle 100, before the colorimeter recording, the samples are cleaned with potable water to remove any rust bleeding or debris.



Figure 8.11 - Konica Minolta CR-10 Plus Color Reader

8.3.4 Response Variable: Thickness Change

To determine the thickness change for the over coating steel paints a PosiTest[®] DFT – dry film thickness gage was used to determine the any deterioration of the over coating paint thickness due to the chamber for accelerated testing. For each over coated steel specimen, the thickness gage is used to analyze three non-corroded sections. The values from the three readings are recorded and averaged together. Thickness gage recordings are taken at cycle 0 (virgin specimens), and cycle 100, when the specimens have completed the accelerated corrosion testing. At the cycle 100, before the thickness gage recording, the samples are cleaned with potable water to remove any rust bleeding or debris.

8.3.5 Response Variable: Visual Inspection

Visual inspection is used to determine significant changes particular to the bolt holes, weld spots and edges where deterioration is expected on a daily basis. If any significant deterioration changes are detected, the cycle and location of the deterioration is recorded.

8.4 Test Results

Table 8.1 shows the different thin coating systems tested for this new protocol. Table 8.2 displays each thin coating systems allowable minimum and maximum thickness. Figures 8.12 to 8.16 display the results from the pull off tests versus master cycles for each of the over coating systems. Figures 8.17 to 8.21 present the creep of corrosion and the calculated effective radius of the thin coating systems. Table 8.9 to 8.13 displays the color recordings for each system. Table 8.14 displays the percent change in the color recordings from cycle 0 to cycle 100. Table 8.15 to 8.19 shows the visual inspection recordings. Figure 8.23 and 8.24 compares the poor and best performing thin coating systems corrosion creep on the 20 millimeter pull off test dollies.

Thin Coating System	Primer Layer	Intermediate Layer	Top Layer
1	Phenalkamine Epoxy	N/A	Aliphatic Acrylic-Polyester Polyurethane
2	Polyamine Bisphenol A Epoxy	N/A	Acrylic Polyurethane
3	Epoxy	N/A	Aliphatic Urethane
4	Polyamide Epoxy - Organic Zinc Rich	Polyamide Epoxy	Aliphatic Acrylic Polyurethane
5	Solvent Based Inorganic Zinc	Cycloaliphatic Amine Epoxy	Aliphatic Acrylic-Polyester Polyurethane

Table 8.1 – Thin Coating Systems

Thin Coating System:	1	2	3	4	5
Minimum Overall Thickness (microns):	175	203	200	275	229
Maximum Overall Thickness (microns):	275	381	350	525	355

Table 8.2 – Thin Coating Systems Allowable Minimum & Maximum Thickness

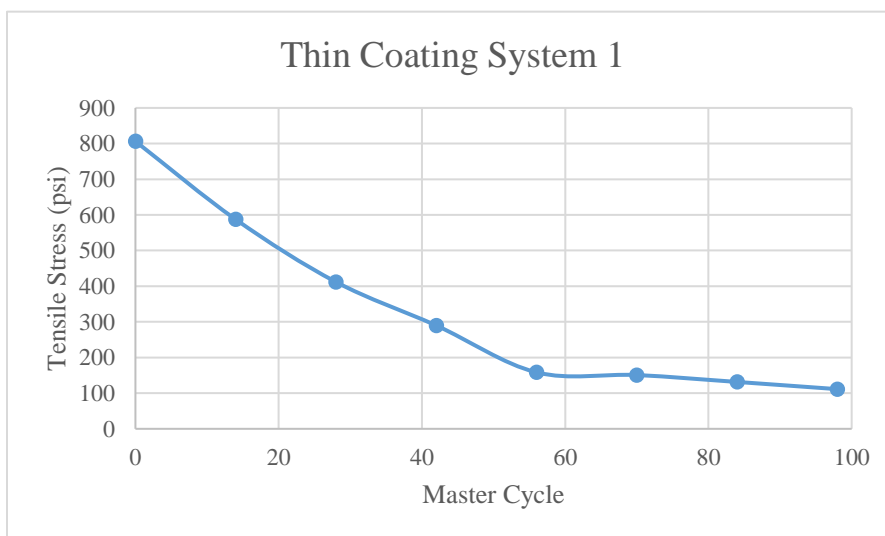


Figure 8.12 - Direct Tensile Stress versus Master Cycles: Thin Coating System 1

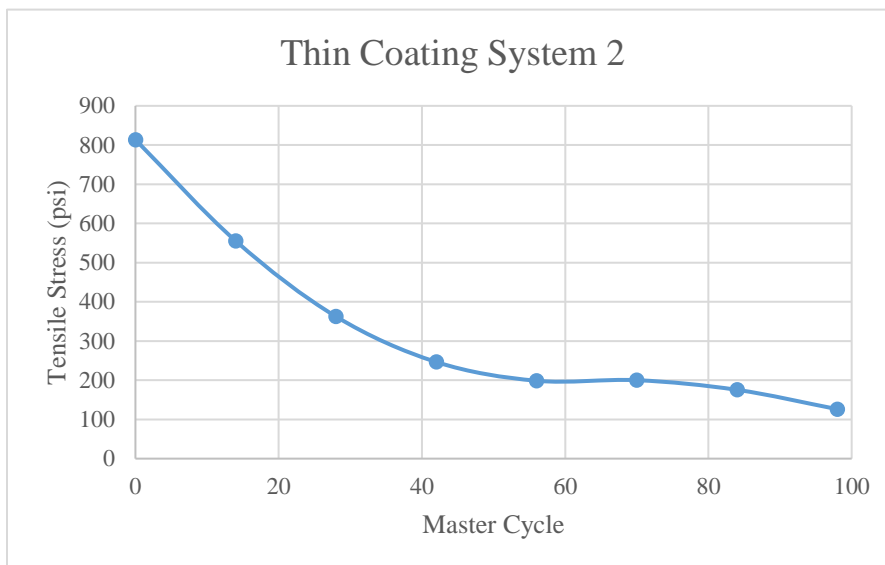


Figure 8.13 - Direct Tensile Stress versus Master Cycles: Thin Coating System 2

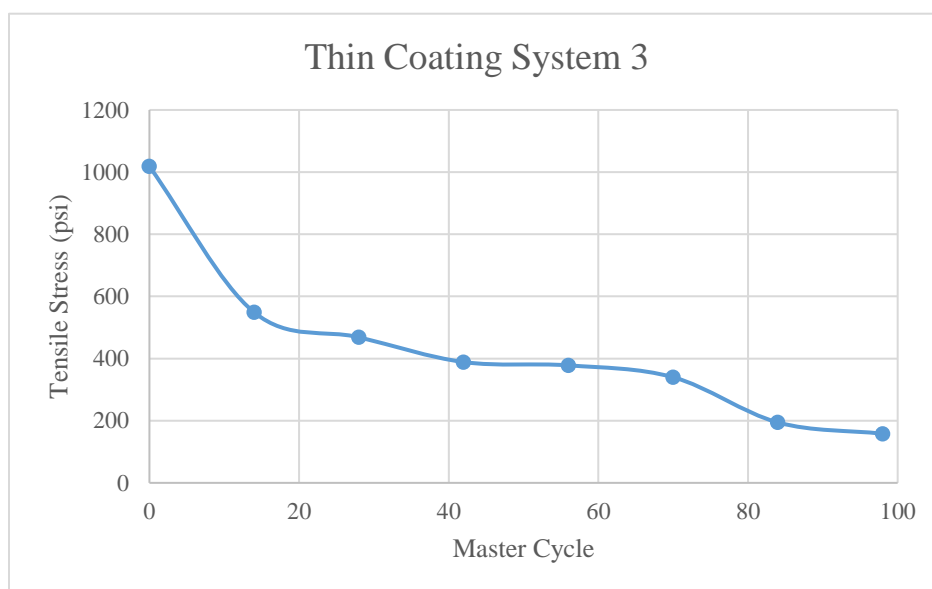


Figure 8.14 - Direct Tensile Stress versus Master Cycles: Thin Coating System 3

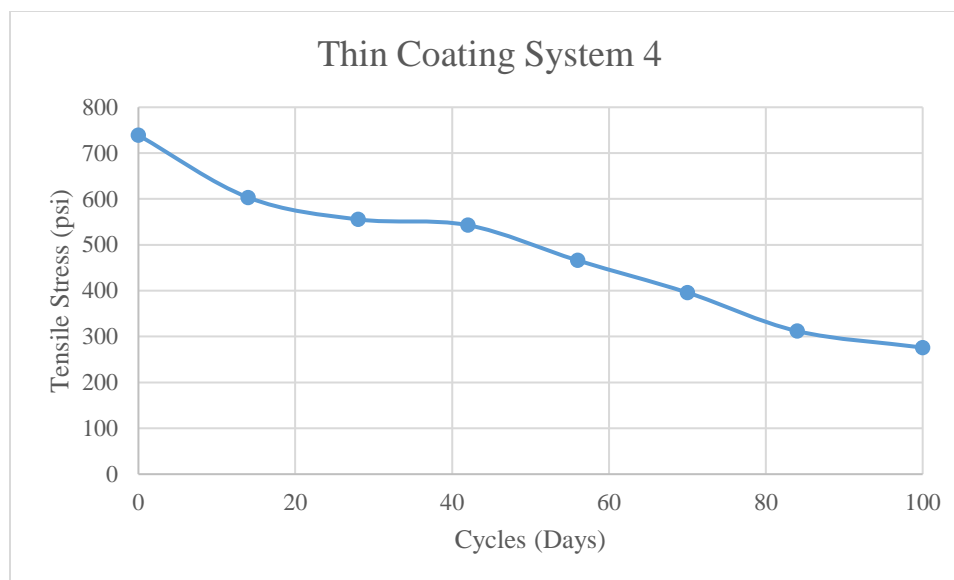


Figure 8.15 - Direct Tensile Stress versus Master Cycles: Thin Coating System 4

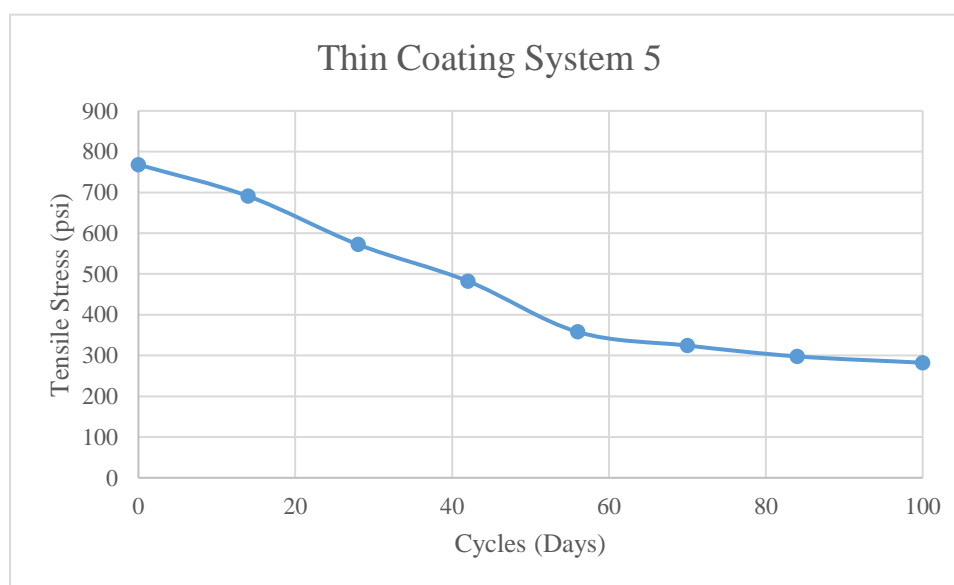


Figure 8.16 - Direct Tensile Stress versus Master Cycles: Thin Coating System 5

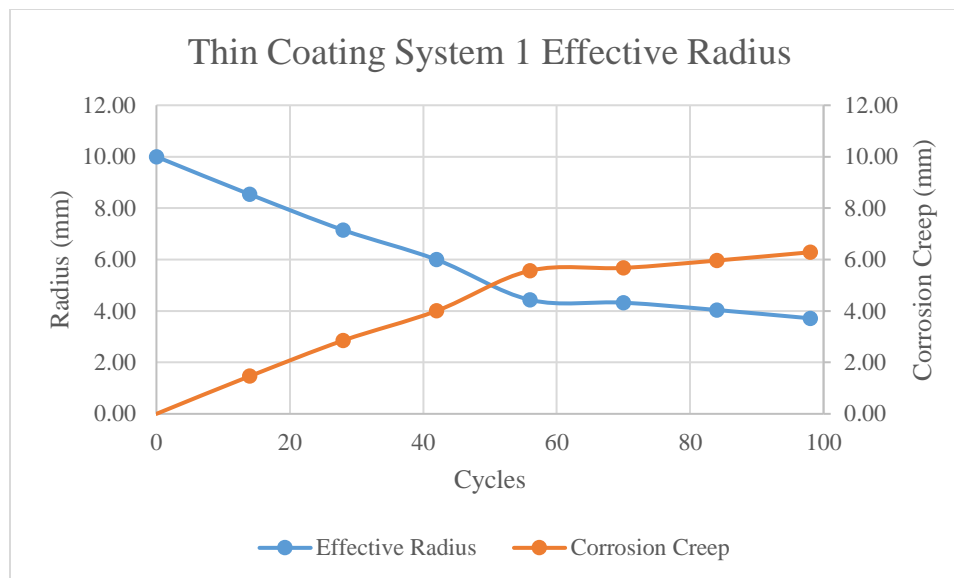


Figure 8.17 - Effective Radius versus Cycles: Thin Coating System 1

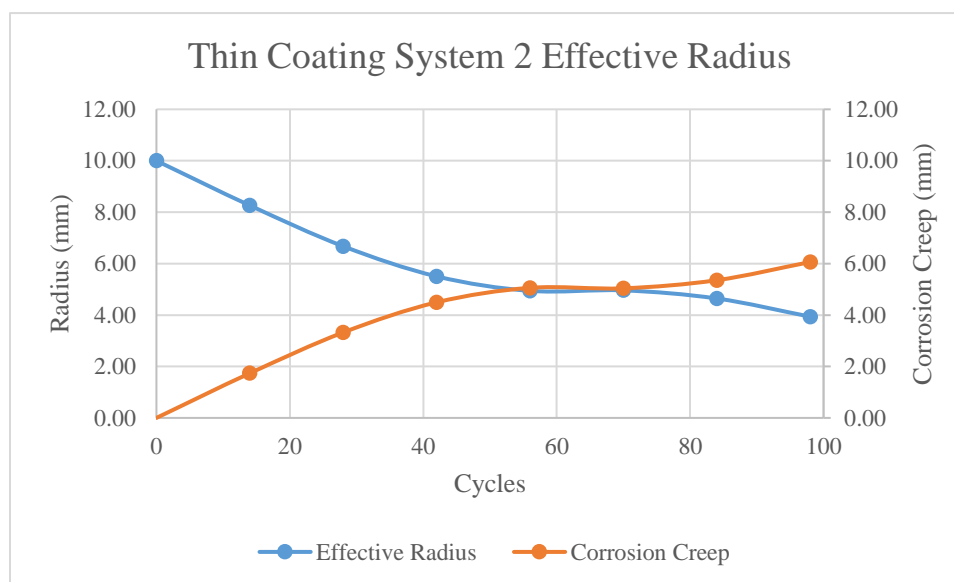


Figure 8.18 - Effective Radius versus Cycles: Thin Coating System 2

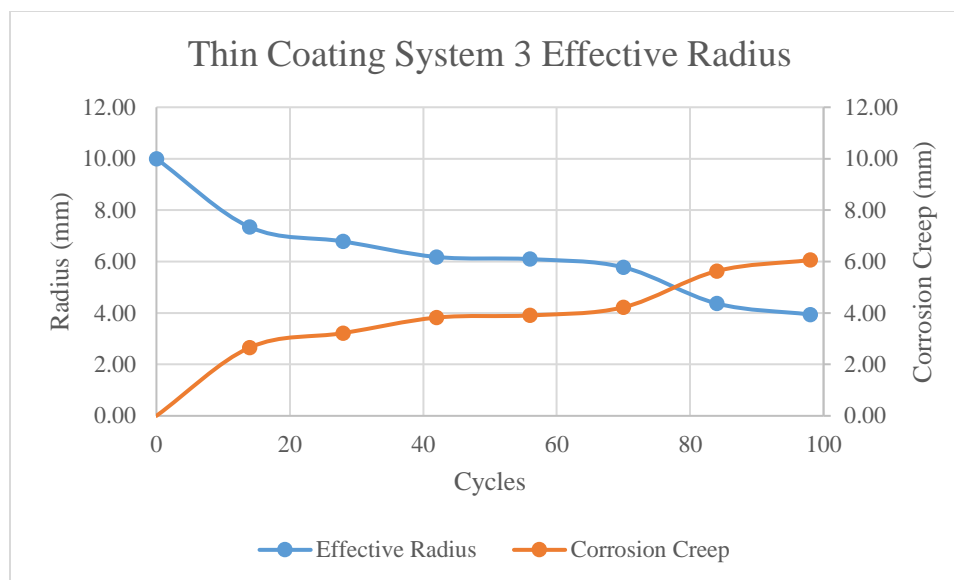


Figure 8.19 - Effective Radius versus Cycles: Thin Coating System 3

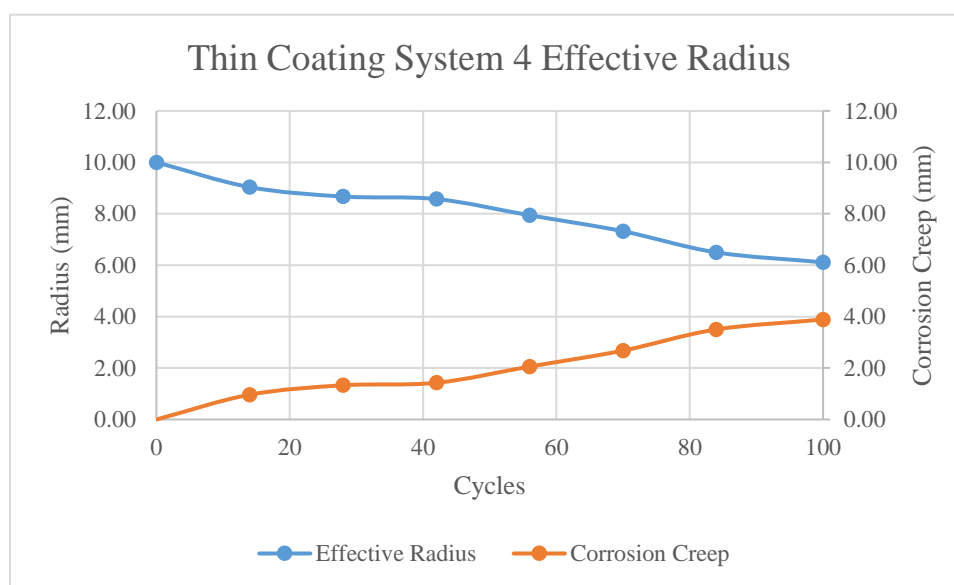


Figure 8.20 - Effective Radius versus Cycles: Thin Coating System 4

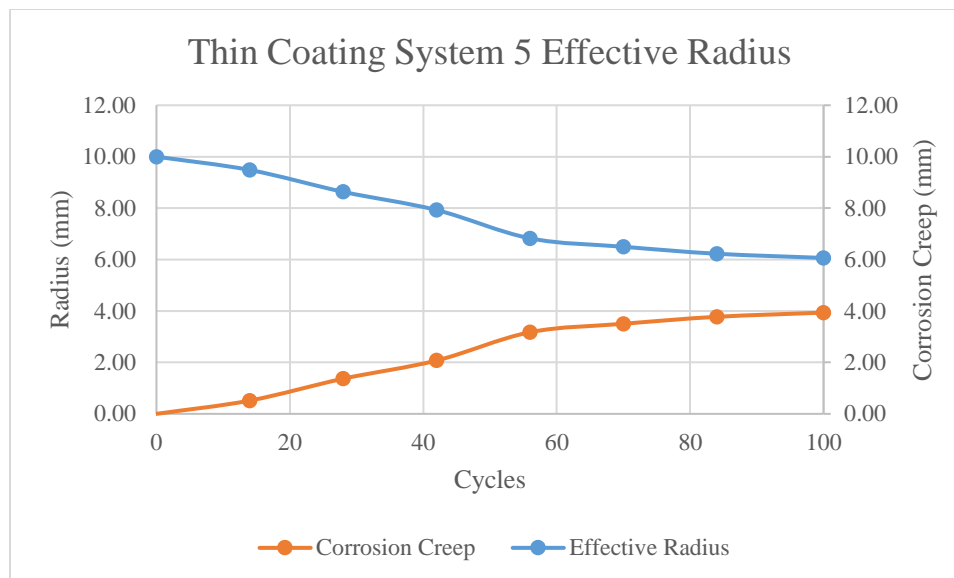


Figure 8.21 - Effective Radius versus Cycles: Thin Coating System 5

		Thin Coating System 1											
		Cycle 0 (Virgin Specimen)					Cycle 100						
Recording (microns):		1	2	3	4	5	1	2	3	4	5		
Sample 1	Leg 1	182	221	210	214	275	229	220	178	193	196		
	Leg 2	205	195	213	229	193	223	196	255	197	216		
	Leg 3	240	141	194	268	205	270	270	260	179	235		
	Leg 4	218	235	176	180	261	179	250	264	201	208		
Sample 2	Leg 1	269	296	300	281	258	209	203	186	243	252		
	Leg 2	201	175	239	271	218	176	196	184	208	190		
	Leg 3	217	205	218	254	202	270	222	225	236	195		
	Leg 4	189	194	181	234	195	237	192	263	235	178		
Sample 3	Leg 1	219	275	211	188	200	248	207	192	234	258		
	Leg 2	273	258	267	215	205	249	178	231	245	216		
	Leg 3	205	166	205	254	286	212	180	198	190	262		
	Leg 4	260	185	187	204	205	254	213	264	206	257		
Sample 4	Leg 1	216	237	208	196	198	269	201	224	260	247		
	Leg 2	205	205	207	239	247	266	208	231	233	250		
	Leg 3	207	245	194	261	233	188	213	198	203	198		
	Leg 4	196	264	205	205	270	270	201	204	208	204		
Sample 5	Leg 1	217	236	242	207	205	269	257	224	236	216		
	Leg 2	194	181	260	183	185	211	255	203	222	275		
	Leg 3	209	270	264	184	205	254	248	206	280	297		
	Leg 4	222	256	214	175	221	239	235	246	257	277		
Sample 6	Leg 1	283	239	290	297	275	222	250	235	201	230		
	Leg 2	290	182	230	247	219	185	179	234	205	185		
	Leg 3	259	227	199	205	194	190	202	202	207	245		
	Leg 4	191	205	207	212	254	184	189	201	196	204		
					Avg.	223						Avg.	223
					S.D.	34						S.D.	29

Table 8.3 – Thickness Readings: Thin Coating System 1

		Thin Coating System 2											
		Cycle 0 (Virgin Specimen)					Cycle 100						
		Recording (microns):	1	2	3	4	5	1	2	3	4	5	
Sample 1	Leg 1	235	261	304	245	352	301	283	309	366	296		
	Leg 2	349	432	385	271	307	357	245	258	309	313		
	Leg 3	235	233	203	233	239	315	283	357	376	263		
	Leg 4	218	218	201	268	245	325	222	286	288	249		
Sample 2	Leg 1	254	215	205	270	214	347	362	265	340	206		
	Leg 2	190	221	314	282	336	342	332	255	327	272		
	Leg 3	222	231	246	209	248	284	245	266	345	245		
	Leg 4	372	279	262	254	304	296	275	289	367	267		
Sample 3	Leg 1	281	290	376	405	380	278	253	255	299	299		
	Leg 2	282	399	453	301	379	257	221	278	309	259		
	Leg 3	299	182	322	304	330	246	272	267	278	278		
	Leg 4	218	264	243	226	169	318	259	217	302	302		
Sample 4	Leg 1	212	302	328	283	323	378	248	266	372	297		
	Leg 2	280	250	296	380	274	257	324	260	364	245		
	Leg 3	233	255	278	214	322	246	287	270	302	249		
	Leg 4	337	280	346	205	238	318	308	302	286	227		
Sample 5	Leg 1	272	315	404	365	312	348	258	283	307	220		
	Leg 2	240	268	300	239	315	289	378	373	250	283		
	Leg 3	422	320	275	238	329	224	224	218	273	292		
	Leg 4	256	196	258	305	289	311	313	218	288	275		
Sample 6	Leg 1	335	354	312	343	320	252	304	365	248	243		
	Leg 2	324	239	332	299	342	236	315	255	255	250		
	Leg 3	205	380	318	315	353	221	301	245	248	232		
	Leg 4	276	329	235	239	223	280	312	305	222	228		
					Avg.	286						Avg.	284
					S.D.	59						S.D.	42

Table 8.4 – Thickness Readings: Thin Coating System 2

		Thin Coating System 3											
		Cycle 0 (Virgin Specimen)					Cycle 100						
Recording (microns):		1	2	3	4	5	1	2	3	4	5		
Sample 1	Leg 1	239	273	262	231	261	296	219	219	261	276		
	Leg 2	235	236	210	214	207	253	296	269	228	211		
	Leg 3	201	209	246	292	211	276	280	280	209	269		
	Leg 4	268	229	212	249	236	220	224	224	269	272		
Sample 2	Leg 1	210	152	292	239	258	222	226	226	245	202		
	Leg 2	257	199	226	216	257	237	274	274	242	260		
	Leg 3	216	194	234	298	217	214	215	215	257	203		
	Leg 4	245	249	206	287	215	209	214	244	201	265		
Sample 3	Leg 1	218	216	205	202	239	253	209	209	244	241		
	Leg 2	297	181	225	298	298	269	211	201	257	208		
	Leg 3	271	228	205	209	207	185	231	244	275	245		
	Leg 4	289	266	279	272	293	217	234	257	264	226		
Sample 4	Leg 1	241	223	262	215	231	289	219	275	296	227		
	Leg 2	223	236	201	295	271	294	206	264	247	251		
	Leg 3	269	208	200	285	207	240	247	214	268	243		
	Leg 4	213	249	277	254	200	275	288	259	233	269		
Sample 5	Leg 1	288	285	225	221	292	264	281	232	224	223		
	Leg 2	234	206	202	226	283	297	207	253	250	223		
	Leg 3	218	261	226	289	280	240	244	244	226	211		
	Leg 4	272	283	298	279	201	287	265	256	207	216		
Sample 6	Leg 1	297	280	311	242	279	224	263	257	208	262		
	Leg 2	220	227	296	208	279	204	240	259	212	261		
	Leg 3	231	244	264	235	227	216	244	208	220	212		
	Leg 4	215	287	240	296	282	284	202	273	240	218		
					Avg.	244						Avg.	242
					S.D.	34						S.D.	27

Table 8.5 – Thickness Readings: Thin Coating System 3

		Thin Coating System 4											
		Cycle 0 (Virgin Specimen)					Cycle 100						
		Recording (microns):	1	2	3	4	5	1	2	3	4	5	
Sample 1	Leg 1	299	351	277	300	294	345	294	353	375	326		
	Leg 2	360	315	300	324	360	285	333	278	281	333		
	Leg 3	286	372	292	330	304	300	363	278	271	340		
	Leg 4	303	291	297	322	351	310	339	337	302	319		
Sample 2	Leg 1	316	296	369	288	318	290	376	339	332	318		
	Leg 2	343	303	272	368	293	278	282	350	361	330		
	Leg 3	322	313	340	372	341	320	330	330	282	311		
	Leg 4	318	352	277	371	315	316	337	311	256	315		
Sample 3	Leg 1	329	341	327	311	294	365	277	278	345	276		
	Leg 2	333	330	336	373	327	289	313	244	286	279		
	Leg 3	304	322	360	297	303	280	288	376	360	347		
	Leg 4	395	340	345	309	288	375	324	284	351	393		
Sample 4	Leg 1	298	325	292	370	328	285	317	360	341	309		
	Leg 2	316	288	307	367	339	346	343	333	369	295		
	Leg 3	280	343	266	301	330	278	363	363	295	282		
	Leg 4	324	373	296	353	348	359	350	306	348	315		
Sample 5	Leg 1	323	324	351	344	324	296	301	292	330	347		
	Leg 2	359	358	336	365	291	366	308	331	333	350		
	Leg 3	321	300	365	314	404	288	323	298	303	298		
	Leg 4	295	339	304	336	288	370	301	364	308	304		
Sample 6	Leg 1	260	288	290	321	363	369	357	342	336	316		
	Leg 2	359	306	292	398	424	311	355	304	322	278		
	Leg 3	306	364	303	289	301	354	348	306	280	279		
	Leg 4	374	334	351	367	331	339	335	346	276	277		
					Avg.	326						Avg.	320
					S.D.	32						S.D.	32

Table 8.6 – Thickness Readings: Thin Coating System 4

		Thin Coating System 5											
		Cycle 0 (Virgin Specimen)					Cycle 100						
		Recording (microns):	1	2	3	4	5	1	2	3	4	5	
Sample 1	Leg 1	293	320	281	281	327	355	368	322	357	304		
	Leg 2	322	331	351	382	368	307	313	357	243	313		
	Leg 3	302	355	368	297	373	289	293	343	287	298		
	Leg 4	318	297	309	295	320	231	315	303	274	259		
Sample 2	Leg 1	305	340	300	314	314	295	309	327	250	351		
	Leg 2	363	304	304	363	363	246	203	294	317	316		
	Leg 3	373	281	343	372	372	293	336	350	330	327		
	Leg 4	302	295	340	339	339	243	284	325	290	354		
Sample 3	Leg 1	320	294	351	304	375	301	226	370	283	338		
	Leg 2	302	371	378	350	357	295	357	326	258	316		
	Leg 3	303	283	349	299	374	366	302	225	280	338		
	Leg 4	351	371	347	289	288	416	228	259	315	325		
Sample 4	Leg 1	361	374	353	359	308	367	296	350	292	285		
	Leg 2	280	287	370	288	375	342	363	360	283	303		
	Leg 3	282	307	343	349	282	329	376	357	301	340		
	Leg 4	300	367	312	326	350	260	353	375	284	284		
Sample 5	Leg 1	294	292	283	283	308	310	263	298	263	299		
	Leg 2	297	343	295	292	313	353	276	292	243	281		
	Leg 3	264	366	293	350	289	343	277	328	371	315		
	Leg 4	352	309	332	334	303	289	278	373	279	360		
Sample 6	Leg 1	393	343	378	308	303	282	360	295	332	360		
	Leg 2	343	389	326	382	301	283	293	302	291	313		
	Leg 3	389	376	412	319	291	281	363	295	324	413		
	Leg 4	393	390	368	384	351	293	272	360	327	297		
					Avg.	331						Avg.	310
					S.D.	35						S.D.	41

Table 8.7 – Thickness Readings: Thin Coating System 5

Thin Coating System	Average Thickness Change (%)
1	0.0
2	0.7
3	0.8
4	1.9
5	6.3

Table 8.8 – Average Thickness Change

	Thin Coating System 1					
	Cycle 0			Cycle 100		
	L*	a*	b*	L*	a*	b*
Sample 1	92.4	0.2	1.2	89.2	0.9	10.6
Sample 1	92.4	0.3	1.6	91.3	0.6	6.9
Sample 1	93.7	0.1	1.0	90.8	0.4	6.4
Sample 2	92.2	0.3	1.2	90.1	0.7	4.7
Sample 2	92.3	0.3	1.3	91.9	0.5	3.4
Sample 2	92.5	0.3	1.3	91.7	0.3	11.8
Sample 3	94.2	0.2	1.4	90.8	0.6	5.8
Sample 3	94.0	0.1	1.1	90.7	0.3	4.2
Sample 3	92.0	0.4	1.7	92.6	0.4	8.0
Average:	92.9	0.2	1.3	91.0	0.5	6.9
Standard Deviation:	0.8	0.1	0.2	1.0	0.2	2.7
Coefficient of Variation:	0.9	39.1	16.3	1.0	35.9	39.1

Table 8.9 - Color Recordings: Thin Coating System 1

	Thin Coating System 2					
	Cycle 0			Cycle 100		
	L*	a*	b*	L*	a*	b*
Sample 1	88.2	-0.2	2.9	86.0	-0.2	4.7
Sample 1	88.0	-0.1	3.1	86.8	-0.2	4.7
Sample 1	88.1	-0.1	2.9	87.2	-0.4	3.9
Sample 2	88.0	-0.1	3.1	85.8	-0.2	3.9
Sample 2	87.5	-0.3	3.2	85.7	-0.2	3.8
Sample 2	88.5	-0.1	2.8	85.4	-0.4	3.7
Sample 3	88.5	-0.3	3.4	83.4	-0.3	3.2
Sample 3	88.1	-0.2	3.0	83.7	-0.6	3.5
Sample 3	88.4	-0.1	3.0	83.9	-0.4	3.0
Average:	88.1	-0.2	3.0	85.3	-0.3	3.8
Standard Deviation:	0.3	0.1	0.2	1.3	0.1	0.6
Coefficient of Variation:	0.3	-49.0	5.6	1.5	-40.8	14.4

Table 8.10 - Color Recordings: Thin Coating System 2

	Thin Coating System 3					
	Cycle 0			Cycle 100		
	L*	a*	b*	L*	a*	b*
Sample 1	95.5	0.5	1.3	95.4	0.9	2.4
Sample 1	95.6	0.5	0.9	95.3	0.9	2.4
Sample 1	94.0	0.4	0.9	93.6	0.9	2.2
Sample 2	96.1	0.5	1.1	95.3	1.1	2.5
Sample 2	95.2	0.6	1.2	95.5	1.2	2.2
Sample 2	95.3	0.4	1.2	95.7	1.0	2.8
Sample 3	94.6	0.4	0.7	95.2	1.0	2.5
Sample 3	95.3	0.5	1.0	93.4	1.0	2.1
Sample 3	94.7	0.4	0.7	93.8	1.0	2.3
Average:	95.1	0.5	1.0	94.8	1.0	2.4
Standard Deviation:	0.6	0.1	0.2	0.9	0.1	0.2
Coefficient of Variation:	0.6	14.3	20.5	0.9	9.4	8.4

Table 8.11 - Color Recordings: Thin Coating System 3

	Thin Coating System 4					
	Cycle 0			Cycle 100		
	L*	a*	b*	L*	a*	b*
Sample 1	52.6	-5.5	-6.0	52.8	-5.9	-4.6
Sample 1	53.5	-5.7	-6.2	50.9	-5.3	-3.6
Sample 1	53.6	-5.7	-6.3	53.8	-5.6	-4.6
Sample 2	51.7	-5.4	-6.1	53.6	-5.5	-5.0
Sample 2	52.5	-5.5	-6.0	53.3	-5.7	-4.7
Sample 2	52.8	-5.6	-6.0	51.9	-5.8	-4.7
Sample 3	52.9	-5.6	-5.9	53.1	-6.0	-4.6
Sample 3	53.9	-5.7	-6.1	51.3	-5.7	-3.0
Sample 3	50.9	-5.3	-5.9	51.7	-5.8	-3.5
Average:	52.7	-5.6	-6.1	52.5	-5.7	-4.3
Standard Deviation:	0.9	0.1	0.1	1.0	0.2	0.7
Coefficient of Variation:	1.7	-2.4	-2.1	1.9	-3.5	-15.4

Table 8.12 - Color Recordings: Thin Coating System 4

	Thin Coating System 5					
	Cycle 0			Cycle 100		
	L*	a*	b*	L*	a*	b*
Sample 1	55.1	-30.3	10.6	53.5	-28.9	11.7
Sample 1	53.0	-29.0	10.4	55.1	-28.1	10.9
Sample 1	54.6	-30.0	10.6	54.1	-30.1	11.2
Sample 2	55.0	-30.2	10.6	54.2	-28.2	11.4
Sample 2	54.7	-30.2	10.7	55.7	-31.2	13.5
Sample 2	54.3	-29.9	10.6	55.2	-30.1	12.4
Sample 3	55.3	-30.2	10.8	54.0	-31.1	11.9
Sample 3	56.1	-31.4	11.3	55.6	-30.1	12.5
Sample 3	55.9	-31.6	11.3	54.3	-27.1	13.5
Average:	54.9	-30.3	10.8	54.6	-29.4	12.1
Standard Deviation:	0.9	0.7	0.3	0.7	1.3	0.9
Coefficient of Variation:	1.6	-2.4	2.8	1.3	-4.6	7.3

Table 8.13 - Color Recordings: Thin Coating System 5

	Difference (%)		
	L*	a*	b*
System 1	2.0	-113.6	-423.7
System 2	3.2	-93.3	-25.5
System 3	0.4	-114.3	-137.8
System 4	0.4	-2.6	29.7
System 5	0.5	2.9	-12.5

Table 8.14 - Color Recordings: Percent Change from Cycle 0 to Cycle 100

Thin Coating System 1		
Specimen	Location of Deterioration	Cycle of Deterioration
1	Hole, Weld	42
2	Weld	42
3	Hole	56
4	Hole	42
5	Weld	42
6	Hole, Weld	42

Table 8.15 - Visual Inspection: Thin Coating System 1

Thin Coating System 2		
Specimen	Location of Deterioration	Cycle of Deterioration
1	Weld	42
2	Weld	42
3	Weld	42
4	Hole	42
5	Hole, Weld	42
6	N/A	N/A

Table 8.16 - Visual Inspection: Thin Coating System 2

Thin Coating System 3		
Specimen	Location of Deterioration	Cycle of Deterioration
1	N/A	N/A
2	Weld	42
3	Hole	42
4	Hole, Weld	42
5	Weld	42
6	Weld	42

Table 8.17 - Visual Inspection: Thin Coating System 3

Thin Coating System 4		
Specimen	Location of Deterioration	Cycle of Deterioration
1	N/A	N/A
2	N/A	N/A
3	N/A	N/A
4	N/A	N/A
5	N/A	N/A
6	N/A	N/A

Table 8.18 - Visual Inspection: Thin Coating System 4

Thin Coating System 5		
Specimen	Location of Deterioration	Cycle of Deterioration
1	N/A	N/A
2	N/A	N/A
3	N/A	N/A
4	N/A	N/A
5	N/A	N/A
6	N/A	N/A

Table 8.19 - Visual Inspection: Thin Coating System 5

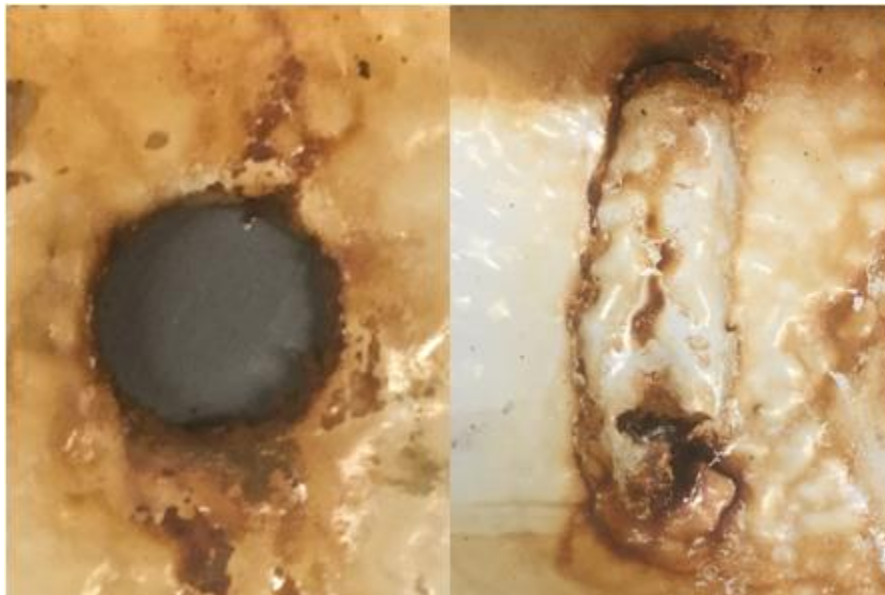


Figure 8.22 – Typical Corrosion Pitting at Simulated Bolt Hole & Weld

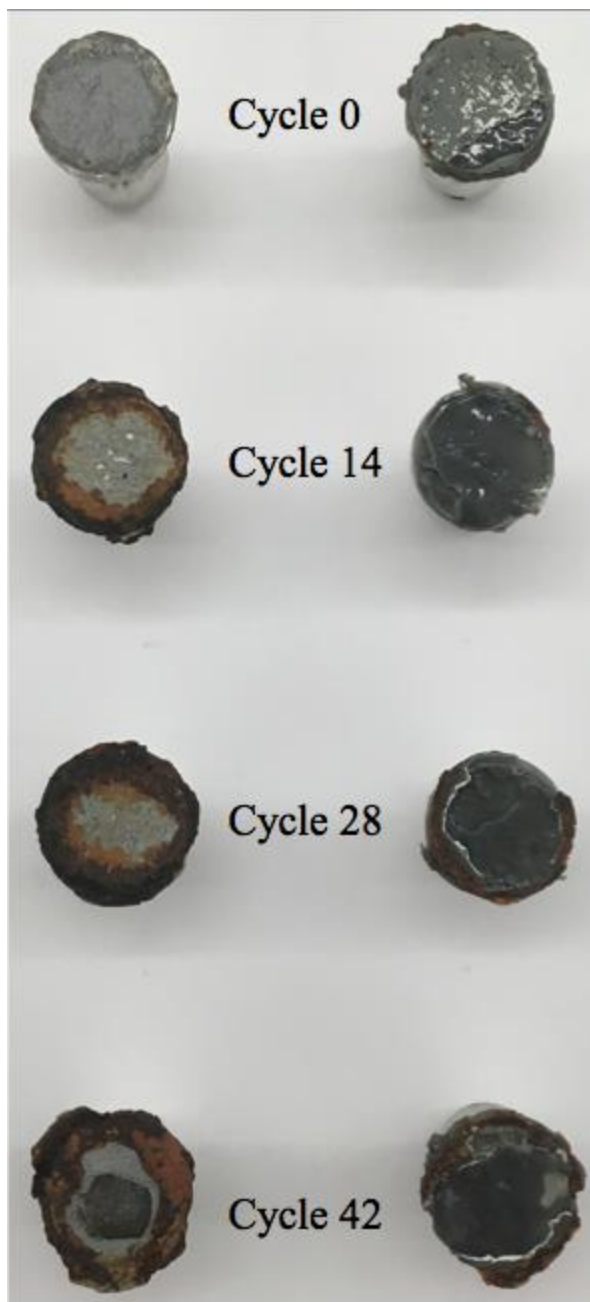


Figure 8.23 – Poor & Best Performing Thin Coating System Pull Test Dollies: Cycle 0 to Cycle 42

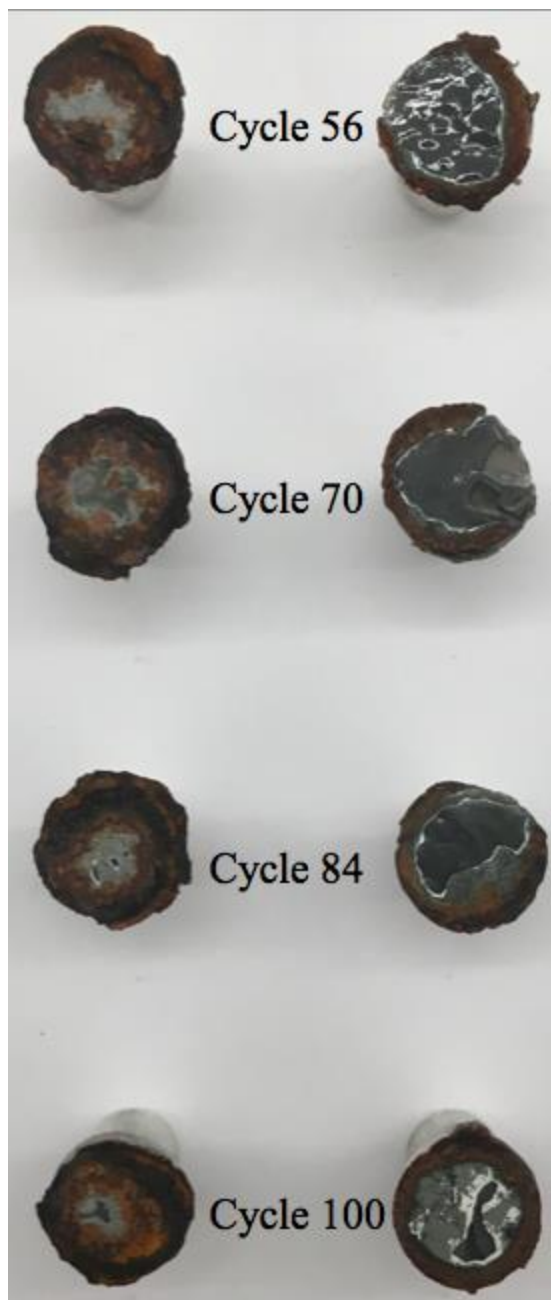


Figure 8.24 – Poor & Best Performing Thin Coating System Pull Test Dollies: Cycle 56 to Cycle 100



Figure 8.25 – Removed Paint After Pull Off Test

8.5 Pull of Test Results Discussion

The results of the pull of test display that the organic and inorganic zinc based over coating paints performed better than the epoxy and aluminum mastic based systems. The corrosion growth for the organic and inorganic zinc systems was significantly lower than for the epoxy and aluminum mastic based systems. At 42 master cycles of accelerated testing thin coating system 1 had a corrosion creep growth of 4.00 millimeters, thin coating system 2 had a corrosion creep growth of 4.50 millimeters, thin coating system 3 had a corrosion creep growth of 3.82 millimeters, thin coating system 4 (organic zinc) had a corrosion creep growth of 1.43 millimeters and thin coating system 5 (inorganic zinc) had a corrosion creep of 2.07 millimeters. At 100 master cycles of accelerated testing thin coating system 1 had a corrosion creep growth of 6.28 millimeters, thin coating system 2 had a corrosion creep growth of 6.06 millimeters, thin coating system 3 had a corrosion creep growth of 6.06 millimeters, thin coating system 4 (organic zinc)

had a corrosion creep growth of 3.89 millimeters and thin coating system 5 (inorganic zinc) had a corrosion creep of 3.94 millimeters.

The epoxy mastic systems experienced a greater loss of tensile strength capacity in the first 42 cycles than the organic and inorganic zinc systems. In the first 42 cycles thin coating system 1 loss 64% of its tensile capacity, thin coating system 2 loss 70% of its tensile capacity and thin coating system 3 loss 62% of its tensile capacity. In the first 42 cycles thin coating system 4 (organic zinc) loss 27% of its tensile capacity and thin coating system 5 (inorganic zinc) loss 37% of its tensile capacity. At the end of the accelerated testing schedule (100 master cycles) thin coating system 1 loss 86% of its tensile capacity, thin coating system 2 loss 85% of its tensile capacity and thin coating system 3 loss 84% of its tensile capacity, thin coating system 4 (organic zinc) loss 63% of its tensile capacity and thin coating system 5 (inorganic zinc) loss 63% of its tensile capacity.

The results from the pull off testing correlate with a 20-year field performance of bridge maintenance systems (Ault & Farsschon, 2011).

8.6 Color Change Results Discussion

The color change from cycle 0 to cycle 100 show variations for all of the thin coating systems. Thin coating system 1 had a 2% change in the L* coordinate, 113.6% change in the a* coordinate and a 423.7% change in the b* coordinate. Thin coating system 2 had a 3.2% change in the L* coordinate, 93.3% change in the a* coordinate and a 25.5% change in the b* coordinate. Thin coating system 3 had a 0.4% change in the L* coordinate, 114.3% change in the a* coordinate and a 137.8% change in the b*

coordinate. Thin coating system had a 0.4% change in the L* coordinate, 2.6% change in the a* coordinate and a 29.7% change in the b* coordinate. Thin coating system had a 0.5% change in the L* coordinate, 2.9% change in the a* coordinate and a 12.5% change in the b* coordinate.

For all thin coating systems, there was a variation greater than 20% for the a* and b* coordinates, and a variation change less than 5% for the L* coordinate. Hence the recommendation is to ignore the a* and b* coordinates, but verify that the variation change for the L* coordinate is less than 5%.

8.7 Thickness Change Results Discussion

There was little variation in thickness change recorded at cycle 0 and cycle 100 for the thin coating systems. Thin coating system 1 had an average thickness change of 0%, thin coating system 2 had an average thickness change of 0.7%, thin coating system 3 had an average thickness change of 0.8%, thin coating system 4 had an average thickness change of 1.9%, and thin coating system 5 had a thickness change of 6.3%. Since the results from the thickness readings for all of the thin coating paint systems did not show any significant change (under 10% variation), and thickness variation is not the primary response variable, the recommendation is to ignore thickness change.

8.8 Visual Inspection Change Results Discussion

Thin coating systems 4 and 5 did not show any significant signs of deterioration. Thin coating systems 1, 2 and 3 showed signs of deterioration around the holes and welds,

typically around cycle 42. The recommendation is to reject any specimen with significant deterioration around the holes or welds.

8.5 Discussion of Test Results

The results of the evaluations display that the organic and inorganic zinc based over coating paints performed better than the epoxy and aluminum mastic based systems. The corrosion growth for the organic and inorganic zinc systems was significantly lower than for the epoxy and aluminum mastic based systems. The results correlate with a 20-year performance of bridge maintenance systems conducted by New Jersey Department of Transportation (Ault & Farsschon, 2011). For all thin coating systems, there was a variation greater than 20% for the a* and b* coordinates, and a variation change less than 5% for the L* coordinate. The thickness readings did not have a large variation, and hence were determined to not have a large impact on determining the systems serviceability. The results from this investigation show that it is possible to determine a thin coatings performance in field conditions, as well as provide a quantifiable method to compare thin coats.

8.6 Proposed Acceptance Criteria

An acceptance criterion is recommended to better determine the over coating paints effectiveness in actual field conditions has been established from the results of the developed protocol. The acceptance criteria are based on the results of the response variables of pull off tests, color change, thickness change and visual inspections. For the results of the pull off tests, any specimen at 42 cycles with a corrosion creep greater than 2.5 millimeters will be rejected. At the completion of 100 master cycles, any specimen

with a corrosion creep greater than 5 millimeters will be rejected. Any specimen after 100 master cycles with a L* coordinate color change greater than 10 percent will be rejected. Any significant deterioration changes detected by visual inspection will result in the rejection of the specimen. If the thin coating system remains within the allowable limits of the corrosion creep, color change, and visual inspection; the thin coating paint system is accepted.

8.5 Summary

- The current ASTM tests to determine thin coating paint performance are intended only for comparative evaluations, and have subjective elements to determine the comparative rating. The results do not represent field performance.
- Current ASTM standards require the removal of over coating paint to measure the rust creepage. There is a potential risk of damaging rust creepage when removing the paint which increases the potential of inaccurate results.
- The newly developed over coating paint procedure still applies the concept of a scribe to simulate typical filed damages, but applies an O-ring during painting to form the outline of the scribe. After the over coating paint cures, the O-rings are removed, exposing the steel with no damage to the over coating paint or steel specimen.
- Water soluble glue is used to attach the O-rings to the steel specimens so it does not add extra corrosion protection for the exposed steel. The glue can be easily removed if any residue is left on the steel specimen.

- For pull off testing, the 20 millimeter dolly fits exactly within the circular scribe. It is not required to remove over coating paint and potentially disturb the corrosive creep on the specimen to conduct pull off testing.
- The new testing procedure provides a calculation to estimate the average corrosion creep based off of the specimens pull off strength. There is no scraping of the specimen's paint or subjective creep measurement required.
- The new test protocol does provide quantitatively measurable results for measuring corrosion vulnerability.
- The results correlate with the field performance results conducted by Ault & Farsschon (2011).
- Of the coating systems, those containing an inorganic zinc or organic zinc primer performed best.
- The epoxy systems and aluminum-mastic systems performed worst.
- The new testing procedure provides a calculation to estimate the average corrosion creep based off of the specimens pull off strength. There is no scraping of the specimen's paint or subjective corrosion creep measurement required.
- The effectiveness of a thin coating system can be analyzed within three months.

CHAPTER 9 – DURABILITY TESTS: RAPID REPAIR SYSTEMS

9.1 Introduction

For the developed chamber for accelerated testing, the experimental schedule emphasizes accelerated degradation by the effect of cyclical wetting and drying, which allows for the deeper penetration of aggressive ions (Moukwa, 1990). Therefore, there will be more focus on the wetting and drying because the cyclical effects accelerates durability problems because it subjects the concrete to the motion and accumulation of harmful materials such as sulphates, alkalies, acids, and chlorides.

There will be a rotational wetting and drying period. The developed experimental system will apply a wetting period of New Jersey Department of Transportation road de-icing salt solution at a 5 percent concentration, followed by a drying period to further accelerate any deterioration that occurred. During the drying period the specimens were exposed to UV irradiation as well. Following the wetting and drying, the specimens were placed into a chamber capable of maintaining a deep freeze. When the specimens are removed from the freezer cabinet and placed into the chamber for accelerated testing, this is considered the beginning of the next cycle. The samples at the end of the wetting/drying rotation end on the wetting process, leaving the specimens saturated with salt solution. Therefore, when the specimens were placed into the freezer cabinet, ice will form and further exacerbated the effects of freeze-thaw.

9.2 Rapid Repair Durability: Test Set Up

To simulate rain and water-run off exposure that occurs with exterior structures, a recycling salt flat spray will be part of the newly developed testing system to simulate

typical rain and water run-off conditions. The developed chamber will ensure that an even coverage of the specimens will still be maintained with a flat spray. The sodium chloride to be used in the system will be typical roadway de-icing salt used by the New Jersey Department of Transportations, to closer simulate field conditions, and deterioration caused on the concrete.

A holding rack for specimens will be part of the chamber for accelerated testing, and its construction will follow the guidelines of ASTM D5894 and ASTM B117. The holding rack will support specimens at an angle between 15° and 30° from the vertical, constructed from a non-corrosive/conductive material capable of resisting deterioration from the components of the chamber and will be placed preferably parallel to the principal direction of the salt spray through the chamber.

Ultraviolet irradiation will also be included new system. As there are no ASTM standards for ultraviolet irradiation of concrete, the accelerated testing system will follow many of the guidelines established in ASTM D5894 and ASTM G154. The type of UV light and placement of UV light will follow the guidelines discussed. Instead of being in a separate UV/condensation cabinet, the UV lights will be part of the main chamber, and included in every cycle.

To provide a deep freeze environment for the chamber for accelerated testing, the concept of freeze-thaw application is derived from ASTM C666. An apparatus suitable with the necessary refrigeration to achieve the specified temperature requirements of $-20 \pm 5^{\circ}\text{F}$ ($-29 \pm 3^{\circ}\text{C}$) will be used. To provide a thawing environment for the chamber for accelerated testing, a heating system capable of achieving and maintaining a temperature

of $122 \pm 5^{\circ}\text{F}$ ($50 \pm 3^{\circ}\text{C}$) within an hour will be applied. For the developed heating system in the chamber for accelerated testing will also act as the drying system.

The chamber for accelerated testing will be a semi-automatic operation, where the operation of the salt sprayers, UV lights, freezing and heating system will be an automatic system. The only manual requirements for the developed system will be the movement of the specimens, and replenishment of the salt solution.

9.3 Rapid Repair Durability: Specimen Preparation

Four 12-inch-wide by 12-inch-long by 1-inch-deep ferrocement square specimens, with a 6-inch-long by 6-inch-wide by $\frac{1}{2}$ inch deep simulated damage were fabricated following the plan in figure 9.1. The specimens were fabricated by constructing 12-inch-wide by 12-inch-long by 1-inch-deep wood forms, and placing 6-inch-wide by $\frac{1}{2}$ inch deep extruded polystyrene foam in the center. Then $\frac{1}{2}$ " by $\frac{1}{2}$ " wide galvanized steel mesh was uniformly placed into the formwork (figure 9.2). Following the galvanized steel mesh placement, a mortar mix was placed into the formwork. Twenty-four hours after the mortar placement, the formwork was demolded (figure 9.3), and the specimens were placed into a 100 percent humidity curing room in the Civil Engineering Laboratory on Busch Campus located in Piscataway, NJ. After 28 days wet curing in a 100 percent humidity curing room, the ferrocement specimens were then removed from the curing room. The most promising formulation (RSHPR) was then casted into the ferrocement specimens simulated damages to replicate a patch repair as shown in figure 9.4. The RSHPR was then air cured for 3 hours in the Civil Engineering Laboratory on Busch

Campus in Piscataway, NJ. Following the 3 hours of curing the specimens were prepared for initial tensile strength testing.

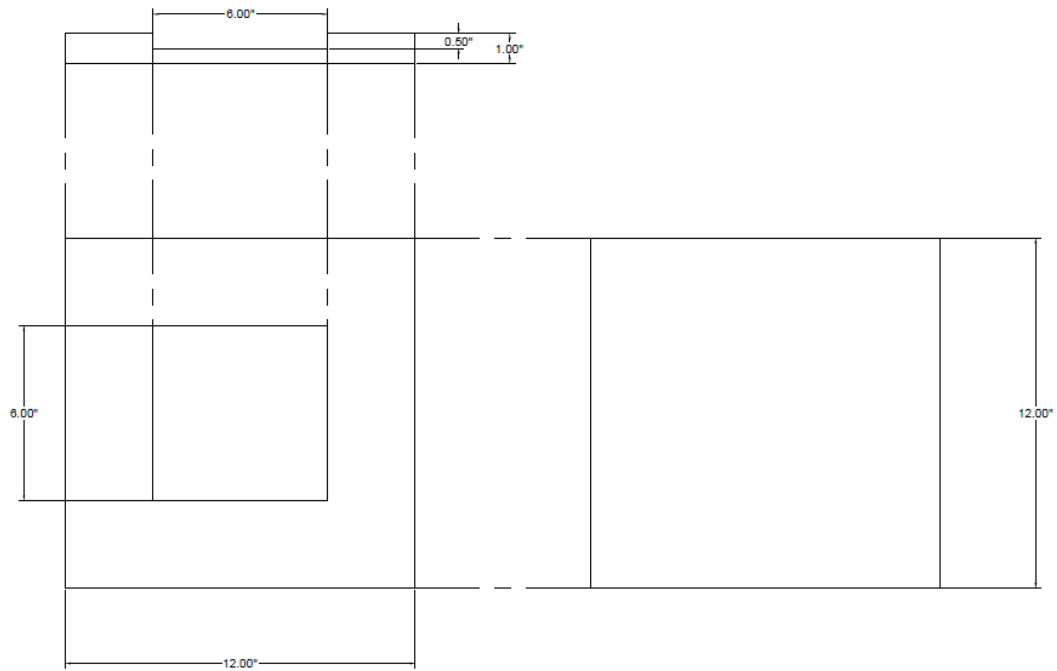


Figure 9.1 – Simulated Damage Patch Design Plan

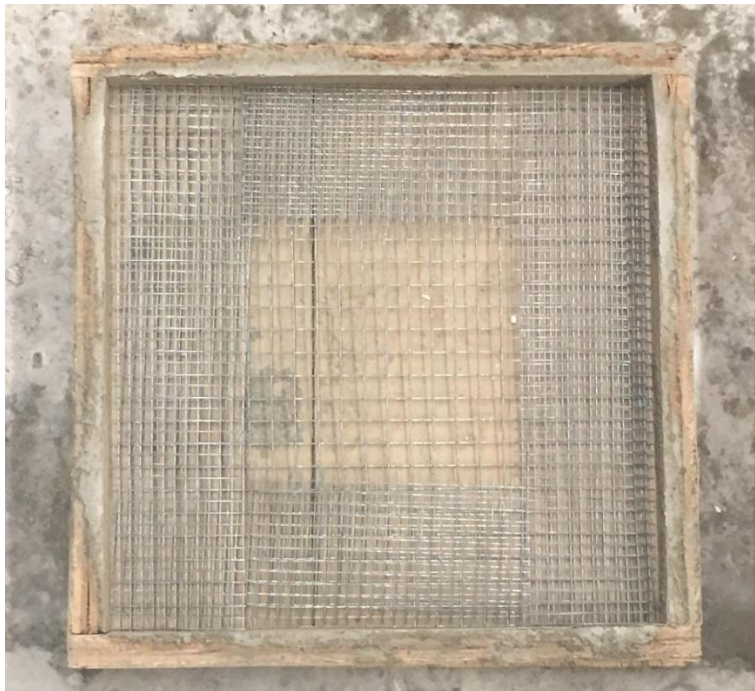


Figure 9.2 – Mesh Wire Placed in Formwork Mold for Simulated Damage Patch



Figure 9.3 – Ferrocement Specimen with Simulated Damage Patch



Figure 9.4 – RSHPR Durability Specimen After Simulated Patch Repair

9.4 Rapid Repair: Test Schedule

The developed chamber for accelerated RSHPR durability testing experimental schedule followed the same sequence as the method for accelerated corrosion testing discussed in chapter 6. For the developed chamber for accelerated testing, the experimental schedule applied a 1-hour wetting period followed by a 1-hour drying period of the RSHPR durability specimens. The wetting and drying periods will rotate one after another for 8 cycles each, over a 16-hour period. During the drying period the specimens were exposed to UV irradiation as well, therefore having a total of 8-hours of irradiation exposure. To include the effects of freeze-thaw interactions, the RSHPR durability specimens were placed into a chamber capable of maintaining a deep freeze for 8 hours after the 16-hours of wetting, drying and UV exposure. Combined these sequences produce a 24-hour period, and will constitute 1-master cycle. When the specimens are

removed from the freezer cabinet and placed into the chamber for accelerated testing, rotated a quarter turn to ensure even exposure coverage. This is considered the beginning of the next cycle. The beginning of the cycle starts with exposure to heat and UV radiation for 1 hour to thaw the specimens as well as dry off any moisture on the specimens from the freezer. The samples at the end of the wetting/drying rotation end on the wetting process, leaving the specimens saturated with salt solution. Therefore, when the specimens are placed into the freezer cabinet, ice will form and further accelerate the detrimental effects of freeze-thaw interactions.

9.5 Rapid Repair Durability: Test Procedure

Before placement of the specimens in the chamber for accelerated testing, the virgin RSHPR durability specimen pull off strength is determined. After the specimens had three hours to air cure in the Civil Engineering Laboratory at Rutgers University, three circular cuts equivalent to the outside diameter of the pull off dollies were drilled $\frac{1}{2}$ inch through the RSHPR to the specimen substrate interface using a wet core drill press and a core bit. The RSHPR specimens were then dried using compressed air. Once the RSHPR slabs were dried, 20 millimeter pull off test dollies were epoxied onto each cut, three for each specimen (figure 9.5). The epoxy was given 24 hours to fully cure as per manufacturer specification before pull off testing. Twenty-four hours after the epoxy has cured, pull off testing is then conducted on the specimens following the guidelines of ASTM C1583, Standard Test Method for Tensile Strength of Concrete surfaces and the Bond Strength of Tensile Strength of Concrete Repair by Direct Tension, to conduct the pull off test. The pull off tester used is a PosiTest[®] AT-M Manual Adhesion Tester. The tensile load was applied at a constant rate of 15 to 20 psi/s. After each failure, the tensile

stress and failure mode are recorded. The pull off dollies are then labeled and kept for comparison. Once testing has been completed, the RSHPR durability specimens are then placed into the chamber for accelerated testing to begin experimentation.



Figure 9.5 – Pull Off Dollies Epoxied on a Rapid Set Repair Durability Specimen

After the required number of master cycles in the chamber for accelerated testing, the RSHPR durability specimens are then removed from the chamber. Three circular cuts equivalent to the outside diameter of the pull off dollies for each RSHPR durability specimen are then drilled $\frac{1}{2}$ inch through the RSHPR to the specimen substrate interface using a wet core drill press and a core bit. The specimens are rinsed with clean water to remove any debris or residue, then gently dried with compressed air. Once the RSHPR slabs were dried, 20 millimeter pull off test dollies were epoxied onto each cut, three for each specimen. The epoxy was given 24 hours to fully cure as per manufacturer specification before pull off testing. Twenty-four hours after the epoxy has cured, pull off testing is then conducted on the specimens following the guidelines of ASTM C1583,

Standard Test Method for Tensile Strength of Concrete surfaces and the Bond Strength of Tensile Strength of Concrete Repair by Direct Tension, to conduct the pull off test. The pull off tester used is a PosiTest® AT-M Manual Adhesion Tester. The tensile load was applied at a constant rate of 15 to 20 psi/s. After each failure, the tensile stress and failure mode are recorded. The pull off dollies are then labeled and kept for comparison. Once testing has been completed, the RSHPR durability specimens are then placed into the chamber for accelerated testing to continue experimentation.

9.6 Test Results

Tables 9.1 to 9.4 displays the pull off test results for each durability specimen. Table 9.5 displays pull off tests conducted on the durability specimens one month after removal from the chamber for accelerated testing, and table 9.6 displays the average tensile strength decrease over 56 cycles. Figures 9.6 to 9.9 displays the tensile stress versus the cycles for each rapid set durability specimen. Figure 9.10 shows the average percentage loss of tensile stress versus cycles. Figure 9.11 shows typical pull off specimens and figure 9.12 displays typical pull outs on rapid set durability specimens.

Rapid Set Repair Durability Specimen 1					
Cycle	Dolly 1 (psi)	Dolly 2 (psi)	Dolly 3 (psi)	Average (psi)	Std. Dev (psi)
0	737	551	363	550	84
14	464	377	451	431	38
28	438	415	386	413	23
42	442	421	384	416	24
56	392	384	426	401	34

Table 9.1 – Pull Off Testing: Rapid Repair Durability Specimen 1

Rapid Set Repair Durability Specimen 2					
Cycle	Dolly 1 (psi)	Dolly 2 (psi)	Dolly 3 (psi)	Average (psi)	Std. Dev (psi)
0	550	683	544	592	64
14	502	461	418	460	34
28	460	421	373	418	36
42	441	416	384	414	23
56	390	406	416	404	11

Table 9.2 – Pull Off Testing: Rapid Repair Durability Specimen 2

Rapid Set Repair Durability Specimen 3					
Cycle	Dolly 1 (psi)	Dolly 2 (psi)	Dolly 3 (psi)	Average (psi)	Std. Dev (psi)
0	508	541	535	528	14
14	451	448	515	471	31
28	Epoxy Failure	499	421	460	39
42	409	354	540	434	78
56	476	328	450	418	65

Table 9.3 – Pull Off Testing: Rapid Repair Durability Specimen 3

Rapid Set Repair Durability Specimen 4					
Cycle	Dolly 1 (psi)	Dolly 2 (psi)	Dolly 3 (psi)	Average (psi)	Std. Dev (psi)
0	592	596	598	595	2
14	524	Epoxy Failure	526	525	1
28	476	489	496	487	8
42	445	457	Epoxy Failure	451	6
56	434	408	441	428	14

Table 9.4 – Pull Off Testing: Rapid Repair Durability Specimen 4

One-Month Testing After Durability Specimen Chamber Removal					
Specimen	Dolly 1 (psi)	Dolly 2 (psi)	Dolly 3 (psi)	Average (psi)	Std. Dev (psi)
1	435	395	383	404	22
2	411	392	417	407	11
3	469	425	434	443	19
4	410	425	415	417	6

Table 9.5 – Pull Off Testing: One-Month Testing After Durability Specimen Chamber Removal

Cycle	Average Tensile Stress (psi)	Loss of Tensile Stress (%)
0	567	0.0
14	472	16.7
28	445	4.8
42	429	2.8
56	413	2.9

Table 9.6 – Average Percentage Loss of Tensile Stress Over 56 Cycles

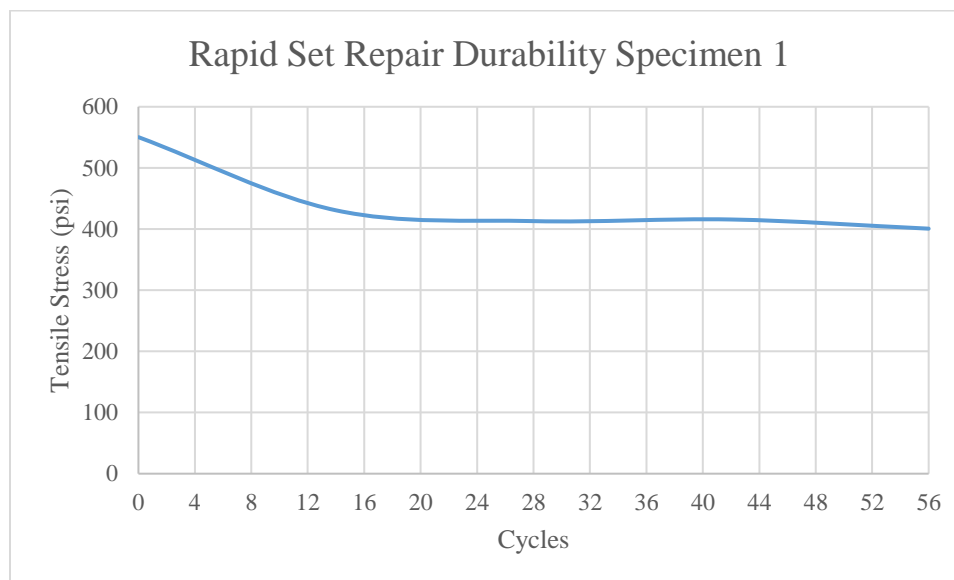


Figure 9.6 – Tensile Stress versus Cycles: Rapid Set Durability Specimen 1

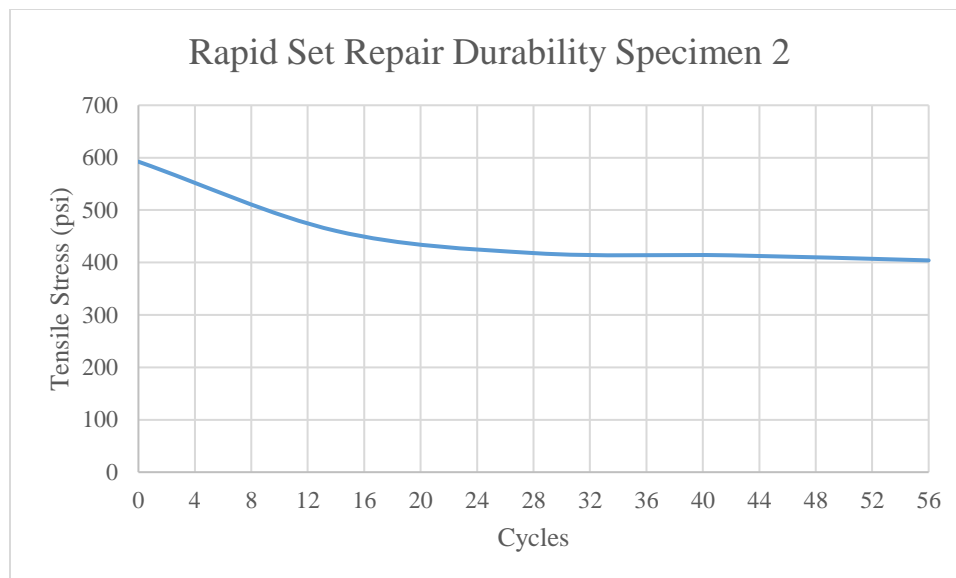


Figure 9.7 – Tensile Stress versus Cycles: Rapid Set Durability Specimen 2

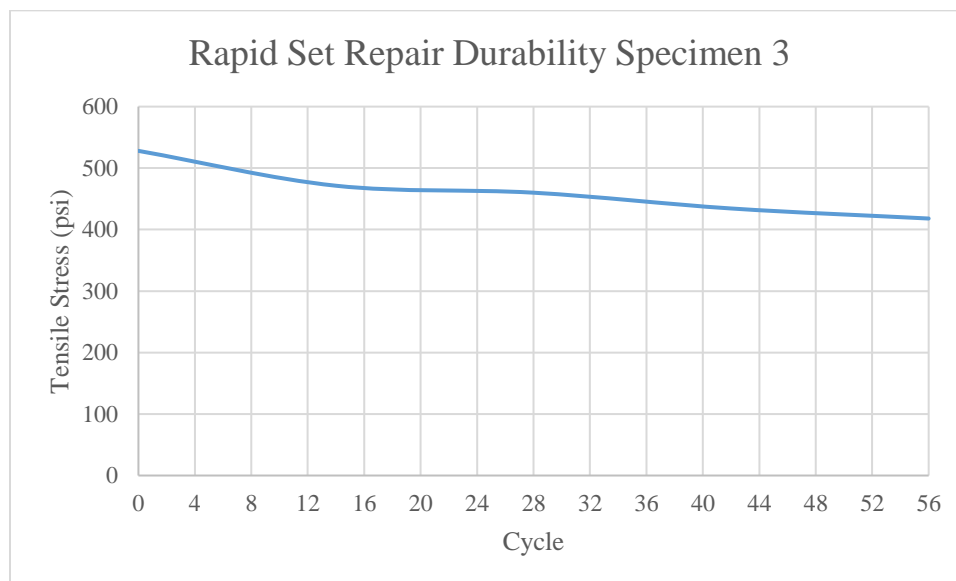


Figure 9.8 – Tensile Stress versus Cycles: Rapid Set Durability Specimen 3

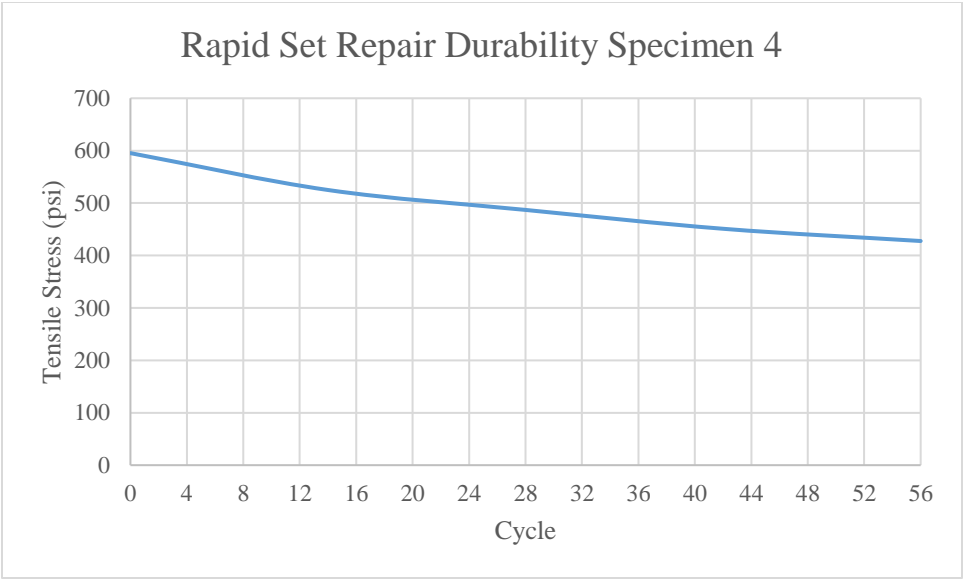


Figure 9.9 – Tensile Stress versus Cycles: Rapid Set Durability Specimen 4

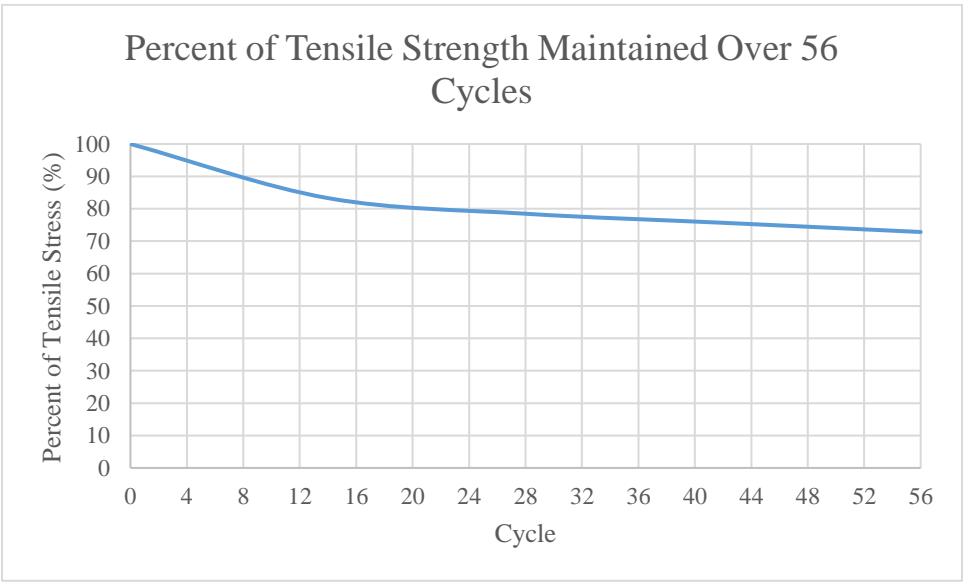


Figure 9.10 – Average Percentage Loss of Tensile Stress versus Cycles



Figure 9.11 – Typical Pull Off Specimens

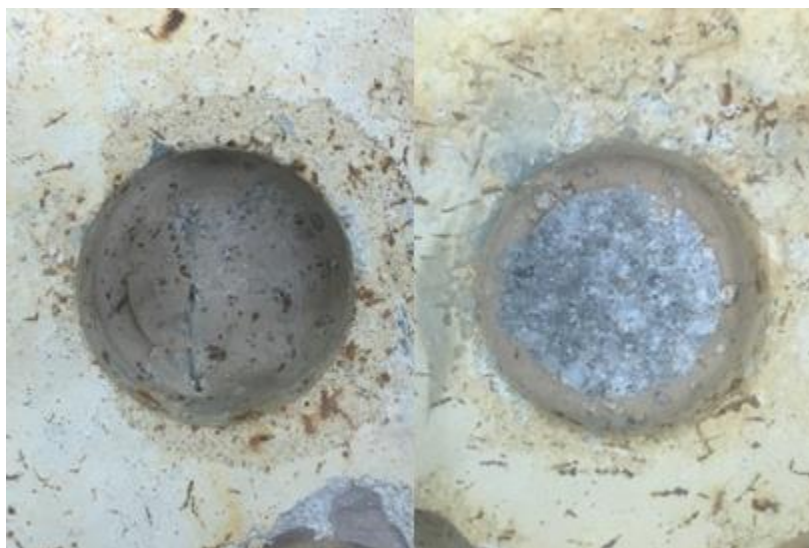


Figure 9.12 – Typical Pull Outs on Durability Specimens



Figure 9.13 – RSHPR Patch Repair: 10 Months After Placement



Figure 9.14 – RSHPR Patch Repair: 10 Months After Placement Interface

9.7 Discussion of Test Results

The results show that there is an initial decrease of approximately 17% from initial bond strength in 14 cycles, followed by an approximate decrease in bond strength of 22% in 28 cycles. After 28 cycles the decrease in bond strength rapidly diminishes, stabilizing approximately at a loss of 27% of bond strength. The results from the pull testing conducted on the rapid set durability specimens at room temperature one month after removal from the chamber of accelerated testing is the same average bond strength undergoing 56 cycles of accelerated degradation. If left in the accelerated chamber, there is a decrease. This test method could possibly be used for evaluating the long term performance under freeze-thaw and UV exposure conditions. Since there are deficient details for the field performance of similar products, the comparative behavior of the developed system could not be numerically determined. As reported from chapter 3, the compressive strength, modulus of rupture and splitting tensile strength capacity of RSHPR increased over 56 days. As these are factors in bond strength, the direct tensile capacity of RSHPR does not diminish if it is not undergoing cyclical degradation. As shown in Figures 9.13 and 9.14, visual inspection of the RSHPR repaired Route 18, County Road 516 overpass bridge deck slabs located outside of the CAIT laboratory on Livingston Campus show no signs of damage after a 10-month period.

9.8 Summary

- There currently no ASTM standards for test methods to assess the effects of deicer salt and freeze-thaw cycling on the durability of concrete repair materials and the concrete substrate.

- It is known that the application of deicing salts over the life of a structure or pavement will negatively impact the long-term durability of the concrete, hence a 5 percent salt solution was used as the wetting agent for the chamber for accelerated testing.
- The developed chamber for accelerated RSHPR durability testing experimental schedule followed the same sequence as the method for accelerated corrosion testing discussed in chapter 6.
- This evaluation simulates the effectiveness of a rapid-set cements bond strength to substrate concrete when it is exposed to cyclical wetting, drying, and freezing conditions. Note that the bond strength of the repair material to substrate concrete is an important factor for durability.
- One master cycle constitutes a 24-hour period.
- Pull off test results provide insight to a rapid-set cements bond strength when exposed to environmental conditions over time. The results can be used to determine the effective durability of a rapid-set cement as a repair material for concrete structures.
- This test method could possibly be used for evaluating the long-term performance under freeze-thaw and UV exposure conditions.

CHAPTER 10 – CONCLUSIONS

Based on the results of this investigation, the following conclusions can be drawn.

- In the area of repair and rehabilitation of concrete structures, rapid hardening formulations are widely used.
- Phosphate cement, calcium sulfoaluminate cement, portland cement with additives and polymer concrete are the common repair systems. The expected compressive strength is 3000 psi within 3 hours. After careful evaluation of the various products, calcium sulfoaluminate was chosen for further enhancement of mechanical properties.
- It is possible to formulate rapid set fiber reinforced concrete with volume fractions of 2 percent that is highly flowable.
- The addition of 2% fibers resulted in a reduction of shrinkage strains by 54 percent.
- Shrinkage stabilized at 28 days, but the compressive strength continued to increase. Therefore, strength gain is not related to shrinkage.
- By formulating compositions with shrinkage strains less than 300 micro strains, it is possible to fabricate crack free repairs leading to durable repairs and structures.
- Using admixtures, the water to cement ratio lower than the manufacturers recommendation could be used and still obtain flowable mix. Reduction in water to cement ratio resulted in shrinkage less than the values reported by the manufacturer.

- The modulus of elasticity measured using the flexural test samples (in flexural mode) is 59% of the modulus of elasticity measured during compression strength testing.
- The rapid set formulations developed in the current investigation (RSHPR), was effectively placed in an active construction zone, with little operating room and strict time constraints. A horizontal patch repair could be completed within 30 minutes.
- Surface preparation before the application of RSHPR is an important factor for an effective repair. Based on this investigation, an unprepared surface can reduce the bond strength of RSHPR to a substrate surface by 27 percent.
- It is possible to pump fiber reinforced concrete volume fractions of 2 percent that is highly flowable, and effectively place both in a horizontal and non-horizontal structural patch.
- A repair procedure was developed for quick repair of vertical surfaces. The system provides a quick one-step repair. There is no need for multiple work-day schedule for placing and removal of formwork.
- Mechanical anchorage of patch repairs provides 44 percent increase in delamination strength, measured using direct tension test.
- The proposed durability evaluation procedure for rapid-set cement repair systems provides insight to a rapid-set cements bond strength when exposed to environmental conditions over time. It is recommended to use this durability testing method for comparing different rapid-set repair systems.

The investigation focusing on the durability and corrosion resistance of thin coatings for steel structures lead to the following conclusions:

- The fundamental weakness of the current accelerated test procedures is that the tests do not provide the estimate of service life in actual field conditions. The tests are intended only for comparative evaluations.
- The test chamber designed and built for this investigation combines wetting, drying, UV exposure, freezing and thawing in 1 master cycle. The existing standards separate these degradation mechanisms. For example, UV exposure is done after the exposure to a saline solution spray. This current process better simulates actual field conditions by combining response variables and can help provide a better estimate of service life in actual field conditions.
- An economical chamber was fabricated for the proposed test protocol.
- The proposed exposure scheme for accelerated testing is as follows:
 - 8 cycles of 1-hour wetting followed by 1-hour drying.
 - 8-hour UV exposure during the drying cycle.
 - 8-hours of deep freezing at a temperature of 0 degrees Fahrenheit.
 - The length of these combined exposures is 24 hours and was designated as 1 master cycle.
- The proposed test protocol provides quantitatively measurable response variables for measuring corrosion vulnerability. The response variables, namely direct tension capacity was used to estimate the average corrosion creep. There is no scraping of the specimen's paint or subjective creep measurement required.

- Of the coating systems, those containing an inorganic zinc or organic zinc primer performed best. The epoxy systems and aluminum-mastic systems performed worst. The results correlate with the 25-year field performance study conducted by Ault & Farsschon (2011).
- The effectiveness of a thin coating system can be evaluated within three months.

The authors suggestions for further research are the following:

- Fiber reinforced rapid set cement for rapid repair and rehabilitation for concrete structures is working well. Further research should be conducted for other rapid set materials to improve the mechanical properties.
- The thin coating evaluation method seems to be working well. More coating types should be evaluated to further evaluate the test protocol and establish variances among test set ups.

REFERENCES

- Abrams, D.A., "The American Concrete Institute and Concrete Research," *ACI Journal*, V. 27, No. 4, Apr. 1931, pp. 953-957.
- ACI (American Concrete Institute) and ICRI (International Concrete Repair Institute). (1999). "Concrete paving technology-guidelines for partial depth repair." Concrete repair manual, Farmington Hills, MI, 467-478.
- ACI Committee 201, Guide to Durable Concrete, 2008: Committee Reports
- ACI 318. 2014. *Building Code Requirements for Reinforced Concrete*. Farmington Hills: American Concrete Institute.
- Adams, M., Browne, R., & French, E. (1975). Using Polymer Concretes. *Batiment International/Building Research & Practice*,3, 212-231.
- Akkaya, Y., Ouyang, C. and Shah, S. P. (2007) "Effect of Supplementary Cementitious Materials on Shrinkage and Crack Development in Concrete," *Cement and Concrete Composites*, Vol. 29, Issue 2, Feb. 2007, pp 117-123.
- Al-Ostaz, A., Irshidat, M., Tenkhoff, B., & Ponnappalli, P. S. (2010). Deterioration of Bond Integrity between Repair Material and Concrete due to Thermal and Mechanical Incompatibilities. *Journal of Materials in Civil Engineering*,22(2), 136-144.
doi:10.1061/(asce)0899-1561(2010)22:2(136)
- American Concrete Institute (ACI), Concrete Repair Guide. ACI Committee 546, ACI 546R-04
- American Concrete Institute (ACI), Report on Fiber Reinforced Concrete (Reapproved 2009). ACI Committee 544, ACI 544.1R-96
- American Society of Civil Engineers, 2017 Infrastructure Report Card – Bridges, Retrieved March 22, 2018, from <https://www.infrastructurereportcard.org/cat-item/bridges/>
- ASTM B117-16 Standard Practice for Operating Salt Spray (Fog) Apparatus, ASTM International, West Conshohocken, PA, 2016, <https://doi.org/10.1520/B0117-16>
- ASTM C1583/C1583M-13 Standard Test Method for Tensile Strength of Concrete Surfaces and the Bond Strength or Tensile Strength of Concrete Repair and Overlay Materials by Direct Tension (Pull-off Method), ASTM International, West Conshohocken, PA, 2013, https://doi.org/10.1520/C1583_C1583M-13
- ASTM C39/C39M-17a Standard Test Method for Compressive Strength of Cylindrical Concrete Specimens, ASTM International, West Conshohocken, PA, 2017
- ASTM C469/C469M-14 Standard Test Method for Static Modulus of Elasticity and Poisson's Ratio of Concrete in Compression, ASTM International, West Conshohocken, PA, 2014

ASTM C490/C490M-17 Standard Practice for Use of Apparatus for the Determination of Length Change of Hardened Cement Paste, Mortar, and Concrete, ASTM International, West Conshohocken, PA, 2017, https://doi.org/10.1520/C0490_C0490M-17

ASTM C496/C496M-11 Standard Test Method for Splitting Tensile Strength of Cylindrical Concrete Specimens, ASTM International, West Conshohocken, PA, 2004

ASTM C666/C666M-15 Standard Test Method for Resistance of Concrete to Rapid Freezing and Thawing, ASTM International, West Conshohocken, PA, 2015, https://doi.org/10.1520/C0666_C0666M-15

ASTM C78/C78M-16 Standard Test Method for Flexural Strength of Concrete (Using Simple Beam with Third-Point Loading), ASTM International, West Conshohocken, PA, 2016

ASTM D1654-08(2016)e1 Standard Test Method for Evaluation of Painted or Coated Specimens Subjected to Corrosive Environments, ASTM International, West Conshohocken, PA, 2016, <https://doi.org/10.1520/D1654-08R16E01>

ASTM D1654-08(2016)e1 Standard Test Method for Evaluation of Painted or Coated Specimens Subjected to Corrosive Environments, ASTM International, West Conshohocken, PA, 2016, <https://doi.org/10.1520/D1654-08R16E01>

ASTM D4541-09e1 Standard Test Method for Pull-Off Strength of Coatings Using Portable Adhesion Testers, ASTM International, West Conshohocken, PA, 2009

ASTM D5894-16 Standard Practice for Cyclic Salt Fog/UV Exposure of Painted Metal, (Alternating Exposures in a Fog/Dry Cabinet and a UV/Condensation Cabinet), ASTM International, West Conshohocken, PA, 2016, <https://doi.org/10.1520/D5894-16>

ASTM D5894-16 Standard Practice for Cyclic Salt Fog/UV Exposure of Painted Metal, (Alternating Exposures in a Fog/Dry Cabinet and a UV/Condensation Cabinet), ASTM International, West Conshohocken, PA, 2016

ASTM D610-08(2012) Standard Practice for Evaluating Degree of Rusting on Painted Steel Surfaces, ASTM International, West Conshohocken, PA, 2012, <https://doi.org/10.1520/D0610-08R12>

ASTM D610-08(2012) Standard Practice for Evaluating Degree of Rusting on Painted Steel Surfaces, ASTM International, West Conshohocken, PA, 2012

ASTM D714-02(2017) Standard Test Method for Evaluating Degree of Blistering of Paints, ASTM International, West Conshohocken, PA, 2017, <https://doi.org/10.1520/D0714-02R17>

ASTM International. (2017). ASTM D3359-17 Standard Test Methods for Rating Adhesion by Tape Test. Retrieved from <https://doi.org/10.1520/D3359-17>

ASTM Subcommittee C09.25, Organic Materials for Bonding, 2010

- ASTM. (2007a). "Standard practice for use of apparatus for the determination of length change of hardened cement paste, mortar, and concrete." ASTM C490-04, West Conshohocken, PA.
- ASTM. (2007c). "Standard test method for length change of hardened hydraulic-cement mortar and concrete." ASTM C157/C157M-06, West Conshohocken, PA.
- Balaguru, P. N., and D. Bhatt. 2000. "Rapid Hardening Concrete." Final report FHWA NJ 2001-03. Piscataway, NJ: Center for Advanced Infrastructure and Transportation, Civil and Environmental Engineering, Rutgers University.
- Balaguru, P.N., Caronia, D, Roda, A.M, (2017). "Development of Concrete Mix Proportions for Minimizing/Eliminating Shrinkage Cracks in Slabs and High Performance Grouts." Final Report CAIT-UTC-NC14. Piscataway, NJ: Center for Advanced Infrastructure and Technology, Rutgers, The State University of New Jersey
- Beck, B., "Evaluation of Minimal Surface Preparation Coatings for Bridge Painting", MDOT, Research Report R-1394, May 2001, MDOT
- Bedi, R., Chandra, R., & Singh, S. (2013). Mechanical Properties of Polymer Concrete. *Journal of Composites*, 2013. <http://dx.doi.org/10.1155/2013/948745>
- Bissonnette, B., Pierre, P., and Pigeon, M. (1999) "Influence of Key Parameters on Drying Shrinkage of Cementitious Materials", *Cement and Concrete Research*, Vol. 29, pp. 1655-1662.
- Bizzozero, J., & Scrivener, K. L. (2015). Limestone reaction in calcium aluminate cement–calcium sulfate systems. *Cement and Concrete Research*, 76, 159-169. doi:10.1016/j.cemconres.2015.05.019
- CCAA (2002). Drying Shrinkage of Cement and Concrete [Pamphlet]. (2002). St. Leonards, NSW: Cement and Concrete Aggregates of Australia. *Cement and Concrete Research* 31, 2001, 455-465.
- Cervo, N. M., & Schokker, A. J. (2010). Bridge Deck Patching Material Evaluation. *Journal of Bridge Engineering*, 15(6), 723-730. doi:10.1061/(asce)be.1943-5592.0000109
- Chong, S.L. (2004, September). Preventing Corrosion in Steel Bridges. Retrieved August 23, 2017, from <https://www.fhwa.dot.gov/publications/publicroads/04sep/08.cfm>
- Darwin, D., Browning, J., Gong, L., & Hughes, S. R. (2007). *Effects of Deicers on Concrete Deterioration* (Rep. No. 07-3). Lawrence, Kansas: Structural Engineering and Materials Laboratory, University of Kansas.
- Kline, E.S (2009). Steel Bridges: Corrosion Protection for 100 Years, *Journal of Protective Coatings and Linings*: pp. 22-31.

- Federal Highway Administration, Steel Bridge Design Handbook: Corrosion Protection of Steel Bridges”, Publication No. FHWA-IF-12-052 – Vol. 19, November 2012
- FHWA Bridge Coatings Technical Note, *Overcoating*, USDOT, Editor. 2000: Washington, D.C.
- Folliard, K.J. and Berke, N.S. (1997) Properties of High-Performance Concrete Containing Shrinkage-Reducing Additives, *Cement and Concrete Research*, Vol. 27, No. 9, pp. 1357-1364.
- Furr, H. L., & Ingram, L. L. (1971). *Bond and Durability of Concrete and Resinous Overlays* (Rep. No. 130-5). College Station, Texas: Texas Transportation Institute.
- Gaudette, P., & Slaton, D. (2007). Preservation Brief 15: Preservation of Historic Concrete. Retrieved July 18, 2017, from <https://www.nps.gov/tps/how-to-preserve/briefs/15-concrete.htm>
- Gilbert, R. I. (2001). Shrinkage, Cracking and Deflection-the Serviceability of Concrete Structures. *Electronic Journal of Structural Engineering*, 1(1). Retrieved July 31, 2017, from <http://www.ejse.org/Archives/Fulltext/200101/02/20010102.htm>
- Gu, P., Beaudoin, J. J., Quinn, E. G., & Myers, R. E. (1997). Early Strength Development and Hydration of Ordinary Portland Cement/Calcium Aluminate Cement Pastes. *Advanced Cement Based Materials*, 6(2), 53-58. doi:10.1016/s1065-7355(97)00008-4
- Houska, C. (2007). Deicing Salt—Recognizing the Corrosion Threat. International Molybdenum Association, Pittsburgh, TMR Consulting.
- J. Ault, C. Farschon, “Selecting and sourcing Bridge Coating Systems”, *Journal of Protective Coatings & Linings*, 2011.
- J. Péra, J. Ambroise, New applications of calcium sulfoaluminate cement, *Cement and Concrete Research*, Volume 34, Issue 4, 2004, Pages 671-676, ISSN 0008-8846, <https://doi.org/10.1016/j.cemconres.2003.10.019>.
- Jiang, H. Y., Liang, B., and Zhang, L.M. Investigation of MPB with super early strength for repair of concrete. *Journal of Building Materials* 4(2), 2001, 196- 198.
- Konica Minolta. (2018). Identifying Color Differences Using L*a*b* or L*C*H* Coordinates. Retrieved March 26, 2018, from <https://sensing.konicaminolta.us/blog/identifying-color-differences-using-l-a-b-or-l-c-h-coordinates/>, Konica Minolta Sensing Americas, Inc.
- Kosmatka, S.H. & Wilson, M.L. (2011). *Design and Control of Concrete Mixtures*, 15th Ed., Portland Cement Association, Skokie, IL.

- Krishna, V., & Kumar, R. (2016). Sustainable Construction Materials & Technologies. In *Water to Cement Ratio: A Simple and Effective Approach to Control Plastic and Drying Shrinkage in Concrete*. Las Vegas, Nevada.
- Kronlöf, A., Leivo, M., & Sipari, P. (1995). Experimental study on the basic phenomena of shrinkage and cracking of fresh mortar. *Cement and Concrete Research*, 25(8), 1747-1754. doi:10.1016/0008-8846(95)00170-0
- Li, S., Geissert, D. G., Frantz, G. C., & Stephens, J. E. (1997). *Durability and Bond of High Performance Concrete and Repaired Portland Cement Concrete* (pp. 1-232, Rep. No. JHR 97-257). Storrs, CT.
- Morgan, D. (1996). Compatibility of concrete repair materials and systems. *Construction and Building Materials*, 10(1), 57-67. doi:0950-0618(95)00060-7
- Moukwa, M. (1990). Deterioration of concrete in cold sea waters. *Cement and Concrete Research*, 20(3), 439-446. doi:10.1016/0008-8846(90)90034-u
- Neville, A. M. (2012). *Properties of concrete*. Harlow: Pearson Education.
- Nocuń-Wczelik, W., Konik, Z., & Stok, A. (2011). Blended systems with calcium aluminate and calcium sulphate expansive additives. *Construction and Building Materials*, 25(2), 939-943. doi:10.1016/j.conbuildmat.2010.06.089
- Ray, I., Parish, G. C., Davalos, J. F., & Chen, A. (2011). Effect of Concrete Substrate Repair Methods for Beams Aged by Accelerated Corrosion and Strengthened with CFRP. *Journal of Aerospace Engineering*, 24(2), 227-239. doi:10.1061/(asce)as.1943-5525.0000030
- Santhanam, M. (2013), Evaluation of superplasticizer performance in concrete, Third International Conference on Sustainable Construction Materials and Technologies, Kyoto, 2013.
- Sarker, A. Investigation of reaction/bonding mechanisms in regular and retarded magnesium phosphate cement systems. *Cement Technology*, 1994, 281-288
- Sarker, A. K. Hydration/dehydration characteristics of struvite and dittmarite pertaining to magnesium ammonium phosphate cement systems. *Journal of Materials Science* 26, 1991, 2514-2518.
- Satoh, A., Satoh, M., & Yamada, K. (2015). Improvement of Adhesion Performance of Mortar-Repair Interface with Inducing Crack Path into Repair. *Frattura Ed Integrità Strutturale*, 34. doi:10.3221/IGF-ESIS.34.44
- Shadravan, S., Ramseyer, C., Gorman, P., & Santamaria, C. R. (2012). Dimensional Stability of Concrete Slabs on Grade. *American Concrete Institute*, 307, 49-69.

- Silfwerbrand, J. (2017). Bonded Concrete Overlays. *Concrete International*,39(5), 31-36.
- Silfwerbrand, J., & Beushausen, H. (2005). Bonded Concrete Overlays - Bond Strength Issues. In Proceedings of the International Conference on Concrete Repair, Rehabilitation and Retrofitting (p. 512). Capetown, South Africa.
- Soliman, M., & Frangopol, D. M. (2014). *Life-Cycle Cost Evaluation of Conventional and Corrosion-Resistant Steel for Bridges*(Tech.). American Society of Civil Engineers. doi:10.1061/(ASCE)BE.1943-5592.0000647
- Soudee, E., and Pera, J. Influence of magnesia surface on the setting time of magnesia-phosphate cement. *Cement and Concrete Research* 32, 2002, 153-157.
- Soudee, E., and Pera, J. Mechanism of setting reaction in magnesia-phosphate cements. *Cement and Concrete Research* 30, 2000, 315-321.
- Sprinkel, M.M. (1983). Thermal Compatibility of Thin Polymer Concrete Overlays. Transportation Research Board Record No. 899.
- The Society for Protective Coatings (1997), *Technology Update No. 3: Overcoating*, SSPC
- The Society for Protective Coatings (2014), *Using SSPC Coating Material Standards*, SSPC
- Tortelli, S., & Marchi, M. (2015). *Performance of Sulpho-Based Rapid-Hardening Concrete* (Vol. 303, pp. 57-68, Special Publication). American Concrete Institute.
- Trauchessec, R., Mechling, J., Lecomte, A., Roux, A., & Rolland, B. L. (2015). Hydration of ordinary Portland cement and calcium sulfoaluminate cement blends. *Cement and Concrete Composites*,56, 106-114. doi:10.1016/j.cemconcomp.2014.11.005
- Tritsch, N., Darwin, D. and Browning J. (2005) "Evaluating Shrinkage and Cracking Behavior of Concrete Using Restrained Ring and Free Shrinkage Tests", *The Transportation Pooled Fund Program Project No. TPF-5(051)*, Structural Engineering and Engineering Materials SM Report No.77, The University of Kansas Center for Research, Inc. at Kansas.
- Vaysburd, A. M., Bissonnette, B., & Von Fay, K. F. (2014). *Compatibility Issues in Design and Implementation of Concrete Repairs and Overlays* (pp. 15-136, Rep. No. MERL-2014-87). Denver, Colorado: Bureau of Reclamation.
- White, A.H. (1914), Volume Changes in Portland Cement and Concrete, *Proceedings of the 17th Annual Meeting*, American Society for Testing Materials, V. 14, Part 2, Technical Papers, West Conshohocken, PA, pp. 203-254.

- Xi, Y., Shing, B., and Xie, Z. (2001) Development of Optimal Concrete Mix Designs for Bridge Decks, *Report No. CDOT-DTD-R-2001-11*, sponsored by the Colorado Department of Transportation, Jun., 60 p.
- Y. Li, B. Chen. (2013) Factors that affect the properties of magnesium phosphate cement, *Construction Building Materials*, 47, pp. 977–983
- Yang, Q., Zhang, S., & Wu, X. (2002). Deicer-scaling resistance of phosphate cement-based binder for rapid repair of concrete. *Cement and Concrete Research*, 32(1), 165-168. doi:10.1016/s0008-8846(01)00651-2
- Yang, Q., Zhu, B., & Wu, X. (2000). Characteristics and durability test of magnesium phosphate cement-based material for rapid repair of concrete. *Materials and Structures*, 33(4), 229-234. doi:10.1007/bf02479332
- Yang, Q., Zhu, B., Zhang, S., & Wu, X. (2000). Properties and applications of magnesia-phosphate cement mortar for rapid repair of concrete. *Cement and Concrete Research*, 30(11), 1807-1813. doi:10.1016/s0008-8846(00)00419-1
- Young, J. F., Mindess, S., Gray, R. J., & Bentur, A. (1998). Chapter 10 - Aggregates. In *The Science and Technology of Civil Engineering Materials* (pp. 189-203). Upper Saddle River, NJ: Prentice Hall.